REPUBLIC OF TÜRKİYE
MUĞLA SITKI KOÇMAN UNIVERSITY
GRADUATE SCHOOL OF
NATURAL AND APPLIED SCIENCES

DEPARTMENT OF GEOLOGICAL ENGINEERING

TEMPORAL AND SPATIAL RELATIONS OF CONTINENTAL DEFORMATION AND TECTONIC CONTROLS WITH PORPHYRY CU-AU AND EPITHERMAL AU MINERALIZATION IN THE KİRAZLI GOLD DEPOSIT

MEHMET ÇAM

PH.D. THESIS

JUNE 2024
MUĞLA

MUGLA SITKI KOÇMAN UNIVERSITY

Graduate School of Natural and Applied Sciences

APPROVAL OF THE THESIS

The thesis submitted by **MEHMET ÇAM** with the title of "**TEMPORAL AND SPATIAL RELATIONS OF CONTINENTAL DEFORMATION AND TECTONIC CONTROLS WITH PORPHYRY CU-AU AND EPITHERMAL AU MINERALIZATION IN THE KİRAZLI GOLD DEPOSIT**" has been unanimously accepted by jury members on the 24th of June, 2024 to fulfil the requirements for degree of Doctor of Philosophy in the Department of Geological Engineering.

THESIS JURY MEMBERS

Prof. Dr. Tolga OYMAN **(Head of Jury)** Signature:

Department of Geological Engineering,
Dokuz Eylül University, İzmir _____

Prof. Dr. İlkay KUŞCU **(Supervisor)** Signature:

Department of Geological Engineering,
Muğla Sıtkı Koçman University, Muğla _____

Prof. Dr. Murat GÜL **(Member)** Signature:

Department of Geological Engineering,
Muğla Sıtkı Koçman University, Muğla _____

Assoc. Prof. Dr. Özgür AVŞAR **(Member)** Signature:

Department of Geological Engineering,
Muğla Sıtkı Koçman University, Muğla _____

Prof. Dr. Nuretdin KAYMAKCI **(Member)** Signature:

Department of Geological Engineering,
Middle East Technical University, Ankara _____

APPROVAL OF THE HEAD OF THE DEPARTMENT

Prof. Dr. Semih GÜRSU Signature:

Head of Department, Geological Engineering
Muğla Sıtkı Koçman University, Muğla _____

Prof. Dr. İlkay KUŞCU Signature:

Supervisor, Department of Geological Engineering,
Muğla Sıtkı Koçman University, Muğla _____

Date of Defence: 24/06/2024

I hereby declare that all information in this document has been obtained and presented in accordance with academic rules and ethical conduct. I also declare that, as required by these rules and conduct, I have fully cited and referenced all material and results that are not original to this work.

Mehmet ÇAM

24/06/2024

ABSTRACT

TEMPORAL AND SPATIAL RELATIONS OF CONTINENTAL DEFORMATION AND TECTONIC CONTROLS WITH PORPHYRY CU-AU AND EPITHERMAL AU MINERALIZATION IN THE KİRAZLI GOLD DEPOSIT

Mehmet ÇAM

Doctoral Thesis (Ph.D.)
Graduate School of Natural and Applied Sciences
Department of Geological Engineering
Supervisor: Prof. Dr. İlkay KUŞCU
June 2024, 113 pages

This thesis work is focused on defining the local structures that are effective in the formation of the Çanakkale-Kirazlı porphyry Cu-Au and high sulfidation (HS) epithermal Au mineralization, the regional tectonic and hydrothermal phases that form these structures and hydrothermal mineralization, and revealing their temporal and spatial relationships. Based on the geometric and kinematic analyses of data collected from the fault surfaces of regional-scale and district-scale areas, 3 different tectonic phases were identified. These tectonic phases and principle stress axes include (1) NW-SE extension (Phase-1: σ1=87°/173°, σ2=01°/057°, σ3=03°/327°), (2) NNE-SSW extension (Phase-2: σ1=69°/286°, σ2=21°/093°, σ3=04°/185°) and (3) NE-SW extension (Phase-3: σ1=32°/306°, σ2=56°/106°, σ3=09°/211°). Comparison of stress axes, extension directions, and predominant fault trends of these phases with the published kinematic data, age and spatial distribution of geological units in the Biga Peninsula, suggests that Phase-1 is related to post-collisional extension in the northern part of the Biga Peninsula, Phase 2 is related to back-arc extensional tectonism and Phase-3 is related to strike-slip tectonism accompanied by faulting event that generated the faults of the North Anatolian Fault zone in the region.

Examination of drill cores intersecting the porphyry Cu-Au mineralization located within the Kale zone and south of the Çatalkaya Zone revealed four distinguishable vein types: sulfide-free quartz veins (A-veins), quartz-sulfide veins (B-veins), sulfide

veins (D-veins), and late-stage carbonate (calcite) veins. The preferred orientations of B-/D-veins observed on the surface are geometrically similar to the predominant orientation of regional faults related to phase-2 tectonism. Petrographic studies on oriented thin-sections also indicate that the growth direction of stretched quartz crystals within B-veins is indicative of NNE-SSW extension and multiple crack-seal events related to Phase-1 tectonism. Analysis of drill cores intersecting the HS epithermal Au mineralization in the Main Zone to the north and the Çatalkaya Zone at the center revealed that the massive silicification forming the core of the system is positioned vertically within a N-S oriented phreatic/hydrothermal breccia providing a background for subsequent quartz-sulfide, grey-quartz, and white-quartz hydrothermal veins. Quartz-alunite alteration of HS epithermal system exhibit a NW-SE spatial distribution, while the clay alteration zone (illite) peripheral to the core of the system is formed parallel the NE-SW and E-W structures crosscutting the quartz-alunite alteration zones, suggesting that marginal alterations of the HS epithermal Au mineralization temporally coincide with structures governed by tectonic Phase-2. Petrographic examinations of oriented thin sections revealed that, while the veins around the Main zone contain fluid-assisted breccia texture with high clast/matrix ratio and no or slightly re-oriented clasts indicating hydraulic assisted fracturing, the veins within illite-montmorillonite zones are thin, breccia-free quartz veins showing NNE-SSW extension referring the increased tectonic contribution related Phase-2 tectonism. The published data and findings in this study revealed that the porphyry-Cu style mineralization and HS-epithermal Au mineralization within Kirazlı district formed along permeable zones resulted by different tectonic phases and an extensional tectonism juxtaposing the Eocene volcano-plutonic and Oligocene volcanic/volcanoclastic sequences along approximately E-W trending faults occurred prior to formation of HS-epithermal Au mineralization implying that the both styles of mineralizations were not temporally linked mineralization systems.

Keywords: Structural Control, Porphyry Cu, HS Epithermal Au, Biga Peninsula, Kirazlı Deposit.

ÖZET

KITASAL DEFORMASYON VE TEKTONİK KONTROLLERİN KİRAZLI ALTIN MADENİNDEKİ PORFİRİ CU-AU VE EPİTERMAL AU CEVHERLEŞMELERİ İLE ZAMANSAL VE MEKANSAL İLİŞKİSİ

Mehmet ÇAM

Doktora Tezi
Fen Bilimleri Enstitüsü
Jeoloji Mühendisliği Anabilim Dalı
Danışman: Prof. Dr. İlkay KUŞCU
Haziran 2024, 113 sayfa

Bu tez çalışması, Çanakkale-Kirazlı porfiri Cu-Au ve yüksek sülfidasyon (YS) epitermal Au cevherleşmelerinin oluşumunda etkili olan lokal yapıların, bu yapıları oluşturan bölgesel tektonik hidrotermal evrelerle zamansal ve mekansal ilişkilerini ortaya koymaya odaklanmıştır. Kirazlı porfiri Cu-Au ve YS epitermal Au cevherleşmeleri sırasıyla, orta-geç Eosen volkano-plutonik ve Oligosen volkanik/volkanoklastik kayaçlar tarafından barındırılmaktadır. Bu magmatik birimler, Permo-Triyas yaşlı Rodop-Pontid zonuna ait temel kayaları üzerler. Saha gözlemleri, farklı yaş aralıklarında oluşmuş ve farklı türde cevherleşmeleri içeren bu magmatik birimlerin genişlemeye bağlı tektonizmaya bağlı normal faylar ile yanyana geldiklerini göstermektedir. Bölgesel ve cevherleşme sahaları içinde yer alan fay yüzeylerinde yapılan ölçümlerin, geometrik ve kinematik analizlerine göre 3 farklı tektonik faz tanımlanmıştır. Bunlar, (1) KB-GD genişleme (Faz-1: σ1=87°/173°, σ2=01°/057°, σ3=03°/327°), (2) KKD-GGB genişleme (Faz-2: σ1=69°/286°, σ2=21°/093°, σ3=04°/185°) ve (3) KD-GB genişleme (Faz-3: σ1=32°/306°, σ2=56°/106°, σ3=09°/211°) tektonik fazlarını içermektedir. Bu fazlara ait stres eksenlerinin, açılma yönlerinin ve hakim fay doğrultularının yaşları literatürde belirtilmiş kinematik veriler, jeolojik birimlerin yaşları ve Biga yarımadası içerisindeki dağılımları ile karşılaştırılması; Faz-1'in orta-geç Eosen magmatik kayaçların Biga yarımadasının kuzey kısmında çarpışma sonrası genişleme yerleşimi ile, Faz-2'nin yay-ardı açılma ve Faz-3'ün ise Kuzey Anadolu Fay zonunun oluşumunu sağlayan doğrultu atımlı evresi ile ilgili olduğunu göstermektedir.

Cevherleşme sahasının güney kısmında, Kale Zonu içerisinde ve Çatalkaya Zonu güneyinde yerleşmiş olan porfiri Cu-Au cevherleşmesini kesen sondaj karot örneklerinin incelenmesiyle, sırasıyla sülfidsiz-kuvars damarları (A-damarları), kuvars-sülfid damarları (B-damarları), sülfid damarları (D-damarları) ve geç evre karbonat (kalsit) damarlarının varlığı tespit edilmiştir. Yüzeyde gözlenebilen B-/D-damarlarının hakim yönleri Faz-2 tektonizmaya ait bölgesel fayların hakim yönleri ile geometrik benzerliğe sahiptir. Ayrıca, yönlü ince kesitler üzerinde yapılan petrografik çalışmalar, B-damarlarının içerisindeki kuvars kristallerinin büyüme yönlerinin, Faz-2 tektonizmasıyla uyumlu olacak şekile KKB-GGD genişlemeyi ve çoklu açılma-tıkanma olaylarını işaret ettiğini göstermektedir. Main ve Çatalkaya zonları içerisinde bulunan YS epitermal Au cevherleşmesini kesen sondaj karotlarının incelenmesiyle, bu sistemin merkezini oluşturan massif silisleşmenin düşey konumlu ve yaklaşık K-G yönlü bir freatik/hidrotermal breş içine yerleştiği ve bu silisleşmiş breşin, sırasıyla birbirini kesen, kuvars-sulfid, gri-kuvars ve beyaz-kuvars hidrotermal damar fazları için bir zemin oluşturduğu belirlenmiştir. YS epitermal Au cevherleşmesinin merkez kesimlerindeki kuvars-alunit alterasyon zonu KKB-GGD yönlü mekansal bir dağılım gösterirken, görece kenar kesimleri oluşturan kil alterasyon (illit) zonu, erken evreyi kesen KD-GB ve D-B yönlü yapılara paralellik göstermesi, YS epitermal Au cevherleşmesinin kenar kesimdeki alterasytonlarının zamansal olarak Faz-2'ye denk geldiğini önermektedir. Yönlü kesitlerde yapılan petrografik çalışmalar, Main zon çevresindeki damarlar yüksek klast/matriks oranına sahip ve az miktarda veya hiç tekrar yönlenmemiş sıvı-destekli breş dokusu içerirken, illit-montmorillonit zonundaki damarlar Faz-2 tektonizma ile ilişkili artan bir tektonik katkıyı kasteder biçimde KKB-GGD açılma gösteren ince breşsiz damarlardır. Yayınlanmış veriler ve bu tezdeki bulgular, Kirazlı sahasındaki porfiri Cu-Au ve YS epitermal Au cevherleşmelerinin farklı tektonik fazların sonucu olan geçirimli zonlar boyunca oluştuğunu ve Eosen volkano-plutonik ve Oligosen volkanik/volkanoklastik sekansları D-B yönlü faylar boyunca yanyana getiren bir açılmalı tektonizmanın her iki cevherleşme türünün zamansal olarak bağlantılı sistemler olmadığını önerecek şekilde YS Epitermal Au cevherleşmesinin oluşumundan önce gerçekleştiğini ortaya koymaktadır.

Anahtar Kelimeler: Yapısal Kontrol, Porfiri Cu, YS Epitermal Au, Biga Yarımadası, Kirazlı Madeni.

To my family,

İsmail, Masume and Selim

ACKNOWLEDGEMENT

I wish to express my deepest gratitude to my advisor, Prof. Dr. İlkay Kuşcu for his patience, encouragements, never-ending support for all the time. In addition to having great contributions at every step of this study, his guidence not only provided me a vision for my academic career but also humanly perspective for my life.

Besides my supervisor I would like to thank, Prof. Dr. Nuretdin Kaymakcı for his great support, valuable suggestions, sincerity and hospitality. I will always feel indebted to him.

I would also like to thank Prof. Dr. Murat Gül for his valuable suggestions, and revisions on my thesis.

I would like to forward my thanks to Exploration Director and Senior Geologist Mehtap Karcı, Senior Geologist Gülsevim Özışık; Exploration Assistants Nazım Tomruk and Sefer Sezgin and Doğu Biga Mining Company (Alamos Gold Inc.) for their great support hospitality and extensive help in every step of this study.

TABLE OF CONTENT

TABLE OF CONTENT……..x

LIST OF TABLES……..…… ..…..xii

LIST OF FIGURES……...……...…xiii

1. INTRODUCTION 1

1.1. Scope and Purpose.....1

1.2. Geographic Setting 3

1.3. Previous Studies 5

1.3.1. Fundamentals on spatio-temporal association between mineralization and structures 5

1.3.2. Studies on regional tectonic and tectono-magmatic evolution of biga peninsula 8

1.3.2.1. Tectonic studies 8

1.3.2.2. Tectono-magmatic studies.....11

1.3.3. Studies on porphyry and epithermal deposits in terms of tectono-magmatic evolution of the biga peninsula 14

1.4. Methodology 16

1.4.1. Field works.....17

1.4.2. Desk and laboratory studies 18

2. REGIONAL GEOLOGY 21

2.1. Basement of Biga Peninsula 21

2.1.1. High-grade metamorphics.....21

2.1.1.1. Kazdağ core complex.....21

2.1.1.2. Çamlıca metamorphics 23

2.1.2. Low-grade metamorphics 23

2.1.2.1. Karakaya complex 23

2.1.2.2. Ezine group 24

2.1.3. Ophiolites.....25

2.1.3.1. Çetmi ophiolitic melange 25

2.1.3.2. Denizgören ophiolite.....25

2.1.4. Magmatism and tectono-magmatic processes.....26

2.1.5. Temporal and spatial distribution of mineral occurrences within biga peninsula 30

3. LOCAL GEOLOGY 32

3.1. Pre-Cenozoic Basement....33
3.2. Cenozoic Magmatics....36
4. STRUCTURAL GEOLOGY....40
4.1. Kinematic Analyses and Characteristics....42
4.1.1. NW-SE extensional phase (phase-1)....42
4.1.2. NNE-SSW extensional phase (phase-2)....44
4.1.3. NE-SW extension phase (phase-3)....45
4.1.4. Spatio-temporal distribution of tectonic phases and related faults....47
4.2. Kinematic Properties and Fault Types of Kirazlı Deposit....51
5. ALTERATION-MINERALIZTION AND VEINS....56
5.1. Alteration-Mineralization Pattern....56
5.2. Vein and Veinlets....58
5.2.1. Veins in the drill core samples....59
5.2.1.1. Porphyry Cu-style veins....60
5.2.1.2. HS-epithermal Au-style veins....64
5.2.2. Veins on surface and predominant vein orientations....68
5.2.2.1. Porphyry Cu-style veins/veinlets....69
5.2.2.2. Epithermal veins/veinlets....72
5.2.2.3. Surface measurements of vein orientations....74
5.3. Association of Au-Grade....78
6. DISCUSSION....80
6.1. Tectonic Phases and Their Spatio-Temporal Association....80
6.2. Correlation Between Regional and District Scale Faults....81
6.3. Spatio-Temporal Association Between Mineralizations and Tectonic Phases....82
6.4. Spatio-Temporal Associations Between High-Permeability Zones and Structural Elements within the District....84
6.4.1. Porphyry-Cu style mineralization....84
6.4.2. HS-epithermal style mineralization....85
6.5. Summary of Temporal Relations Between Tectonism and Mineralization Within District....87
7. CONCLUSION....90
REFERENCES....93
APPENDICES....104
CURRICULUM VITAE....111

LIST OF TABLES

Table 4.1. List of measurement sites, resultant principle stress orientations and lithology ages related to phase-1 (R= Ratio of principle stress differences, n/nt= working/total data).....43
Table 4.2. List of measurement sites, resultant principle stress orientations and lithology ages related to phase-2 (R= Ratio of principle stress differences, n/nt= working/total data).....44
Table 4.3. List of measurement sites, resultant principle stress orientations and lithology ages related to phase-3 (R= Ratio of principle stress differences, n/nt= working/total data).....46
Table 4.4. List of measurement sites, resultant principle stress orientations and lithology ages related to Phase-1 (R= Ratio of principle stress differences, n/nt= working/total data).....51
Table 4.5. List of measurement sites, resultant principle stress orientations and lithology ages related to Phase-2 (R= Ratio of principle stress differences, n/nt= working/total data).....52
Table 4.6. List of measurement sites, resultant principle stress orientations and lithology ages related to Phase-3 (R= Ratio of principle stress differences, n/nt= working/total data).....52

LIST OF FIGURES

Figure 1.1. (A) Major Tectonic units of Türkiye (blue square encirling the Biga Peninsula), (B) Biga Peninsula (big and small red reticles respectively marking the regional and district-scale areas), (C) Kirazlı District and mineralized sectors/ore zones. (IAESZ: İzmir-Ankara-Erzincan Suture Zone, IPS: Intra-Pontide Suture, BZSZ: Bitlis-Zagros Suture Zone).....4

Figure 1.2. (A) Re-oriented sample in sand pool based on marked orientation of reference surfeace and smaple that vertical N-S and (B) horizontal planes marked on.....18

Figure 1.3. Prepared oriented chip sample. (N= North) 20

Figure 2.1. (A)Tectonic units of Turkiye and location of Biga Peninsula (blue square), (B) Geological map and locations of mineral occurrences of Biga peninsula. (Revised after Yiğit, 2012; Duru et al, 2014; Brunetti, 2016; Leroux, 2016; Sanchez et al, 2016). (IAESZ: İzmir-Ankara-Erzincan Suture Zone, IPS: Intra-Pontide Suture, BSZ: Bitlis Suture Zone).....22

Figure 2.2. Compiled magmatic ages of plutonic and volcanic rocks, magmatic and tectonic stages of Biga Peninsula. (References for Plutonism= Delaloye and Bingöl, 2000; Beccaletto and Bonev, 2007; Altunkaynak and Genç, 2008; Karacık and Yılmaz, 2008; Kuşcu, 2009; Altunkaynak et al, 2012; Yiğit, 2012; Black et al, 2013; Brunetti, 2016; Kuşcu et al, 2019; Volcanism= Ercan et al, 1995; Aldanmaz et al, 2000; Altunkaynak and Genç, 2004; Kuşcu et al, 2019; Erenoğlu and Billor 2022; Magmatic stages = Altunkaynak and Genç, 2008; Kuşcu et al, 2019; Hydrothermal stages = Brunetti, 2016; Leroux, 2016; Kuşcu et al, 2019; Tectonic history = Brun and Sokoutis, 2007; Brun and Faccenna, 2008; Agostini et al, 2010; Jolivet and Brun, 2010; Sanchez et al, 2016; Kuşcu et al. 2019; Schaarschmidt et al.2021; Gülyüz et al., 2024).....27

Figure 3.1 Geological map of Kirazlı District, A-B-C-D composite cross-section and E-F crossection. 33

Figure 3.2. Outcrops of Çamlıca Metamorphics at the eastern part of district. (A) Strongly folded, micaschists with boudinaged quartz lenses, (B) Well foliated, undeformed micaschists without quartz lenses. 34
Figure 3.3. (A) Contact between serpentinite of Denizgören and micaschists of Çamlıca unit, (B) close view of dark green/blue colored, blocky and well-deformed serpentinites of Denizgören ophiolite from northeastern sector of Kirazlı District.....35
Figure 3.4. Outcrop view of units belong to Karakaya Complex from southeastern sector of Kirazlı District. (A) Fine grained, well-sorted sandstones and (B) polymictic, matrix supported conglomerate.....35
Figure 3.5. (A), (B) Outcrop view of Cenozoic volcanics at the western sector of Kirazlı District. Dark colored Plagioclase-phyric andesite (PPA) forms the footwall of nearly E-W striking extensional faults and light light - medium gray Basaltic Andesite (BA) forms the hangingwall. 37
Figure 3.6. (A) Altered plagioclase crystal from PPA (x-pl), (B) Embayed and fractured magmatic quartz crystals from BA (x-pl), (C) and (D) Amphibole pseudo-crystals from clay altered BA (x-pl).....37
Figure 3.7. Drillcore samples from andesitic tuff sequences. (A) Lithic-tuff including rounded to subrounded clast, (B) unwelded/welded lithic+crystal tuff (silicified), (C) fine grained layered tuff (silicified and oxidized). 38
Figure 3.8. (A),(B) Clay altered and silicified, angular to subangular clast bearing phreatic breccia from Kirazlı Main Zone.....39
Figure 4.1. (A) Lithological-structural map of regional-scale study area and locations of kinematic measurement sites, (B) Stereoplots and p-t axes of measurement sites, (C),(D),(E),(F) Stereoplots of fault planes, principle stress axes; roseplots of predominant fault strikes, dip amounts of fault planes and striations from determined tectonic phases. (Lithologies are same as in the Figure 2.1.) 41
Figure 4.2. Stereoplots of fault planes, principle stress axes; roseplots of predominant fault strikes, dip amounts of fault planes and striations from phase-1. (Small arrows on arcs indicate slip senses).....43

Figure 4.3. Stereoplots of fault planes, principle stress axes; roseplots of predominant fault strikes, dip amounts of fault planes and striations from phase-2. (Small arrows on arcs indicate slip senses).....45
Figure 4.4. Stereoplots of fault planes, principle stress axes; roseplots of predominant fault strikes, dip amounts of fault planes and striations from phase-3. (Small arrows on arcs indicate slip senses).....46
Figure 4.5. (A) Spatial distribution of basemen and volcano-plutonic rocks of Biga Peninsula based on predominant directions. (B) Contour diagram of kinematic data indicating NE-SW extension and spatial distribution of shear-senses within Kemer Micaschists (Beccaletto et al.,2007), (C) Contour diagrams of kinematic data indicating NNE-SSW extension and spatial distribution of shear-senses within Northwestern margin of Kazdağ Core Complex and Alakeçili Shear Zone (Okay et al, 2000; Beccaletto et al.,2007). 50
Figure 4.6. (A) Lithological-structural map of district-scale study area and locations of kinematic measurement sites, (B) Stereoplots of measured faults and p-t axes of measurement sites, (C),(D),(E),(F) Stereoplots of fault planes, principle stress axes; roseplots of predominant fault strikes, dip amounts of fault planes and striations from determined tectonic phases. (Lithologies are same as in the Figure 3.1.).....53
Figure 4.7. Geometric correlations of regional and district scale tectonic phases based on predominant fault orientations, principle stress orientations, p-t axes and related shear models. 54
Figure 5.1. The alteration map showing the main alteration types (after Aluç et al. 2023) and structures mapped during this study.....57
Figure 5.2. (A) and (B) The spatial distribution of HS-epithermal-style, and (C) porphyry Cu style alterations in the Kirazlı district (after Aluç et al., 2023) 58
Figure 5.3. Topography map with alterations and structures also showing the locations and hole ID of the drill holes for core sampling in this study (alteration map after Aluç et al.,2023).....60

Figure 5.4. Drill cores with early-stage A-veins (A) arrays of veins and (B) offset by micro faults.....61
Figure 5.5. Drill core samples showing (A) to (D) quartz- sulfide, and (E) and (F) sulfide only veins post-dating the quartz-sulfide veins. 62
Figure 5.6. Drill cores showing (A) sulfide only veins, and (B) stockwork veins post-dating the quartz-sulfide veins 63
Figure 5.7. Drill cores showing (A) calcite-only late carbonate vein, (B) close-up view of A, (C) pyrite-bearing late carbonate vein and (D) close up view of C 63
Figure 5.8. (A)Vuggy-textured quartz from the drill cores within the HS epithermal Au system and (B) close-up view of A.....64
Figure 5.9. Drill core showing the dark-gray quartz-sulfides cementing the breccia.65
Figure 5.10. Drill core (A) showing dark grey quartz cement, vein breccia and (B) cross cutting quartz-sulfide veins 65
Figure 5.11. A,C) Drill cores showing quartz-sulfide veins, (B) close view of A and (D) close view of C.....66
Figure 5.12. (A) and (B) gray quartz vein crosscutting phreatic breccia and quartz-sulfide veins.....66
Figure 5.13. Drill cores showing white sulfide-free quartz veins truncating (A) gray quartz vein and (B) quartz-sulfide veins.....67
Figure 5.14. Topography map with alterations, structures, sampling lines and locations of oriented samples (alteration map after Aluç et al.,2023).....68
Figure 5.15. Stereographic projection and contour diagram from poles of vein planes measured from chip samples.....69
Figure 5.16. Oriented samples showing (A) and (B) Oxidized B-type (quartz-sulfide veins) and (C) and (D) stockwork type D-veins, note that the N and S are shown as “K” and S”, respectively on the samples. 70
Figure 5.17. (A) The predominant strike direction of B-veins and (B) D-veins from chip samples. 71
Figure 5.18. Photomicrographs illustrating (A) to (F), quartz veinlets from oriented thin sections, elongated and stretched quartz minerals within veins. Note

that blue arrows showing extension directions based on elongation axes of quartz minerals. 72
Figure 5.19. Chip samples showing various types of silicified breccia (A) vein containing silicified angular vein breccia with high clast/matrix ratio, (B) vein with low clast/matrix ratio, and (C) oxidized vein array with milled clasts formed under tectonic contribution. Note the direction of North is marked on the samples.....73
Figure 5.20. Photomicrograph illustrating (A) vuggy-quartz from silica core, (B) and (C) hydrothermal-breccia veinlets, (D) oxidized vein with milled breccia clasts, (E), (F) quartz veinlets exampling NE-SW and N-S extension. Note that red arrows pointing direction of extension. 74
Figure 5.21. (A) Geological map with alterations (after Aluç et al. 2023) and observation points where vein orientations are measured at the field, and (B) predominant strike orientation of the porphyry Cu and epithermal Au-style alteration (yellow colored rose plots for the measurement on porphyry Cu-style and red for the epithermal Au-style veins) 75
Figure 5.22. Field photos showing (A) stockwork veins within the epithermal Au exposure, (B), (C) and (D) quartz-sulfide (B-veins) 76
Figure 5.23. Photo showing the, (A) veins breccias from the epithermal Au system and (B) close up view of A. 77
Figure 5.24. (A) Geological map of Kirazlı District and map distribution of Au grades, (B) A-B-C-D composite cross-section and vertical distribution of Au grades, (C) E-F cross-section and vertical distribution of Au grades, (D) and (E) close-up views of distribution of Au grades from cross-sections in B and C, (F) alteration types and Au grade in porphyry styale mineralization.....79
Figure 6.1. Regional and district scale temporal relations between tectonic, magmatic and hydrothermal events. (Regional Magmatic stages = Altunkaynak and Genç, 2008; Kuşcu et al, 2019; Regional Hydrothermal stages = Brunetti, 2016; Leroux, 2016; Kuşcu et al, 2019; Regional Tectonic history = Brun and Sokoutis, 2007; Brun and Faccenna, 2008; Agostini et al, 2010; Jolivet and Brun, 2010; Sanchez et al, 2016; Kuşcu et al. 2019;

Schaarschmidt et al.2021; Gülyüz et al., 2024; District scale magmatic and hydrothermal chronology = Aluc et al.,2023) 89

1. INTRODUCTION

1.1. Scope and Purpose

Migration and circulation of hydrothermal solutions is recognized as precondition for hydrothermal ore formation (Connolly and Cosgrove,1999). The fractures play a significant role in the hydrothermal systems as they provide both channel ways for the fluid migration-circulation and also pre-existing open spaces for mineral precipitation from fluids (Sibson, 1987; Sibson et al., 1988; Robert et al., 1995; Micklethwaite and Cox, 2004). Since hydrothermal fluid flow and precipitation take place along structural permeability zones, geometries of ore bodies governed by general trends of regional and district scale structural zones resulted by specific geodynamic events and tectonic environments. As can be understood from previous statements, regional tectonics and related local stress conditions decide the emplacement geometry of hydrothermal ore deposits by governing the formations of permeable pre- or syn-mineral fracture systems during convergent or divergent geodynamic events.

Porphyry-Cu style hydrothermal system mainly form either in subduction related magmatic-arc/back-arc or post-collisional extensional environments that were experienced regional stress regimes resulted by contractional to moderately extensional tectonics resuted by syn-collision and post-collison events (Tosdal and Richards, 2001; Hou et al., 2003; Cooke et al.,2005; Hou and Cook 2009; Richards, 2009; Sillitoe, 2010). Besides the arc settings, minor porphyry mineralizations may also form related to intracontinental settings (Richards, 2009; Hou et al., 2011). Within subduction-related environments, porphyry-Cu and porphyry-Cu related epithermal-Au-Ag systems, spatially and genetically associated with intermediate to felsic, calc-alkaline and high-K calc-alkaline intrusions and volcanism (Cooke and Simmons, 2000; Richards, 2004; Seedorf et al.,2005; Richards et al., 2009;).

The epithermal deposits occur in close association with volcanism and fractures related to various extensional tectonic regimes including intra-arc, back-arc and post-

collisional rift settings, in shallow crustal levels (Arribas, 1995, Simmons et al., 2005; Taylor, 2007, Rhys et al., 2020). They are generated by the circulation of acidic to neutral, low to moderate temperature fluids throughout the brittle fault and fracture meshes (Sillitoe and Hedenquist, 2003; Cox, 2005; Simmons et al., 2005; Micklethwaite et al., 2010; Rhys et al., 2020).

Kirazlı (Çanakkale) deposit includes both Porphyry Au-Cu (PCD) and a High Sulfidation (HS) epithermal Au-Ag deposits with breccia to vein ore bodies hosted by altered volcanic rocks. The ore body geometries are controlled by structures formed during Cenozoic regional tectonic regime. The available data on the porphyry-Cu and porphyry-Cu-related epithermal deposits within the Biga Peninsula culminated data on the mineralization and alteration types, vein distributions and textural specifications and genetical aspects and timing of several porphyry-Cu and porphyry-Cu-related hydrothermal mineralization. Besides, the structural evolution of the Biga province along with regional tectonics and stress directions on fracture types are widely documented (Okay and Satır, 2000a; Beccaletto et al., 2007; Kaymakcı et al., 2007; Brun and Faccena, 2009; Şengün et al., 2011; Yiğit, 2012; Sözbilir et al., 2016; Sanchez et al., 2016; Gürer et al., 2021). However, the data on spatio-temporal association between the structural features and PCD and epithermal Au-Ag mineralization have been partly investigated. Apart from several works on the association between regional tectonics and mineralization in Biga province (Brunetti, 2016; Gülyüz et al., 2016,2024; Leroux, 2016; Sanchez et al., 2016) , the district to deposit-scale association between the vein geometry and fracture pattern and their temporal association have not been fully provided. This requires deposit to district-scale studies on (1) understanding of the ore-vein textures and preferred ore geometries, (2) the correlation between fracture pattern and ore geometries with respect to regional tectonics, types and mechanisms of the faults and (3) temporal-spatial relations between fractures and veins. Such database would be of great help for a better understanding of hydrothermal evolution and favourable sites for mineralization that collectively direct the exploration efforts in mineralization targets. Furthermore, the information on the kinematic history of the structures, the timing of mineralization relative to displacement, and whether regional shear zones were active at the time of mineralization are also poorly known. Establishing the structural timing

relative to mineralization would provide an effective tool in the exploration efforts for the Kirazlı district.

This study focuses mainly on examining the geometric and spatial relationship between mineralization and structures and establishing the relative timing of mineralization as pre-, syn-, or post-deformational with respect to structures that host or are associated with the mineralization. Therefore, this study aims to (1) map the faults in conjunction with the regional tectonic regime that formed the regional and district scale faults, (2) determine the kinematics of the faults, (3) understand temporal and spatial relationship between mineralization and district scale structural architecture and the textural and/or mineralogical evidence, and (4) structural evolution of the Kirazlı (Çanakkale) porphyry and high-sulfidation epithermal gold deposit.

1.2. Geographic Setting

The field works in this thesis include; (1) district-scale works at the Kirazlı district, and (2) regional-scale works in a larger, approximately 2300 km² area surrounding the Kirazlı district and covering the central Biga Peninsula (Figure 1.1A-B). The regional-scale works cover an area between Çanakkale city center and Çan (Çanakkale) town center to north , and Kazdağ mountain to the south (Figure1.1B). The Kirazlı district is located in the north western sector and closer to center of regional-scale area between coordinates of (UTM-WGS84 Zone 35N) 4431450-4426970 North and 473460-478910 East. Several porphyry-Cu and porphyry-Cu-related epithermal deposits including the Kirazlı prospect are present within the Kirazlı district (Figure 1.1C). The closest deposits to the Kirazlı project are (1) porphyry-Cu deposits including, Halilağa, Aladağ (Kuşçayır), Palamutoba, Tongurlu and Kocayayla, (2) HS-epithermal deposits including, Dededağ, Bodurlar, Sarpdağ, Kartaldağ, TV Tower, Kuşçayır, Karıncalı, Pirentepe, Çaltıkara, Hamamtepe, Seyrattepe, Halilağa-North, Dedeler, Doğancılar, Alanköy and (3) LS-epithermal deposits including Akbaba and Madendağ (Figure 1.1B).

The Kirazlı project includes five sectors or ore zones from to south as Kirazlı-Main at the north, Çatalkaya at the center, Kale Zones at the south, Rockpile at the west and İri Zone at the east (Figure 1.1C).

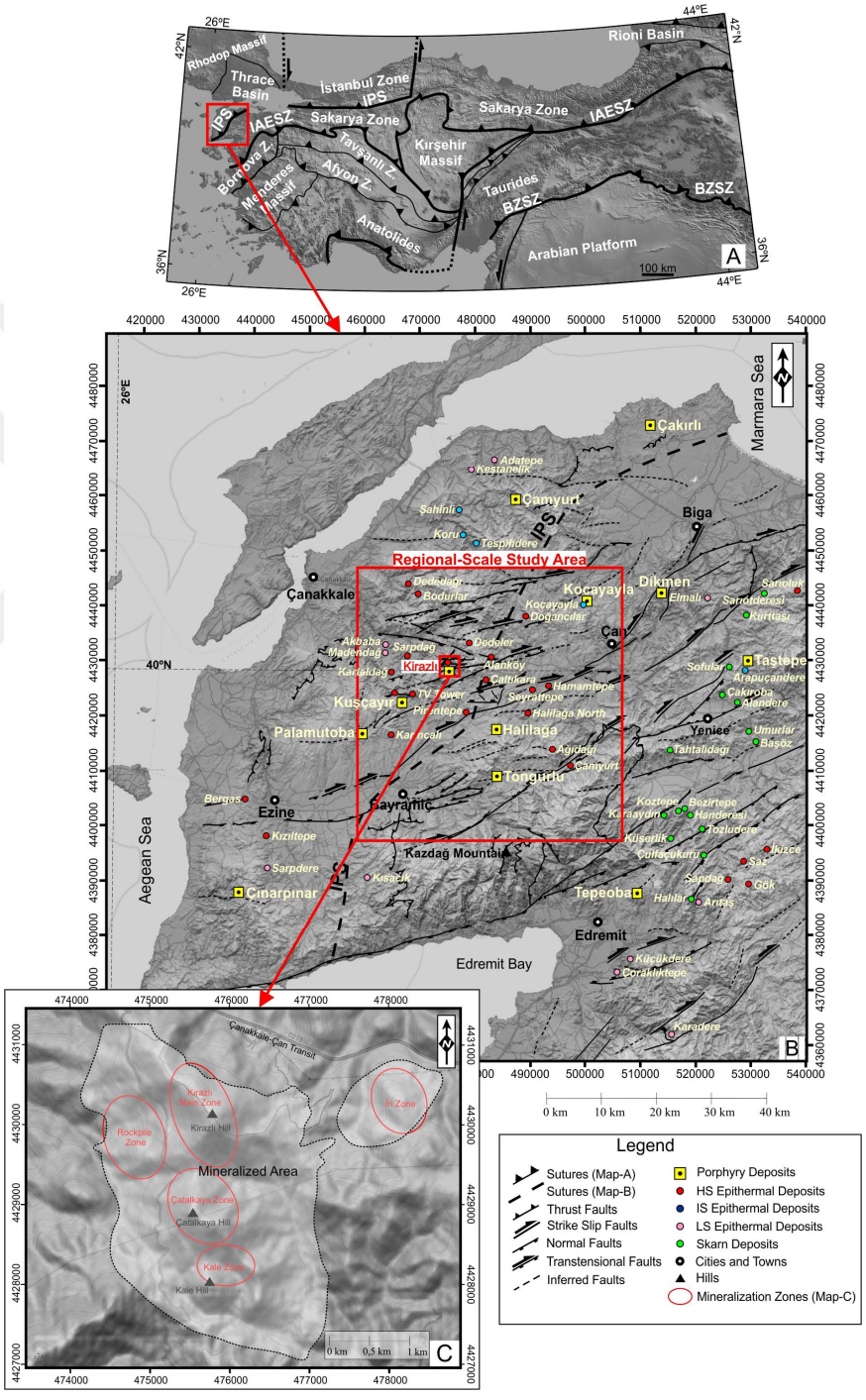

Figure 1.1. (A) Major Tectonic units of Türkiye (blue square encirling the Biga Peninsula), (B) Biga Peninsula (big and small red reticles respectively marking the regional and district-scale areas), (C) Kirazlı District and mineralized sectors/ore zones. (IAESZ: İzmir-Ankara-Erzincan Suture Zone, IPS: Intra-Pontide Suture, BZSZ: Bitlis-Zagros Suture Zone)

1.3. Previous Studies

The previous studies that summarize the current understanding of the work done in the scope of this thesis, are classified into three groups as (1) the fundamental works culminated in the literature on the temporal-spatial association between mineralization and structures, and those (2) on regional tectonic and tectono-magmatic evolution of the Biga Peninsula and (3) on porphyry-Cu and epithermal Au-Ag deposits in terms of tectono-magmatic evolution of the Biga Peninsula. The main points in these are summarized below.

1.3.1. Fundamentals on spatio-temporal association between mineralization and structures

Temporal and spatial association between the porphyry-Cu and epithermal au-Ag deposits and structures have largely been well documented. It is commonly stated that porphyry-Cu deposits are generally generated at the convergent or collisional plate margins and subsequent tectonic transition during post-collisional period from contraction to extension (Tosdal and Richards, 2001; Richards, 2003; Cooke et al., 2005; Sillitoe, 2010).

Epithermal Au-Ag deposits are hosted by volcanic-subvolcanic rocks formed in close genetic association with faults/fractures developed under extensional and/or strike-slip tectonics mostly in post-collisional back-arc settings (Reid, 1975; Oliver, 1986; Sibson, 1987; Connoly and Cossgrove, 1999; Sillitoe and Hedenquist, 2003; Cox, 2005; Simmons et al. 2005; Mickeltwaithe, 2010)

Reid (1975) explained that occurrence of openings favourable to ore deposition depends on fault deflection by refraction and favourable fault movement direction and net-slip direction may be interpreted from extension joint orientation or by other means, and predictions can be made as to the location and orientation of ore shoots.

Oliver (1986) suggested that fluid migration in a tectonically active region occur dominantly in response to a physical rather than chemical and thermal driving mechanism, since the mean stress is the most important physical parameter affecting the fluid pressure in pore-spaces and fractures.

Sibson (1987) explained that brittle fault-fracture systems and related zones of brecciation which best developed in extensional and/or strike-slip settings, work as channels for hydrothermal fluid flow and sites for ore deposition. He specified that epithermal Au mineralization is commonly localized in dilatational jogs related fault-fracture systems developed in the brittle carapace of regions undergoing magmatic and related geothermal activity.

Connoly and Cossgrove (1999) argued that stress distribution around a fault system controls fluid movement and formation of secondary fractures at the same time. They described that in a stable system, it is possible to evaluate hydrothermal fluid movements by using fault geometry and stress values obtained from secondary structures together instead of only using mean stress data alone. Therefore, they concluded that determining the development of a normal fault and fracture systems and effects on epithermal systems in an extensional regime, plays a key role during exploration phase.

Tosdal and Richards (2001), stated that porphyry Cu deposits are resulted by the dynamic inter-play occurred between tectonic, magmatic and hydrothermal processes within the convergent margins. Magmas generated at subduction zones rise into the upper crust, commonly along high permeability zones of breccias or fractures. Geometries and spatio-temporal distributions of these fractures and resultant veins in porphyry-Cu system differs vertically; concentric and radial arrays are more common above or in the upper parts of the stocks, whereas linear arrays dominate at depth. Formation of common orthogonal or conjugate fracture and resultant vein systems require repetitive differential stress changes and low horizontal differential stresses. Such specific stress conditions may occur in areas removed from active deformation, or during periods of stress relaxation and low strain in the magmatic arc.

Sillitoe and Hedenquist (2003) explained that most epithermal-Au deposits are associated with bimodal volcanic suites in a broad spectrum of extensional tectonic settings intra-, near- and back-arc, as well as post collisional rift environments.

Cooke et al. (2005), reviewed 25 giant porphyry deposits and described Cooke et al. (2005), reviewed 25 giant porphyry-Cu deposits and suggested that subsequent periods of compressional and extensional regimes are crucial for their formation. They

pointed out the compressional regime promotes necessary volatile saturation and large volumes within the magma chambers and prevents formation of apophyses possibly due to lack of extensional faulting, subsequent rapid uplift extension and erosion promotes transport of magmatic-hydrothermal fluids due to abrupt decompression.

Cox (2005), stated that deposit-scale localisation of fluid flow is strongly dependent on fluid-driven growth of fracture permeability in structurally controlled sites. He explained that permeability enhancement is associated particularly with jogs and other irregularities on faults, shear zones and fault intersections and fold-related dilatation sites. He concluded that understanding how fracture permeability may develop in different geologic situations can help to predict the location of fluid pathways and thus the location of potential ore zones.

Simmons et al. (2005), stated that epithermal Au ore bodies occur in diverse morphologies that reflect the influence of structural and lithological controls and they represents high permeability zones within the shallow parts. He suggested that the epithermal-Au ore bodies occur in vertical to subvertical veins that formed by dilatation and extension and these veins are mostly hosted by minor second and third order fractures with small displacement instead major faults.

Tosdal et al (2009), documented that porphyry-Cu deposits generally form near the end of magmatic episode when the arc is experiencing limited contraction as the result of changing deformational style. In contrast, the geological setting of epithermal-Au deposits is more variable, including volcanic dome fields, peripheral areas of volcanoes and rift zones.

Mickelwaithe (2010), explained that the structural analysis is applied to identify how deformation influenced the enhancement or decrease of permeability in rocks both spatially and over time. He stated that veins and faults in structurally controlled mineralized areas show typically schematic patterns in geometry and scale which are cumulative result of multiple slip events. He also specified that fluid flow particularly depends on changes of permeability in and around shear zones over time.

Sillitoe (2010), noted that porphyry Cu systems show a marked tendency to occur in linear, typically orogen-parallel belts along convergent plate boundaries and are generated mainly in magmatic arc - back-arc environments subjected to a spectrum of

regional-scale stress regimes, apparently ranging from moderately extensional through oblique slip to contractional. Among other factors, trench advance or rollback and the degree of obliquity of the plate convergence vector may effect stress regime.

1.3.2. Studies on regional tectonic and tectono-magmatic evolution of biga peninsula

1.3.2.1. Tectonic studies

The geological evolution of the Biga Peninsula has been the subject that of many works for a long time. These put constraints on the tectonic and tectono-magmatic evolution of the Biga Peninsula in close relation to the evolution of the Tethyan realm.

Okay et al. (1991), described four NE-SW trending zones within the Biga Peninsula as Gelibolu, Ezine, Ayvacık-Karabiga and Sakarya Zones juxtaposed during late Palaeocene to early Eocene. According to Okay et al (1990), Sakarya zone forming the eastern sector of Biga Peninsula consists of four tectono-stratigraphic units inluding Nilufer, Hodul Orhanlar and Çal units defined in the Karakaya Complex. Apart from the Karakaya complex, the Biga Peninsula also contains several fragments with more Rhodopean affinities including Ezine zone, ophiolitic rocks, melange (Çetmi melange and Denizgören ophiolite) and metamorphic rocks (Çamlıca and Kemer metamorphics). The Karakaya Complex is separated from rest of the units in the western part of Biga Peninsula by IPS formed by a north subducting passive-active continental collision during the closure of Karakaya marginal Basin (1991).

Okay and Mostler (1994), suggested that the Karakaya Complex exemplifies an accreted active margin and consists of Permo-Triassic oceanic units.

Pickett and Robertson (1996), concluded that the Karakaya Complex is a PaleoTethyan accretionary complex, rifted off from the North Gondwanan margin and drifted northwards towards Eurasia. According to them, genesis of rock units are related to both northward and southward subductions.

Okay and Satır (2000a), conducted geochemical and radiometric studies to determine metamorphism stages of Kazdağ core complex, an exhumed metamorphic package in

the Karakaya complex. They concluded that the Kazdağ range is an extensional metamorphic core complex exhumed at 24 Ma along a ductile shear zone.

Okay and Satır (2000b), according to petrographic and geochronologic works on the the Çamlıca-Kemer Metamorphics outcroping western part of Biga Peninsula, and they suggested that they differ from Sakarya Zone and exhibits features suggesting to a Rhodopean origin in terms of lithology, tectonic settings and mineralogical assemblage.

Beccaletto and Jenny (2004), suggested that the Ezine Group and overlying Denizgören ophiolites at western part of Biga Peninsula, were originated from Rhodopean domain instead of being a part of Sakarya Zone and juxtaposed with the Sakarya Zone after early Cretaceous.

Beccaletto et al. (2005), inspected and examined the biostratigraphic properties of NE-SW trending Çetmi Ophiolitic Melange between Kazdağ core complex and Çamlıca-Kemer metamorphics. They compared the Çetmi melange with the previously known ophiolites of IPS and IAESZ, and concluded that the Çetmi melange shares common origin with the Rhodopean realm compared to IPS and IAESZ.

Beccaletto et al (2007), examined the methamorphism conditions and kinematic properties of Çamlıca-Kemer Metamorphics and concluded that, Çamlıca-Kemer metamorphics show a continuous ductile to ductile–brittle extensional shearing, due to a NE–SW-oriented extensional regime between syn- and post-orogenic extension in the Aegean region.

Kaymakcı et al. (2007), inspected the Neogene-Quaternary tectonic evolution of northern Thrace Basin and Biga Peninsula and role of block rotatins linked to kinematic history of the region by examining palemagnetism and 40Ar–39Ar geochronology of alkaline basaltic lava flows exposed along localized shear zones. They concluded that, based on geochronological data basaltic rocks of Thrace basin and Biga Peninsula formed synchronously and paleomagnetic results indicate 73° and 33° clockwise rotations respectively for Thrace basin and Biga Peninsula, resulted by a dextral strike-slip deformation. They also stated that ENE-WSW trending active faults zones (Ganos, Etili, Yenice and Edremit fault zones) are formed prior to and reactivated by North Anatolian Fault Zone during Pliocene times.

Brun and Faccenna (2008), specified that the exhumation of high-pressure metamorphism in the Aegean region is associated in time and space with the slab-rollback and trench retreat.

Cavazza et al. (2009), documented apatite-fission track data, structural and stratigraphical analyses and indicated that the Kazdağ core complex was exhumed during late Oligocene to middle Miocene . They also suggested two-stage structural evolution model for the complex;the first stage comprising late Oligocene - early Miocene low-angle detachment faulting and the second stage dominated by Plio-Quaternary strike-slip faulting related to the westward propagation of the North Anatolian fault system.

Ring et al (2010), explained that the Cenozoic geodynamic evolution of the Aegean region including Rhodope-Sakarya zones at the northernmost part are related to subduction, accretion, arc magmatism, exhumation, normal faulting, and large-scale continental extension from ∼60 Ma until the Recent. They concluded that exhumation of metamorphic core complexes took place At 23–19 Ma due to large-scale lithospheric extension related to slab-retreat and -rollback.

Jolivet and Brun (2010), examined the Cenozoic geodynamic evolution of Aegean domain showed that slab-rollback and southward migration of single slab and backarc extension processess controlled the geodynamic evolution of Aegean domain.

Şengün et al. (2011), according to petrographic and structural results, concluded that Çamlıca metamorphics, in contrast to previous works did not undergo high-pressure metamorphism related to subduction-accretion. It is stated that, Çamlıca metamorphics experienced single-stage greenschists facies metamorphism and juxtaposed with HP rocks by “ductile-semi brittle” dextral strike-slip faults formed under effect of NE-SW extension and NW-SE compression. The age of dextral deformation concluded as late Cretaceous – early Eocene.

Sözbilir et al. (2016), describes three discrete deformation phases based on stratigraphic, structural and kinematic analyses along southern margin of Kazdağ Core Complex during Mio-Pliocene as, (1) pure N-S extension related detachment faulting, (2) strike-slip deformation related to progression of southern section of NAFZ and (3) high-angle normal faulting realted to NNE-SSW extension of Edremit Fault Zone.

Gürer et al. (2021), examined types, formation times and kinematics of young fault systems within the western Biga Peninsula. It is concluded that, there where three distinct tectonic phases as (1) Mio-pliocene NW-SE extension, (2) late Pleistocene NNE-SSW compression and (3) late Pleistocene – Holocene NE-SW extension. It is also stated that the extension of western Anatolia was active during Miocene-Pliocene times, since late Pliocene - Holocene times NAFZ effected the tectonomorphology of Biga Peninsula and surrounding region.

Koçyiğit (2023), describes the pull-apart basins including Sarıköy, İnova, Kazabat, Çan and Ezine-Bayramiç basins. It is concluded that both Sarıköy-Inova and Çan-Bayramiç-Ezine fault zones are recently active fault zones formed respectively on the pre-Miocene and lower-middle Miocene graben associated basins. Also Çan and Bayramiç-Ezine depressional basins include faults that formed during Miocene extension and reactivated by recent dextral strike-slip tectonism.

1.3.2.2. Tectono-magmatic studies

Delaloye and Bingöl (2000), suggested that the granitoids in the Biga Peninsula are clustered in six isochronological belts as older Granitoids (Cambrian), late Cretaceous, early Palaeocene, late Eocene, late Oligocene, Oligo-Miocene, Miocene and late-Miocene based on the petrographical, geochemical and geochronological studies. They also indicated that they become younger from north to south.. They specified that the granitoids formed in a post-collisional environment and their geochemical features are more consistent with a subduction-related origin related to N-dipping subduction of Neotethys.

Yılmaz and Karacık (2001), distinguishes two magmatic episodes related to Tethyan northward subduction as, late Cretaceous to Eocene post/syn collisional episode and late Miocene-Pliocene N-S directed back-arc extensional episode. They stated that the geochemistry of Oligo-Miocene magmatic rocks in Biga Peninsula, closely resemble to arc-derived magmas.

Dilek and Altunkaynak (2007), summarized the geochemical signatures of the Cenozoic post-collisional magmatism in western Anatolia. They deduced concluded that magmatism in western Anatolia occurred in discrete pulses and propagated from north to south after early to middle Eocene period. They proposed that the magmatic

rocks exhibit a shift from subduction enriched mantle in a collisional environment to post-collisional extension from north to south and Eocene to late Miocene, and these are ascribed to slab-breakoff followed by regional scale lithospheric extension.

Altunkaynak (2007), conducted geochemical and geochronological studies on two granitoid belts to south of Marmara (northern Biga Peninsula)within northwestern Anatolia. They specified that the geochemical characteristics of both granitoid belts indicate a metasomatized litospheric mantle source for middle to late Eocene granitoids in NW Anatolia, and that they were formed in a post-collisional setting after the collision of the Anatolide-Tauride platform with the Sakarya continent along the IAESZ. It is concluded that such geochemical and petrogenetic features can be best explained with a slab-breakoff model that is compatible with the geodynamic evolution of the region.

Karacık et al. (2008), described two granitoid belts within Biga Peninsula as Eocene and Miocene belts located respectively to north and south. They adopted slab-breakoff model in a subduction and post-collision environment to explain geochemical signature of both belts.

Altunkaynak and Genç (2008), described five discrete magmatic episodes from early Eocene to Pliocene younging from north to south within Biga Peninsula.Researchers reported that composition of magmatic rocksdisplay shift from decreasing subduction signature to increasing crustal component between early Eocene to middle Miocene, and followed by a decreasing crustal component. They suggested that all these features indicate a magmatism formed during syn- and post- collisional tectonic environment followed by crustal-extension.

Altunkaynak et al (2012), examined the geochemistry and petrography of several plutons within the western Anatolia. They concluded that western Anatolian granitoids exhibit an increasing crustal signature from 24 to 18 Ma coinciding with crustal exhumation (Kazdag and Menderes core complexes) and extension in western Anatolia. The widespread early to middle Cenozoic magmatism was resulted from thermal weakening and a significant syn-convergent extension, exhumation and thinning during Tethyan orogen in western Anatolia.

Ersoy et al. (2017), based on geochemical analysis from two domain namely BOVR (Biga orogenic volcanic rocks) and SOVR (Sakarya orogenic volcanic rocks), states

that, volcanic rocks of Biga Peninsula and Central Sakarya (with medim-K calc-alkaline to ultra-K characteristic) emplaced at 43-15 Ma and 53-38 Ma respectively. It is suggested, magma generation processes within Biga Peninsula related to "subduction rollback processes and associated with post-collisional extension".

Aydın et al. (2019), based on resultant characteristics derived from geochemical analyses, stated that, granitoids in Biga Peninsula produced during Eocene (Dikmen, Kuşçayır, Güreci, Karabiga) and Oligo-Miocene (Alanköy, Çamyayla, Evciler, Eybek, Kestanbol, Yenice, Sarıoluk) and linked to post-collisional magmatism subsequent to closure of northern branch of Neotethys between Sakarya and Anatolide-Toride platforms. They also concluded that, granitoid in the Biga Peninsula, derived from a mantle source signifying subduction zone.

Erenoğlu et al., (2020), describes six Eocene-Oligocene magmatic units including Laledağ granodiorite and Beyçayır, Kızıldam, Dededağ, Kırcalar, Harmancık volcanics in terms of lithostratigraphy and chronostratigraphy. Results of geochronology studies from volcano-plutonic units of northern Biga Peninsula indicate an active magmatism from middle Eocene to late Miocene. They also concluded that, two different source characteristics including Eocene calc-alkaline (medium-high-K) and Oligocene alkaline (high K and shoshonitic) sources related respectively subduction and breakup of a subducting plate.

Aslan et al. (2020), examined two early Miocene plutons within eastern Biga Peninsula namely Göloba and Şaroluk based on their geochemical and petrographical characteristics and they stated that Neogene magmatism occurred in Biga Peninsula has I-type, high-K calc-alkaline characteristics indicating post-collisional environment.

Schaarschmidt et al. (2021), compiled the age of volcanic centers ranging in age from 33 Ma along two NNE-SSW trending traverse including northwestern Anatolia and Greece from northern Aegean towards south to Hellenic trench. They concluded that the age progressive profiles reveal continuous southward arc-normal migration caused by slab rollback since 32 Ma.

1.3.3. Studies on porphyry and epithermal deposits in terms of tectono-magmatic evolution of the biga peninsula

In Biga Peninsula, numerous porphyry-Cu and epithermal Au deposits close to study area were investigated. These studies mostly focused on alteration types and paragenesis, textures, temperature, salinity and sources of fluid and metals in these deposits. They concluded that (1) these deposits were developed in volcano-plutonic settings and (2) vein orientations are conformable to predominant fault orientations. Most studies present evidence or data on how the veins and faults correlate and why hydrothermal solutions favoured or channelized along some faults in the region, are not clearly documented. Only few studies addressed how stress directions played a role on mineralization and vein formation. These studies briefly are summarized below.

Yiğit (2012), conducted geochronological studies on twelve significant Au-bearing deposits within Biga Peninsula. He presented wide-range regional data on lithology, stratigraphy, structural, tectono-magmatic features of several occurrences in the Biga Peninsula. Yiğit (2012) concluded that the timing of significant gold mineralization within Biga Peninsula is between 38 and 22 Ma and this also corresponds to rollback of the Aegean subduction.

Brunetti (2016), examined the magmatic-hydrothermal evolution of the Halilağa porphyry-Cu deposit located in a close proximity to northern flank of Kazdağ range. She mapped deposit-scale structures and presented a structural-hydrothermal evolution model for Halilağa porphyr type mineralization related to regional tectono-magmatic evolution. .According to this model, two magmatic pulses described in Halilağa district as middle Eocene (39-37 Ma) and late Oligocene (28-26 Ma) related to Kestane porphyry (39 Ma) and Pirentepe epithermal (28 Ma) respectively. Brunetti states that NW-SE striking extensional faults formed under NE-SW extension pre-dates the subsequent faulting events and mineralizations. Formation of Kestane porphyry deposit is linked to middle Eocene NNW-SSE extension and resultant ENE-WSW and E-W striking syn-mineral normal faults. Subsequent NW-SE extension and resultant NE-SW striking extensional faulting was effective during the formation of Pirentepe epithermal deposit. Pliocene dextral tectonic regime forms the post-mineral faulting event and controls the latest geometry of mineralizations.

Leroux (2016), studied the stratigraphic and petrographic characteristics of Kirazlı and Tv Tower epithermal Au systems located to west of Kirazlı district. He obtained comprehensive database on the type and geochemistry of the hydrothermal alterations, stratigraphy and alteration features of the host volcanic sequences, and correlated the host rock geometries with the structural zones and regional tectonics.

Sanchez et al (2016), examined the crustal extension and its relationship to porphyry-Cu and epithermal au-Ag type systems within the Biga Peninsula in terms of geochemistry, geochronology, stratigraphy and structural geology. He visited numerous well-known plutons, volcanic associations and mineralization sites to determine regional scale association between tectono-magmatic and hydrothermal evolution of northwestern Anatolia. As a result, they described six tectono-magmatic phases within the Biga Peninsula during its Cenozoic evolution as (1) early Eocene (~65–49 Ma), (2) middle-late Eocene (~49–35 Ma), (3) late Eocene-Oligocene (~35–23 Ma), (4) latest Oligocene - early Miocene (~23–17 Ma), (5) middle Miocene (~17-14 Ma) and (6) late Miocene (~14-5 Ma). According to Sanchez et al. (2016). Porphyry-Cu-Au (Mo) deposits specific to two time periods; late Eocene (phase 2) and late Oligocene (phase 3) in spatio-temporal relation with core-complex formation within Biga Peninsula.

Gülyüz et al. (2018), determined the structural controls on mineralization in Kestanelik low sulfidation epithermal Au deposit. They explained the kinematic characteristics of vein hosting faults, vein geometries and their spatial distribution. They also differentiated hydrothermal phases with respect to their crosscutting relations and textural features. They concluded that dilatational veins tend to host fluid flow events and earthquake rupturing and fluid-assisted hydrothemal brecciation are two major mechanisms controlling the permeability during epithermal gold mineralization.

Kuşcu et al. (2019), documented the special association between porphyry-Cu deposits and associated magmatic rocks of Pontides, western Anatolia, central Anatolia and southeastern Anatolia in terms of geochemistry, geochronology, structural geology, both in country and regional scale. They stated that, four major metallogenic episodes are recognized within the western Anatolia, early-middle Eocene, middle Eocene, Oligocene and middle-late Miocene. They also pointed out that the porphyry Cu systems form regional belts that mimic the a spatial and temporal shift from esrly

Eocene to middle Miocene from north to south. The porphyry Cu, skarn and epithermal Au-Ag systems in the Biga province are integral segment of the Aegean subduction accompanied by southward younging extension since the middle Eocene.

Aluc et al. (2023), examined geochemical, petrographic, and geochronologic properties of porphyry-Cu and HS-epithermal Au-Ag mineralizations of Kirazlı district and mineralization hosting Cenozoic magmatic rocks. Aluc et al. concluded that, magmatic rocks of Kirazlı district include two magmatic episodes with the ages of; (1) Eocene intrusive rocks (41,2-40,5 Ma) and plagioclase-phyric andesite lava flow (38,4-37,9 Ma) and (2) Oligocene basaltic andesite lava flow (32,7-31,9 Ma) and volcanoclastic rocks (32,4 Ma). Porphyry-cu mineralization related to Eocene intrusive rocks and yields two episodes at 36,7 Ma and 33,7 Ma while the Hs-epithermal-Au-Ag mineralization related to Oligocene volcanism and yields 32 Ma (Yiğit, 2012). They also concluded that spatially associated porphyry-Cu and HS-epithermal mineralizations of Kirazlı district are genetically unrelated and they have formed during post-collisional tectonism based on geochemical signatures of host rocks.

Gülyüz et al. (2024), applied a new approach based on low-T thermochronology method to determine rate of tilting event linked to extensional tectonic in Halilağa porphyry Cu-Au deposit. Based on paleo-geothermal gradient it is calculated that the 64° tilting occurred towards 207°N as the earliest response to backarc extension in Western Anatolia approximately between ~24-18 Ma at north. Following tectonically stable period since ~18 Ma lasted until initiaton of NAF in northwestern Anatolia around 2-1,5 Ma.

1.4. Methodology

The works consist of “field works” and “desk and laboratory” studies for data and sample collection on field and data-sample processing stages. Field works simply include mapping of rock units exposed within the regional and deposit scale study area, structures, and veins, collecting attitude and slip vector data from faults and veins, and collecting oriented samples for microstructural and petrographical analysis. Desk and laboratory studies include (1) structural data evaluation, data correction for slip

measurements and illustrating the structural data (2) sample preparation for analysis on oriented samples, and (3) petrographical examination of thin sections from the oriented samples.

1.4.1. Field works

Field works include; (1) mapping of rock units, structural elements and veins for a better understanding of regional and district-scale geometry of faults and veins, (2) attitude and slip data collection on the fault planes and veins in the ore zones and (3) oriented-sampling. The lithology and alteration maps were provided by Doğu Biga Madencilik which is descendant of Alamos Gold Inc. Provided data were used and revised where necessary on field by tracing lithological borders and veins by tablet PC (IOS-operated) with built-in GPS and GISPro software. During mapping, the traces fault planes were mapped, and attitudes and slip vector data on fault planes and veins have been recorded as vector data on the tablet PC. Sampling campaign conducted along pre-determined lines those were traversing the main structural zones perpendicular/sub-perpendicular along mineralized zones. All data collected at the field were georeferenced by the tablet. Georeferencing was applied using UTM system (Universal Transverse Mercator) with ED50 datum. The direction and orientation of the traverses were designed so as to hit maximum number of veins with different directions along the same traverse. The data stored at the tablet, then, were ready to be transferred to any other computer applications commonly in common formats (kmz, shp or tab). The field studies also included the understanding of the stratigraphy of volcanic-volcanoclastic sequences and basement rocks.

Attitudes of the faults and veins and slip vector data have been recorded by both Brunton Compass and eGEO Compass application installed on the android mobile phone. The measurements include strike-dip values of observed veins-veinlets and faults also Aki-Rake slip sense data on faults. These measurements provided the main data necessary to understand the type and nature of the tectonic regime in the regional and district-scale, and for geometric correlations between predominant fault sets and veins.

The oriented sampling has been conducted on the vein-bearing localities. The oriented samples and microstructural analysis on these samples are crucial to understand the order or relative timing of hydrothermal phases, ore-vein textures, geometric relation between veins and microfractures. From southwest to northeast, 112 oriented samples have been collected within four mineralized zones including Kirazlı Main, Çatalkaya, Kale and İri zones. During sampling on field, exposed flat surface of each sample was chosen as reference surface and attitude values (Strike-Dip-Dip Direction) were marked on reference surface. By help of a sand pool, collected samples re-oriented based on recorded attiutdes on field and horizontal and N-S vertical planes marked (Figure 1.2A,B) on samples to be used for sawing process.

Figure 1.2. (A) Re-oriented sample in sand pool based on marked orientation of reference surfeace and (B) sample that vertical N-S and horizontal planes marked on.

1.4.2. Desk and laboratory studies

Desk studies include structural data correction, data evaluation and interpretation. The digitally georeferenced data is an important component of the desk studies. The laboratory studies include sample preparation for petrographical and micro-structural works and petrographical analysis. The slip-vector data collected from the fault planes have been recalculated and corrected to be used for further structural data interpretation. Slip data have been processed by Win Tensor software in order to find main pressure-tension axes and stress directions. According to collected data, stereoplots showing the principle stress directions, fault attitudes, P-T axes and slip

vectors were produced. Faults were grouped first according to their processed kinematic axes (P-T and principle stresses) predominant directions and predominant directions. Also strike/dip data for the veins have been transferred to the stereographic diagrams to find out the predominant trends and sets of veins. This has also helped to establish geometric relation between faults and veins in field scale

Drill-log data of Kirazlı prospect shared by project owner company Alamos Gold Inc. The provided drill-logs include, lithology and ore grade data. This data processed by Leapfrog Geo (Bentley-Seequent) software to establish spatial relations between structural zones, relatively high ore grades and vein phases.

The laboratory works consist of sawing of oriented samples collected during field works to chip-samples, thin-sectioning of oriented chip-samples and petrographical, and micro-structural analyses on the thin-sections. The spatial correlation between the vein orientation and fault orientation is not only based on two dimensional attitude data but also on distinguishing the phases and textures of each vein. Therefore, the oriented samples collected from the field have been thin-sectioned at the Geological Engineering Department at Dokuz Eylül University (İzmir, Türkiye). The oriented samples have been firstly sawed to chip-samples according to previously marked horizontal and vertical planes on the sample in laboratory of Geological Engineering Department of Muğla Sıtkı Koçman University (Muğla, Türkiye) (Figure 1.3). Produced chip-samples were prepared so long axis of thin section (parallel to vertical plane) is set to fit to north-south line marked on the samples. The thin sections, were then prepared using these oriented chip-samples, and were examined under trinocular polarizing (Leica DMP) microscope to measure the strike of veins and veinlets at each sample using the rotating stage with 360^{o} incremental reading, and all strike measurements were recorded in a table presenting the strike measurement. To compare predominant strike directions for different phases, veins and veinlets have been grouped with respect to their crosscutting relations and strike values from each phases have been reclassified to be used on rose diagrams.

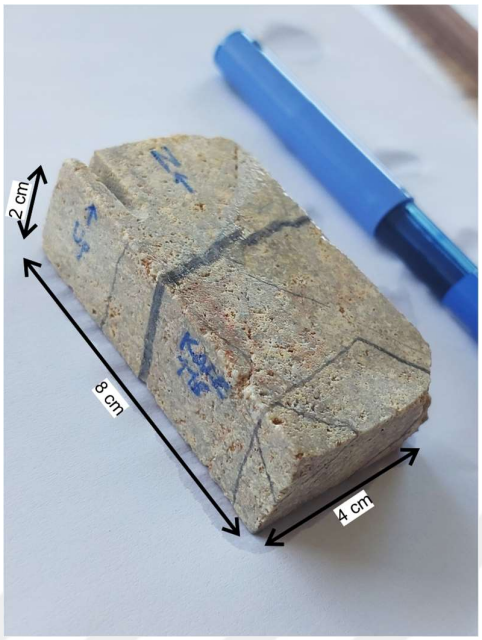

Figure 1.3. Prepared oriented chip sample. (N= North)

In order to model the tectonics, kinematics of the structures as a function of structural evolution (1) main stress and pressure-tension directions obtained from attitudes and slip vector data have been used, (2) predominant strike directions of different veins with silicification phases have been compared with main fault and vein orientations measured on field (3) ore grades from drill-logs and texture have been correlated with predominant deformation zones.

2. REGIONAL GEOLOGY

The Biga Peninsula is located northwestern part of Turkiye where pre-Cenozoic crystalline basement consisting of two main terranes, Sakarya and Rhodope zones and overlying Cenozoic magmatic rocks are exposed. (Figure 2.1A,B). The Rhodope zone is represented by Ezine Group, Çamlıca Metamorphics-Kemer micaschists, ophiolites. The Sakarya zone in this part of Turkiye is composed of Kazdağ core complex, Çetmi Melange and Karakaya Complex are situated in an active tectonic region characterized by back-arc extension related to the southward moving Hellenic subduction system (Bonev and Beccaletto, 2007).

2.1. Basement of Biga Peninsula

2.1.1. High-grade metamorphics

2.1.1.1. Kazdağ core complex

Kazdağ core complex forms the lowest crustal levels of Sakarya Zone within the Biga Peninsula (Duru et al.,2004). Kazdağ core complex occurs as NE trending, double plunging anticlinorium cropping out as a tectonic window under the Karakaya Complex (Okay, 1991;Duru etal.,2004; Yiğit, 2012). It covers a large area at the southwestern part of Biga Peninsula (Figure 2.1B). Kazdağ core complex consists mainly of intercalations of felsic gneiss, amphibolite, marble; meta-ophiolite at the middle and sillimanite-bearing paragneisse and migmatite at the top (Okay et al. 1991; Duru et al. 2004; Bonev and Beccaletto 2015). The metamorphic rocks in the Kazdağ Core Complex are subdivided from bottom to top as Fındıklı Formation (intercalation of amphibolite bearing gneiss and marble), Tozlu Formation (metaophiolite), Sarıkız Marble and Sutuven Formation (sillimanite bearing paragneiss and migmatite) (Duru et al.,2004). The metamorphism in the Kazdağ core complex includes early eclogite facies metamorphism (308 ± 16 Ma; Okay et al., 1996) middle Carboniferous (Hercynian-Variscan) and late amphibolite facies metamorphism in the Oligocene to early Miocene (Okay and Satır 2000; Duru et al., 2004; Cavazza et al., 2009). According to apatite fission-track ages, exhumation of Kazdağ core complex took

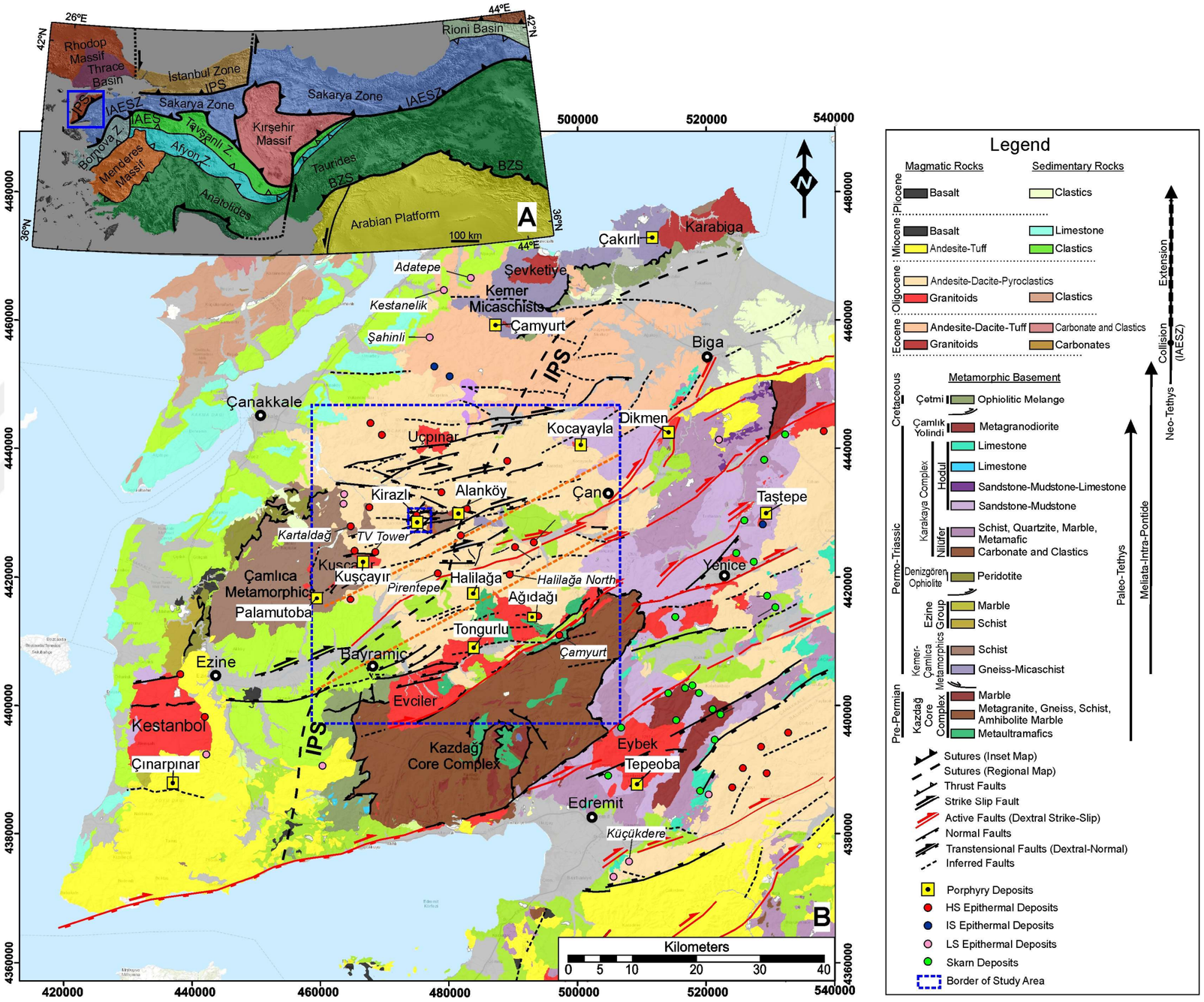

Figure 2.1. (A)Tectonic units of Turkiye and location of Biga Peninsula (blue square), (B) Geological map and locations of mineral occurrences of Biga peninsula. (Revised after Yiğit, 2012; Duru et al, 2014; Brunetti, 2016; Leroux, 2016; Sanchez et al, 2016). (IAESZ: İzmir-Ankara-Erzincan Suture Zone, IPS: Intra-Pontide Suture, BSZ: Bitlis Suture Zone)

place between 24 and 17 Ma (Bonev et al., 2009; Cavazza et al., 2009;Gülyüz et al., 2024). The metamorphic rocks have been juxtaposed to surrounding pre-Miocene units due to extensional tectonism in western Anatolia and exhumation of Kazdağ Core Complex during Oligo-Miocene.

2.1.1.2. Çamlıca metamorphics

Çamlıca metamorphics and Kemer micaschist are located in western and northern parts of Biga Peninsula (Figure 2.1B). Çamlıca metamorphics overlain by the Denizgören ophiolite forms the basement of Rhodope Zone in Biga Peninsula, and are mainly composed of quartz micaschists with intercalated calc-schists, phyllite, marble, amphibolite and quartzite (Okay et al.,1991; Sanchez et al., 2016). Çamlıca metamorphics has protolith ages of 582 ± 30 Ma and 559 ± 17 Ma (Ediacaran; Tunç et al., 2012) and underwent HP-LT metamorphism between the latest Cretaceous to earliest Paleogene they (Okay and Satır, 2000; Beccaletto, 2007). Fine-grained and banded foliations of Çamlıca metamorphics exhibit 20° to 50° dip to the west and NE-trending mineral lineations with top to NE kinematics (Sanchez et al., 2016).

2.1.2. Low-grade metamorphics

2.1.2.1. Karakaya complex

Karakaya Complex covers the eastern and southeastern parts of Biga Peninsula (Figure 2.1B). The complex tectonically overlies the rock unşts in the Kazdağ core complex, and consist of partly metamorphosed and moderately to strongly deformed, Permo-Triassic clastics, carbonates, and metaconglomerates restricted to Sakarya Zone (Bingöl et al., 1975; Okay,1989; Okay et al., 1991; Okay and Altiner, 2004). From bottom to top Karakaya complex consists of four tectono-stratigraphic units, Nilufer Unit, Hodul Unit, Orhanlar Greywacke and Çal Unit (Okay et al., 1991). The recent works subdivide the Karakaya Complex in to two tectono-stratigraphic units as termed as Upper (Hodul Unit, Orhanlar Graywacke and Çal Unit) and Lower (Nilufer Unit) Karakaya Complexes (Okay and Göncüoğlu, 2004; Federicci et al., 2010). Lower Karakaya Complex also known as Nilufer Unit is generally foliated, isoclinically folded, and consists of highly deformed and metamorphosed metabasite, phyllite and

marble, with minor amounts of metachert, metagabbro and serpentinite (Okay & Göncüoğlu 2004; Federicci et al., 2010). In Biga Peninsula, conodonts from marble interbedded with the metabasite give middle Triassic age (Kozur et al., 2000). Upper Karakaya Complex includes a thick quartzo-feldspathic sandstone-shale series (Hodul Unit) with a continental granitic source, a greywacke-shale sequence (Orhanlar Unit) and series of basalt, debris flows, and grain flows containing upper Permian limestone clasts (Çal Unit) (Okay et al., 1991; Pickett and Robertson, 1996; Okay and Göncüoğlu, 2004; Federicci et al.,2010). The Lower and Upper Karakaya Complex are juxtaposed to each other almost everywhere in the Sakarya Zone (Federicci et al., 2010) The Karakaya complex is described as a subduction and accretion complex formed in fore-arc basin of an active margin (Picket and Robertson, 1996). Okay et al. (1991) also suggested that the Karakaya Complex could be accepted as a rift basin opened on southward dipping Paleothetys subduction zone and reflects entire active margin tectono-stratigraphy including back-, intra-, fore-arc and accretionary units. Also, it is widely accepted that Karakaya Complex were formed by intra-oceanic subduction or, during subduction of oceanic seamounts (Pickett & Robertson, 2004) or an oceanic plateau (Okay 2000).

2.1.2.2. Ezine group

Ezine group (Karadağ Unit, Okay et al., 1991) outcrops on the western an eastern flanks of the Çamlıca Metamorphics and Kemer micaschist respectively (Beccaletto and Jenny, 2004; Sanchez et al., 2016) (Figure 2.1B). This group includes Geyikli, Karadağ and Çamköy formations (Beccaletto and Jenny, 2004) that consist of greenschists facies sedimentary sequence . From bottom to top Ezine Group includes gently folded silty-sand intercalated recrystallized limestones (Geyikli Formation), limestone-conglomeratic limestone intercalations (Karadağ Formation) and silty-sandy carbonate turbidites (Çamköy Formation). These formations were formed during syn-rift sedimentation of middle–late Permian to middle Triassic age, or most probably pre-rift transgressive sedimentation in the early–middle Permian, followed by syn-rift sedimentation in the early–middle Triassic (Beccaletto and Jenny, 2004).

2.1.3. Ophiolites

The ophiolites in the Biga Peninsula include two tectonostratigraphical rock units, Çetmi ophiolitic melange and Denizgören ophiolites. The meta-ophiolites within the Sakarya Zone (Upper Karakaya and Kazdağ Group) are not included in this classification. They are exposed west of Kazdağ core complex in the south and northwest of Ezine Group in the north Figure (2.1B).

2.1.3.1. Çetmi ophiolitic melange

The Çetmi ophiolitic mélange (Çetmi melange) is referred to as an accretion-related ophiolitic mélange (Okay et al. 1990; Beccaletto et al. 2005). The Çetmi melange tectonically overlie the Çamlıca metamorphics and is unconformably overlain by Palaeogene–Neogene sedimentary and volcanic rocks. It is the tectonically juxtapose with the high grade metamorphics of Kazdağ core complex through a detachment fault (Beccaletto et al., 2004;2005). Basically The Çamlıca metamorphics tectonically overlies the Çetmi mélange in the north of the Peninsula. (Okay et al., 1990; Beccaletto et al., 2005). It consists of deformed blocks of altered basaltic to andesitic and pyroclastic rocks, blocks of Upper Triassic neritic and pelagic limestones, detritic greywacke–shale matrix, tectonic lenses of sandstone–shale turbiditic sequences, slices of serpentinite/listvenite, exotic lenses of garnet–micaschists and eclogite, blocks of radiolarite and radiolarite–red mudstone alternations and, lower to middle Triassic limestones (Beccaletto et al., 2005). Beccaletto et al. (2005) indicated that thr Çetmi mélange does not have any direct correlation and common characteristics with the other melanges along İzmir-Ankara and İntra-Pontide sutures in western Anatolia. It is also suggested that the mélange may represent an isolated fragment of the Rhodope Zone and mélange forming processes stopped between the early Albian and the latest Albian-Cenomanian (Beccaletto et al., 2005).

2.1.3.2. Denizgören ophiolite

Denizgören ophiolite reflects a northeast trending belt and tectonically overlies the Permo-Triassic sedimentary rocks Ezine Group in the east (Becaletto and Jenny, 2004). The Denizgören ophiolite is almost totally made up of partially serpentinized

harzburgite (Okay et al. 1991). It is explained that characteristic rock types including gabbros, sheeted dykes, basalts, pelagic sediments in a typical ophiolitic suite are absent in the Denizgören ophiolite (Beccaletto et al., 2005). Amphibolites taken from the base of the Denizgoren ophiolite give Ar/Ar radiometric ages of 117 ± 1.5 Ma and 118.3 ± 3.1 Ma (Okay et al., 1996) and 125±2 Ma (Beccaletto and Jenny, 2004).

2.1.4. Magmatism and tectono-magmatic processes

Pre-Cenozoic period (Permian-late Cretaceous) involves subduction and closure of Paleotethys, opening of Neotethys and closure of Neotethys oceanic system. During late Cretaceous, magmatism developed in a contractional tectonic environment, and this regime resulted in crustal thickening (Schefer et al., 2010). This period gave rise to a porphyry-Cu and volcanogenic massive sulfide (VMS) belt in northeastern Turkiye (Yiğit, 2009). This has lasted until the latest Cretaceous - early Cenozoic time when Izmir-Ankara Ocean was totally consumed, and Anaolide-Tauride block (TAB) collided with the Sakarya zone forming the E-W running Izmir-Ankara-Erzincan Suture Zone (IAESZ). The late Cretaceous and early Palaeocene marks the period during which continental subduction and amalgamation of TAB and Sakarya zone took place. Since the convergence between the Afro-Arabian and Eurasina plates was still active, the convergence was accommodated by initiation of a new subduction event by the closure of the Ionian Sea, remaining Neotethys Ocecan during middle Eocene. In other words, the N-S convergence resulted in a subduction-jump to the west, and creation of an active margin between African and Eurasian plates (Rolland et al. 2012). This resulted in the generation of the Hellenic-Aegean subduction starting from middle Eocene (Figure 2.2). The Hellenic subduction transformed from northward advancing subduction front to southward retreating plate boundary that resulted in back-arc crustal thinning (Figure 2.2; Sanchez et al., 2016). During the Cenozoic extensional period gravitational collapse of thickened crust due to slab break-off and slab role-back of subducting plate took place (Bonev and Beccaletto, 2007; Ring et al., 2010). Northward stretching and thinning of the continental crust were resulted in basement shear zones in the lower crust and regional extensional fault systems in the upper brittle crust (Bonev et al., 2009; Cavazza et al., 2009). The first one resulted in the footwall exhumation of metamorphic core complexes, the second resulted in NW- and NE-trending half-graben basins (Şengör, 1987; Bozkurt and Sözbilir, 2004). In western

Anatolia, magmatic belts generated during this period were emplaced along sub-parallel arcs within footwall blocks of basin-border normal faults and hanging-wall basins in Eocene, Oligocene, early-middle Miocene and Holocene (Brun and Faccenna, 2008; Çiftçi and Bozkurt, 2009; Helvacı et al., 2009; Jolivet and Brun., 2010; Innocenti et al., 2010; Altunkaynak et al., 2012).

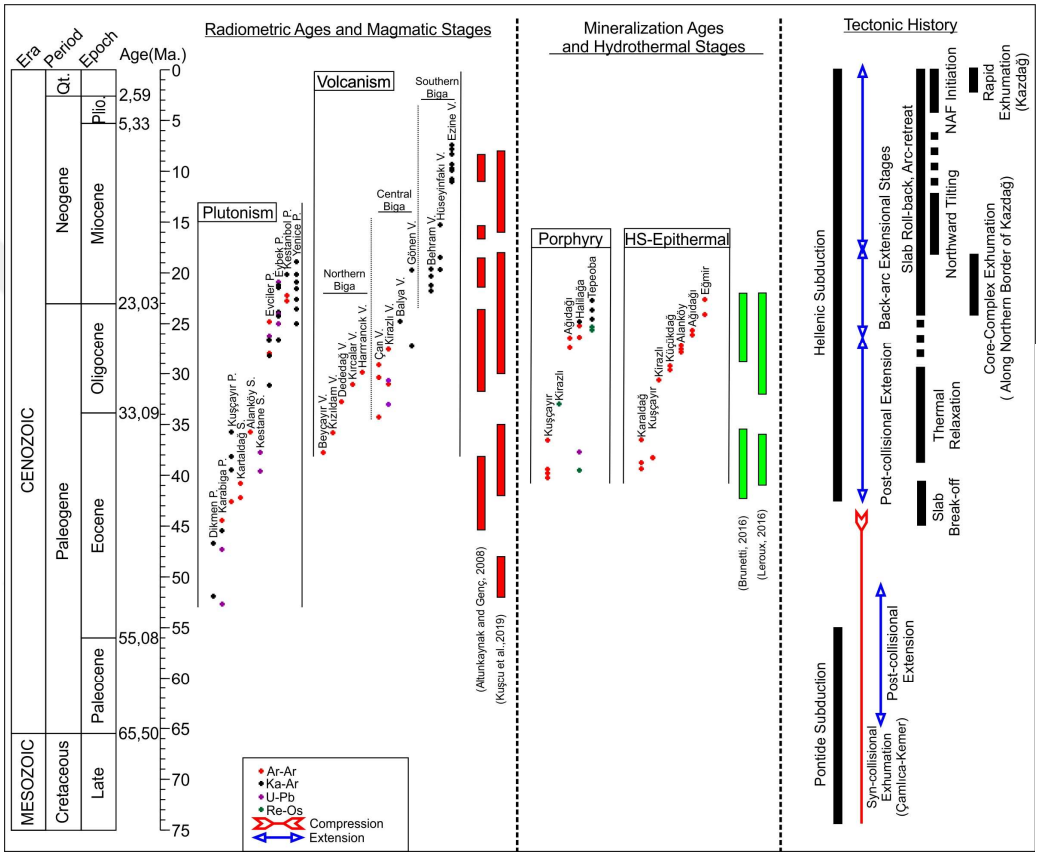

Figure 2.2. Compiled magmatic ages of plutonic and volcanic rocks, magmatic and tectonic stages of Biga Peninsula. (References for Plutonism= Delaloye and Bingöl, 2000; Beccaletto and Bonev, 2007; Altunkaynak and Genç, 2008; Karacık and Yılmaz, 2008; Kuşcu, 2009; Altunkaynak et al, 2012; Yiğit, 2012; Black et al, 2013; Brunetti, 2016; Kuşcu et al, 2019; Volcanism= Ercan et al, 1995; Aldanmaz et al, 2000; Altunkaynak and Genç, 2004; Kuşcu et al, 2019; Erenoğlu and Billor 2022; Magmatic stages = Altunkaynak and Genç, 2008; Kuşcu et al, 2019; Hydrothermal stages = Brunetti, 2016; Leroux, 2016; Kuşcu et al, 2019; Tectonic history = Brun and Sokoutis, 2007; Brun and Faccenna, 2008; Agostini et al, 2010; Jolivet and Brun, 2010; Sanchez et al, 2016; Kuşcu et al. 2019; Schaarschmidt et al.2021; Gülyüz et al., 2024)

Convergence between Eurasia and African plates resulted collision of these plates and played a major role in distribution of magmatic rocks during Cenozoic within Biga Peninsula. In northwestern Anatolia, the main magmatic belts are resulted from the syn- and post-collisional periods and extensional arc magmatism (Yılmaz et al., 2001; Dilek and Altunkaynak, 2007; Altunkaynak and Genç, 2008; Sanchez et al.,2016;

Kuşcu et al., 2019). By the recent researchers (Altunkaynak and Genç, 2008; Sanchez et al. 2016; Kuşcu et al., 2019) these main magmatic episodes occurred as discrete pulses and with varying compositions, and are ascribed to vanning stage of closure of Izmir-Ankara Ocean and early stage of closure of Ionian sea due to Africa and Eurasia convergence. For the formation of these magmatic belts several tectono-magmatic phases are suggested between the ages of Palaeocene - early Eocene (post-collisional events due to slab break-off, *ca.*65–49 Ma), middle-late Eocene (extensional arc, *ca.*49–35 Ma), late Eocene-Oligocene (back-arc extension and exhumation due to slab rollback, ~35–23 Ma), late Oligocene (core-complexing, *ca.*23–14 Ma) and late Miocene-Pliocene (*ca.*14–5 Ma) (Sanchez et al, 2016; Kuşcu et al., 2019).

Exhumation of Çamlıca metamorphics and Kemer micaschists was resulted by NE-directed Syn-orogenic extension (Bonev and Beccaletto, 2007) and was accompanied by Palaeocene - early Eocene intrusions. late Palaeocene - early Eocene magmatism was produced by metasomatized magma as a result of melting of upwelling asthenosphere after syn- to post-collisional slab break-off (Altunkaynak and Dilek, 2007; Altunkaynak and Genç, 2008). The post-collisional stage during Palaeocene-early Eocene (*ca.* 65–49 Ma; Bonev and Beccaletto, 2007) is a significant time period where volcanic rocks occupy a large area in the northern part of the Biga Peninsula and area between east of Marmara to Ankara. The early Eocene period resulted in emplacement of a nearly E-W to NW-SE trending belt of post-collisional and slab break-off driven granitoids from northern part of Biga Peninsula, including Armutlu, North and South Kapıdağ and Karabiga plutons towards Sivrihisar-Kaymaz plutons (Ankara). This magmatism is characterized by subduction modified, medium- to high-calcalkaline magmas exhibiting I-type character with variable composition from diorite to granite (Altunkaynak et al., 2012). The middle Eocene Kuşçayır pluton Eocene marks the product of intrusive magmatism of the Hellenic-arc and their emplacement into metamorphic basement of Biga Peninsula (Altunkaynak and Genç, 2008; Kuşcu et al, 2019). It is reported that middle Eocene volcanism in the northern Biga Peninsula produced voluminous in lavas and pyroclastics with the intermediate to felsic compositions (Ercan et al.,1995; Dönmez et al.,2005; Altunkaynak and Genç, 2008). The early Oligocene andesites and felsic tuff sequences covered the northwestern part of Biga Peninsula and southern parts of Bayramiç-Çan half-graben (Sanchez et al.,2016). Oligo-Miocene the extension was accompanied by the initiation

of core complex exhumation of Kazdağ by shallow detachment faults and well known granitic plutons of Evciler, Eybek, Kestanbol and Yenice plutons emplaced into metamorphic basement at the flanks of Kazdağ horst (Okay and Satır, 2020; Altunkaynak and Genç, 2008; Yiğit, 2012; Sanchez, 2016). Evciler and Eybek plutons intruded respectively northern and southern flanks of Kazdağ respectively during latest Oligocene mostly along the detachment planes and it is suggested that intrussion of Evciler and Eybek plutons are coeval with the exhumation of Kazdağ Core Complex (Okay and Satır, 2000). The extension directions related the exhumation is proposed as NNW-SSE and N-S within the western part of Kazdağ Core Complex (Okay and Satır, 2000; Beccaletto et al.,2007; Bonev and Beccaletto, 2007) Oligo-Miocene episode is marked by formation of Half-graben basins, increased half graben subsidence and southward migration of magmatism (Sanchez et al.,2016) originated from back-arc extensional tectonism caused by arc-retreval and slab-rollback (Aldanmaz et al., 2000; Altunkaynak and Dilek, 2006; Bonev and Beccaletto, 2007; Dilek and Altunkaynak, 2008; Altunkaynak and Genç, 2008; Brun and Faccenna, 2008; Ring et al., 2010; Schaarschmidt et al. 2021). At the early Miocene, the plutonism migrated towards the south of Edremit graben and Kozak pluton was emplaced into the metamorphic rocks s between around 22-20 Ma (Oyman, 2010; Black et al., 2013).

Cenozoic magmatism in Biga Peninsula is explained through several different mechanisms including tectonic escape (Dewey and Şengör, 1979; Şengör, 1979, 1982, 1987; Şengör et al., 1985), back-arc extension (Jackson and McKenzie, 1988; McKenzie, 1978; Meulenkamp et al., 1994; Okay and Satir, 2000a) orogenic collapse (Dewey, 1988; Seyitoglu and Scott, 1997) and slab-breakoff (Aldanmaz et al., 2000; Altunkaynak and Dilek, 2006; Dilek and Altunkaynak, 2008; Altunkaynak and Genç, 2008). It is well established that Cenozoic magmatism in Biga Peninsula is a related to north-dipping subduction of Tethyan ocean. Recent model proposed by Altunkaynak and Genç (2008) suggests that Cenozoic magmatism in Biga Peninsula during Eocene and Oligo-Miocene periods strongly affected by partial melting of mantle which was enriched by subduction derived fluids.Temporal relations of tectonism, magmatism, compiled ages of volcanic and plutonic associations are given in Figure 2.2.

2.1.5. Temporal and spatial distribution of mineral occurrences within biga peninsula

Porphyry-Cu and epithermal-Au-Ag show close temporal relation to two specific time periods during middle-late Eocene and middle-late Oligocene (Sanchez et al.,2016; Kuşcu et al., 2019). These two periods tectonically linked to extensional tectonism during post-collision (middle-late Eocene) and back-arc extension periods respectively associated by slab-breakoff and slab-rollback events.

Porphyry-Cu systems are hosted by 42.6 to 18.2 Ma. aged andesite porphyry, diorite to granite intrusions (Kuşcu et al., 2019) and spatially distributed NE-SW trending magmatic belts generally bounded by extensional fault systems that were played a role as loci for the emplacement of the magmatic rocks (Sanchez et al.,2016; Kuşcu et al., 2019). The known ages of porphyry-Cu deposits within the Biga Peninsula include, Kuşçayır (42,68 Ma), Halilağa (26,27 Ma), Ağıdağı (27,2 Ma), Alanköy (26,27 Ma.) and Tepeoba (24,70) (Yiğit et al, 2012; Leroux, 2016; Kuşcu, 2009; Kuşcu et al, 2019). These ages tend to reflect a younging direction from north to south (Figure 2.2). The temporal shift in the age of porphyry Cu systems from north to south is also indicative of a shift from arc to progressive extensional events by slab-breakoff followed by core complexing to slab-rollback (Sanchez et al. 2016; Kuşcu et al. 2019). Temporal and spatial shift pattern of the porphyry Cu systems within Biga Peninsula are associated with NW-SE trending magmatic belts bordered by regional NE-SW trending large scale structures since the middle Eocene.

Epithermal Au-Ag systems of the Biga Peninsula mostly consisted of high-sulfidation (HS)-type and relatively small number of low sulfidation (LS)-type (Figure 2.1). The HS-type epithermal Au systems are hosted by Oligocene volcanics in central and SE Biga Peninsula (Figure 2.1). Nevertheless, there are small numner of HS-type hosted by Miocene volcanics to southwest. Known intermediate sulfidation (IS)- and LS-type epithermal Au-Ag systems appear to form by a rough circle around HS-type epithermal Au systems (Figure 2.1), and are hosted by Eocene to Miocene volcanics respectively from north to south (Figure 2.2). The temporal and spatial association between the magmatic rocks, epithermal Au systems and regional structures are suggestive of a temporal and spatial shisft from north to south, and progression from early extensional arc to core complexing and slab rollback events that collectively

formed the extensional western Anatolian volcanic province and associated mineralization (Kuşcu et al. 2019).

Besides porphyry Cu and epithermal Au-Ag systems occurences, skarn mineral occurrences are also clustered along a NNE-SSW trending zones to the eastern and southeastern Biga Peninsula where the Cenozoic plutons were intruded in to basement units belong to Karakaya Complex. Ages of skarn occurrences changes range between 20,05-28,44 Ma consistent with the middle-late Oligocene (Yiğit, 2012; Kuşcu, 2009; Leroux, 2016; Kuşcu, 2019).

Compiled geochronology on the magmatic, porphyry-Cu and HS epithermal geochronology Au systems ages indicate specific time intervals (Figure 2.2). Porphyry-Cu and HS-epithermal-Au-Ag mineralization ages those were presented by previous researchers show that mineralization periods concentrated in two main time interval as late Eocene - early Oligonene and Oligocene to early Miocene (Brunetti, 2016; Leroux, 2016). These periods coincide with the previously given magmatic episodes of Cenozoic magmatic activity of Biga Peninsula during the syn- and post collisional geodynamic evolution of Neo-tethyan era (Figure 2.2).

3. LOCAL GEOLOGY

The Kirazlı district is located in central Biga Peninsula where the pre-Cenozoic basement consisting of Sakarya and Rhodop zones and ophiolites outcrop, and are unconformably overlain by Cenozoic volcanic associations. Permo-Triassic basement rocks cover the eastern and southeastern sectors of the district and buried under the Cenozoic volcanic rocks at the central and western sectors (Figure 3.1). From bottom to top, basement rocks simply consist of Çamlıca metamorphics, Denizgören ophiolite and Karakaya Complex. The Cenozoic magmatic rocks unconformably cover the basement and their subvolcanic counterparts are emplaced into the basement rocks. They form the main rock types covering entire district (Figure 3.1) and include granodioritic rocks, andesite, basaltic-andesitic lava flow and pyroclastic rocks respectively from bottom to top. The age of these rocks range between 41.20-37.88 Ma and 32,69-31,93 Ma (Aluç et al., 2023).

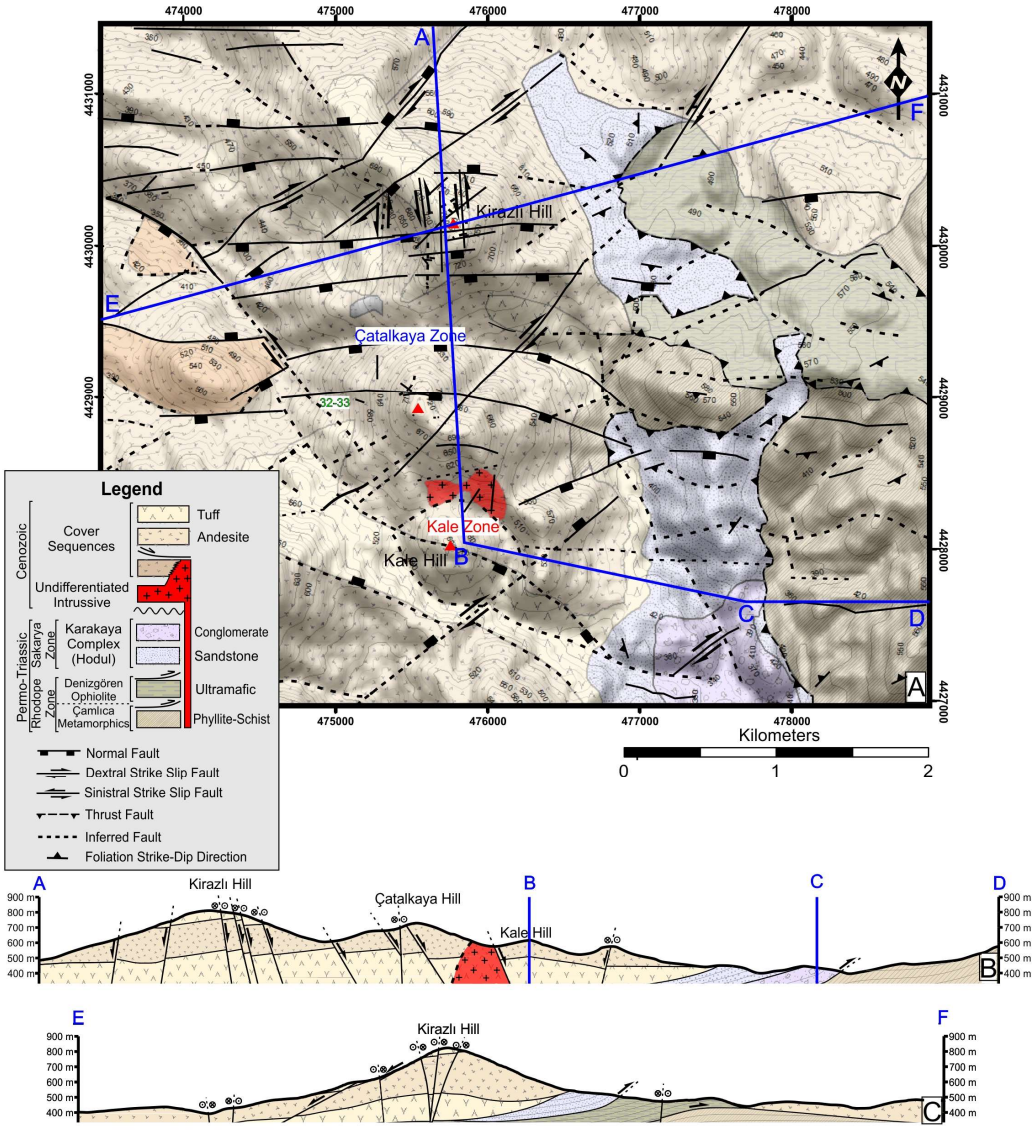

Figure 3.1. Geological map of Kirazlı District, A-B-C-D composite cross-section and E-F crossection.

3.1. Pre-Cenozoic Basement

The Çamlıca metamorphics consist of well foliated, medium to dark gray colored phyllite, mica-schists with augen-textured quartz (Figure 3.2A,B). They generally reflect strong deformation mostly by folding and contain boudinage and stretched minerals especially along the contacts with overtrusting units (Figure 3.2A). The Çamlıca metamorphics has protolith ages of 582 ± 30 Ma and 559 ± 17 Ma (Ediacaran;

Tunç et al., 2012). However, they underwent HP-LT metamorphism during the latest Cretaceous to earliest Paleogene (Okay and Satır, 2000; Beccaletto, 2007).

Figure 3.2. Outcrops of Çamlıca Metamorphics at the eastern part of district. (A) Strongly folded, micaschists with boudinaged quartz lenses, (B) Well foliated, undeformed micaschists without quartz lenses.

Denizgören Ophiolite overlies the Çamlıca Metamorphics along a thrust fault (Figure 3.3A). Denizgören ophiolite is characterized by dark green/blue color, blocky and well-deformed appearance reflecting only existence of serpentinized ultramafic rock within eastern sector of the district (Figure 3.3B). Okay et al. (1991) and Beccaletto et al. (2005) similarly signify that Denizgören ophiolite is almost totally made up of serpentinized harzburgite and sequences characteristics to ophiolitic suite (gabbro, sheeted dyke, basalt, pelagic sediments) absent in the Denizgören ophiolite. Ar/Ar geochronology of Denizgören ophiolite gives age between 117 ± 1.5 Ma to 118.3 ± 3.1 Ma (Okay et al., 1996) and 125±2 Ma (Beccaletto and Jenny, 2004) indicating the early-middle Cretaceous.

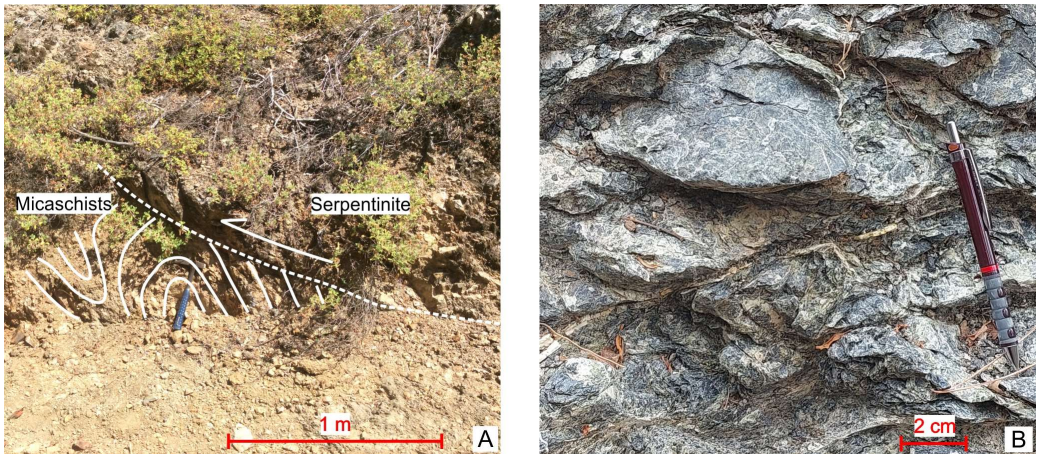

Figure 3.3. (A) Contact between serpentinite of Denizgören and micaschists of Çamlıca unit, (B) close view of dark green/blue colored, blocky and well-deformed serpentinites of Denizgören ophiolite from northeastern sector of Kirazlı District.

The Karakaya Complex in the deposit area is represented mostly by metaclastics that belong to the Hodul unit (Duru et al, 2012). They tectonically overlie the Çamlıca metamorphics and ophiolitic rocks, and are unconformably overlain by the cover seqeunces (Figure 3.1) The Karakaya basement is exposed at the eastern part of Kirazlı district sandwiched between the Denizgören ophiolite and and Cenozoic volcanics along a N-S trending valley (Figure 3.1). From bottom to top these rocks respectively include medium to dark gray, fine grained, well-sorted meta sandstone (Figure 3.4A) and gray/light-blue, thickly bedded polymictic, matrix-supported conglomerate levels (Figure 3.4B).

Figure 3.4. Outcrop view of units belong to Karakaya Complex from southeastern sector of Kirazlı District. (A) Fine grained, well-sorted sandstones and (B) polymictic, matrix supported conglomerate.

3.2. Cenozoic Magmatics

The Cenozoic volcanic rocks in the Kirazlı district refer mostly to volcanic and pyroclastic associations cut across by subvolcanic domes and rare intrusives. The intrusives are sporadic or commonly exposed outside the Kirazlı district. They form the predominant rock association covering unconformably the basement rocks (Fig. 3.1). The intense hydrothermal alteration appears to obliterated the original textural and mineralogical features. Consequently, it is challenging to determine the composition of the volcanic rocks. This also applies for the counterparts in the drill core samples. The geochronological data for these associations reveal an age range between 41.20-37.88 Ma (undifferentiated intrusive-plagioclas phyric andesite lava flow) and 32.69 to 31,93 Ma (basaltic andesite-pyroclastics) (Aluç et al, 2021; Aluç et al., 2023). From older to younger these rock associations include intensely altered intrusive rocks (Aluç et al., 2023) (middle-late Eocene); plagioclase-phyric andesite lava flow (late Eocene), basaltic andesite lava flow, tuffs and volcanic breccias (early Oligocene).

The intrusive rocks crop out at the southern sector of the district, between Çatalkaya and Kale hills. Since the unit subjected to intense alteration textural and petrographical identification on field or in core samples was not possible. Also lateral and vertical contact relations between post-dating units are stay uncertain since there is no drills intersecting the transitition between units. Yet this unit well defined by Aluç et al.(2023) based on geochemical, petrographical and geochronologic studies. This rocks is the main host for the porphyry-Cu type mineralization in the district (Aluç et al., 2023). Identifiable mineral composition of altered intrusive is reported as quartz and plagioclase within district (Aluç et al., 2023). Minor exposures of the same rocks approximately 2 km southeast of the Kirazlı district are reported by Leroux (2016). He reported that it is consists of quartz, biotite, hornblende and plagioclase. Age of the intrusion is given as 40,19±0,34 Ma (U-Pb ;Leroux, 2016) and 40,47±0,33 Ma to 41,20±0,45 Ma (U-Pb; Aluç et al., 2023).

Volcanic rocks consist of plagioclase-phyric andesite lava flow (late Eocene) , basaltic andesite lava flow, tuffs and volcanic breccias (early Oligocene). with an increasing pyroclastic compostition ratio from bottom to top. Lava flows within the district form two different levels in the sequence based on their age and composition (Leroux, 2016;

Aluç et al, 2023). Relatively older plagioclase-phyric andesite lava flow (late Eocene) crops out at the western part of study area and juxtaposed with the younger basaltic andesite flow unit (early Oligocene) along extensional faults (Figure 3.5). This sequence can be differentiated by dark green/brown color (Figure 3.5). The older andesitic lava flow is dominated by plagioclase and quartz, plagioclase is being phenocrystal constituent and termed as plagioclase-phyric andesite (Figure 3.6.A)(Aluç et al, 2023).

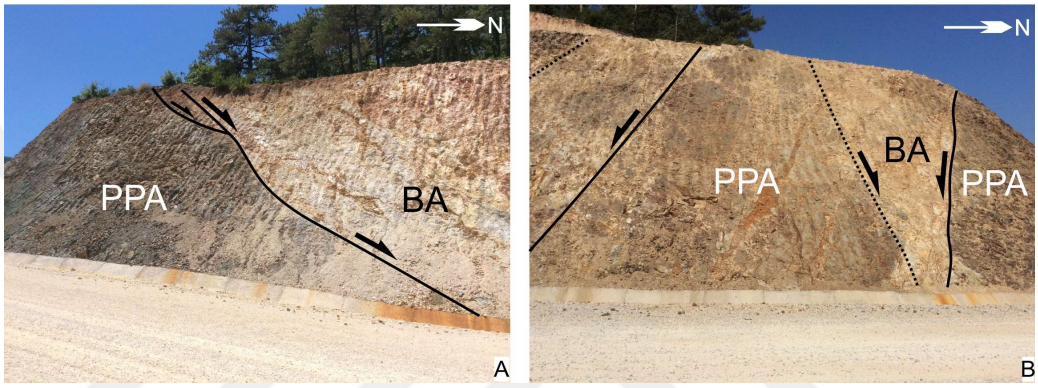

Figure 3.5. (A), (B) Outcrop view of Cenozoic volcanics at the western sector of Kirazlı District. Dark colored Plagioclase-phyric andesite (PPA) forms the footwall of nearly E-W striking extensional faults and light light -medium gray Basaltic Andesite (BA) forms the hangingwall.

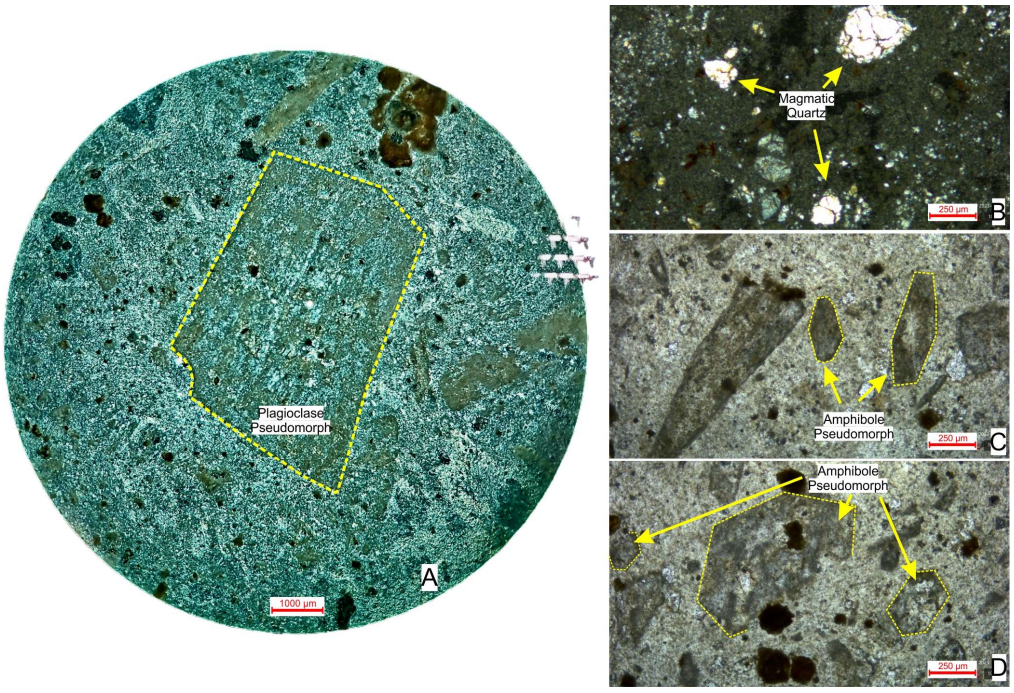

Figure 3.6. (A) Altered plagioclase crystal from PPA (x-pl), (B) Embayed and fractured magmatic quartz crystals from BA (x-pl), (C) and (D) Amphibole pseudo-crystals from clay altered BA (x-pl).

The relatively younger levels of the volcanic association consist of basaltic-andesite lava flow, tuff and phreatic breccia (Figure 3.1 and Figure 3.7A-C). They represent the major rock associations covering the largest area within central and western parts of the district. The upper sequence is distinguishable by its light to medium gray color. It is pervasively clay-altered, silicified or oxidized at the Kirazlı, Çatalkaya and Kale hills. Tuff-bearing levels form the peak and western flank of Kirazlı hill, eastern part of the neck between Kirazlı and Çatalkaya hills and southern flank of Kale hill (Figure 3.1A). Mineral composition of upper andesitic lava is composed of quartz, intensely altered plagioclase and hornblende pseudomorph (Figure 3.6B-D) (Aluç et al, 2023). Tuff-bearing levels mainly consist of angular to sub-rounded lithic fragments and defined as lithic-tuff (Figure 3.7A-C). Phreatic breccia mainly observed at the mineralized sectors of the Kirazlı hill. It contains angular to sub-angular silicified rocks, oxidized or clay altered phreatic breaccia clasts (Figure 3.8A-B).

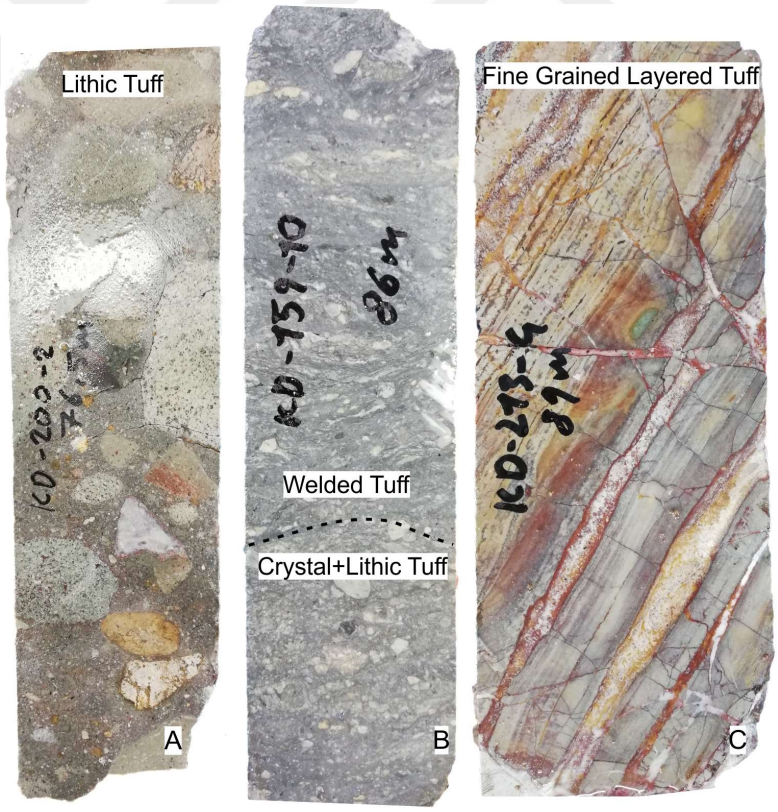

Figure 3.7. Drillcore samples from andesitic tuff sequences. (A) Lithic-tuff including rounded to subrounded clast, (B) unwelded/welded lithic+crystal tuff (silicified), (C) fine grained layered tuff (silicified and oxidized).

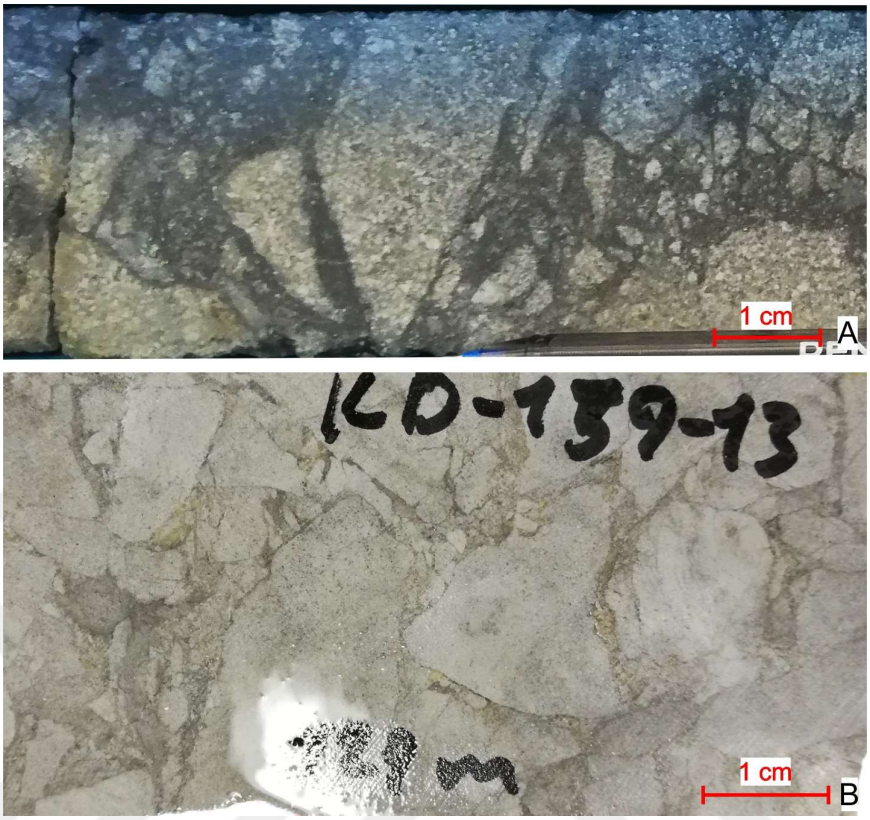

Figure 3.8. (A),(B) Clay altered and silicified, angular to subangular clast bearing phreatic breccia from Kirazlı Main Zone.

4. STRUCTURAL GEOLOGY

Structural studies aiming to explain the relationship of Kirazlı deposit with regional tectonics and deformation, were conducted through both regional and district-scale study areas. Regional-scale study area covers the central Biga Peninsula where the Permo-Triassic Rhodopean and Sakarya basements are covered by Neogene volcanics. These lithologies bordered and offset by various types of extensional, oblique and strike-slip faults formed during syn/post-collisional Neogene extension subsequent to closure of the NeoTethyan ocean and initiation of dextral strike-slip deformation related to North Anatolian Fault System (NAFS).

The field works on structural features began firstly with the lineament analysis using satellite images and digital elevation maps (DEM) of the region and district. Satellite images and DEM indicated a dense population of parallel to sub parallel sets of faults belong to different kinematic characteristics. These faults appears to have controlled the morphology and landscape of the district. Field studies were directed to focus on the lineaments as potential faults on the regional and district-scale purposes. Then, the field studies on structural features include mapping of faults and recording of attitude and kinematic data on observed fault planes. During the regional-scale field works, 100 fault planes from 32 sites/zones were identified, and the attitudes of faults and slickenlines at each site were recorded (Figure 4.1A). Recorded data were evaluated and grouped according to host rock ages, kinematic characteristics (principle stress directions, p-b-t axes) and fault plane orientatitons. The data recorded from the fault planes have been transferred to the rose and stereographic diagrams to determine the predominat trends and sets of faults with different kinematic characteristics (Figure 4.1B-E). The slip data was processed by Win Tensor™ software in order to define main pressure-tension axes and stress directions of each kinematic group.

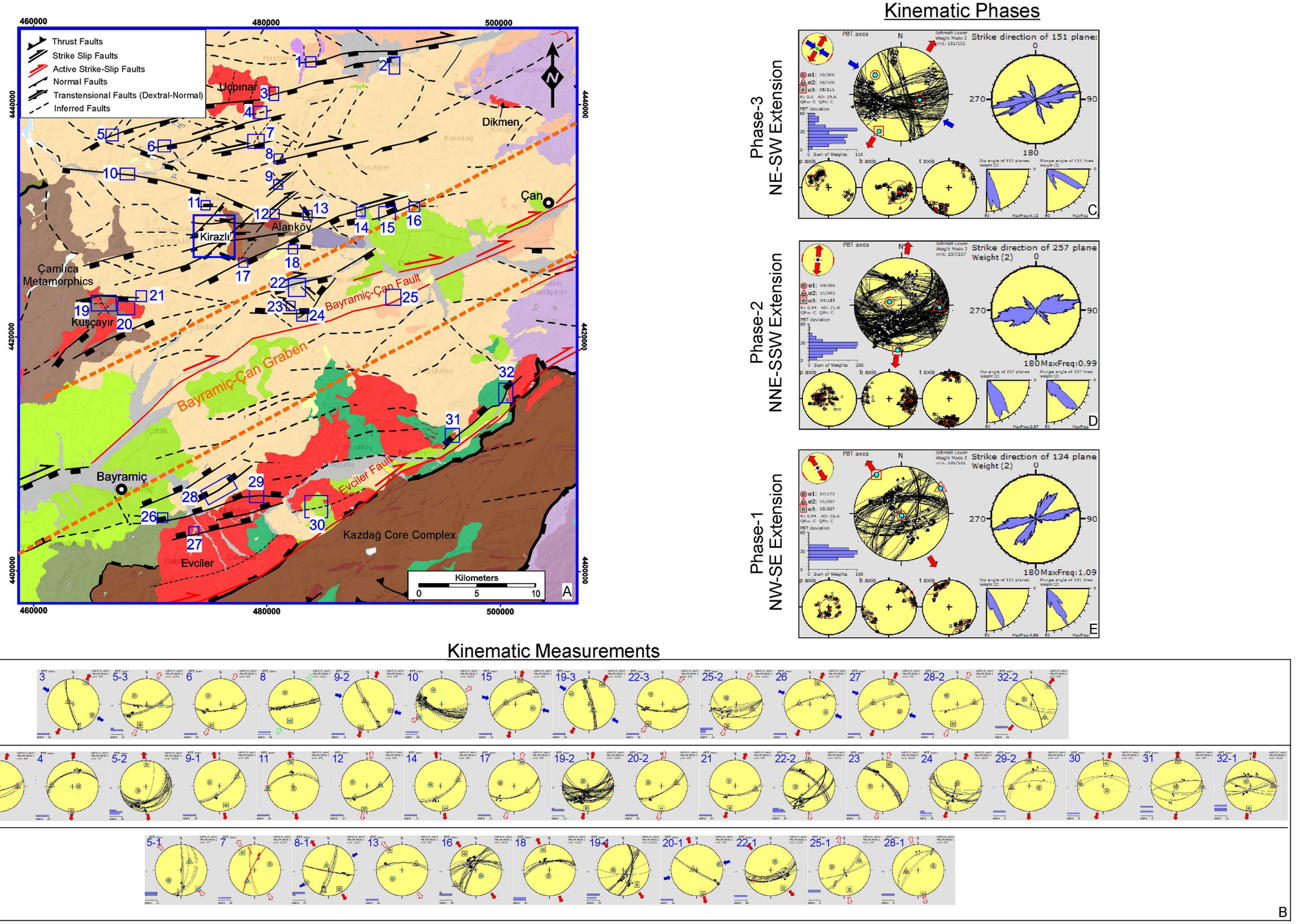

Figure 4.1. (A) Lithological-structural map of regional-scale study area and locations of kinematic measurement sites, (B) Stereoplots and p-t axes of measurement sites, (C),(D),(E),(F) Stereoplots of fault planes, principle stress axes; roseplots of predominant fault strikes, dip amounts of fault planes and striations from determined tectonic phases. (Lithologies are same as in the Figure 2.1.)

4.1. Kinematic Analyses and Characteristics

Stereoplots of collected data including fault plane orientation, slip vector, resultant principle stress axes and pressure-tension axes for each site are presented in Figure 4.1. The processed data from the measurement sites (Figure 4.1) that indicates several principle stress orientations and pressure-tension directions. Also, the processed data (Figure 4.1B) clearly indicates that three different kinematic characteristics (Figure 4.1C-E) govern the generation of faults within the central Biga Peninsula. These kinematic characteristics are represented and mentioned with respect to their extension axes as (1) NW-SE, (2) NNE-SSW and (3) NE-SW (Figure 4.1C-E). For each kinematic grup, predominant fault strikes and dip amounts and plunges of striations given in Figure 4.1C-E.

4.1.1. NW-SE extensional phase (phase-1)

Kinematic analyses of 134 measurements on fault plane attitude and slip vector data during the regional-scale works reveal an NNW-SSE extension. The sites, resultant orientations of resultant principle stress axes and rock ages related to this phase given in Table 4.1. Based on fault orientations two predominant trends emerge as (1) N25°-35°E and (2) N75°-90°E with dip amounts varying between 60°-85° (Figure 4.2). Plunges of slip data measured on fault planes show generally close relation to dip angle of fault planes (Figure 4.2). Slip vectors on N25°-35°E faults with moderately dipping geometry generally indicate dominantly dip-slip sense of movement with lesser strike-slip component (Figure 4.2). Also slip vectors on approximately E-W striking faults with steeply dipping geometry indicate a sinistral-normal oblique slip but with dominant dip-slip characteristic (see small arrows on fault plane arcs on Figure 4.2).

Table 4.1. List of measurement sites, resultant principle stress orientations and lithology ages related to phase-1 (R= Ratio of principle stress differences, n/nt= working/total data)

Sites	Principle Stress Orientations (plunge/trend)			R	n/nt	Lithology Age
	σ1	σ2	σ3			
5-1	38°/230°	52°/045°	02°/138°	0,35	7/7	Oligocene
7	37°/069°	47°/214°	18°/324°	0,50	10/10	Oligocene
8-1	02°/241°	75°/337°	15°/150°	0,66	11/11	Oligocene
13	49°/227°	40°/067°	10°/329°	0,50	5/5	Oligocene
16	66°/139°	02°/234°	24°/325°	0,55	36/36	Oligocene
18	71°/188°	08°/075°	17°/342°	0,49	10/10	Oligocene
19-1	58°/271°	21°/037°	23°/137°	0,54	22/22	Eocene
20-1	11°/075°	78°/277°	04°/166°	0,50	5/5	Eocene
22-1	60°/028°	26°/241°	15°/144°	0,48	20/20	Oligocene
25-1	49°/284°	32°/059°	23°/165°	0,66	5/5	Eocene
28-1	39°/075°	51°/263°	04°/168°	0,63	5/5	Oligocene
Phase-1 (NW-SE Extension)	87°/173°	01°/057°	03°/327°	0,54	101/134	

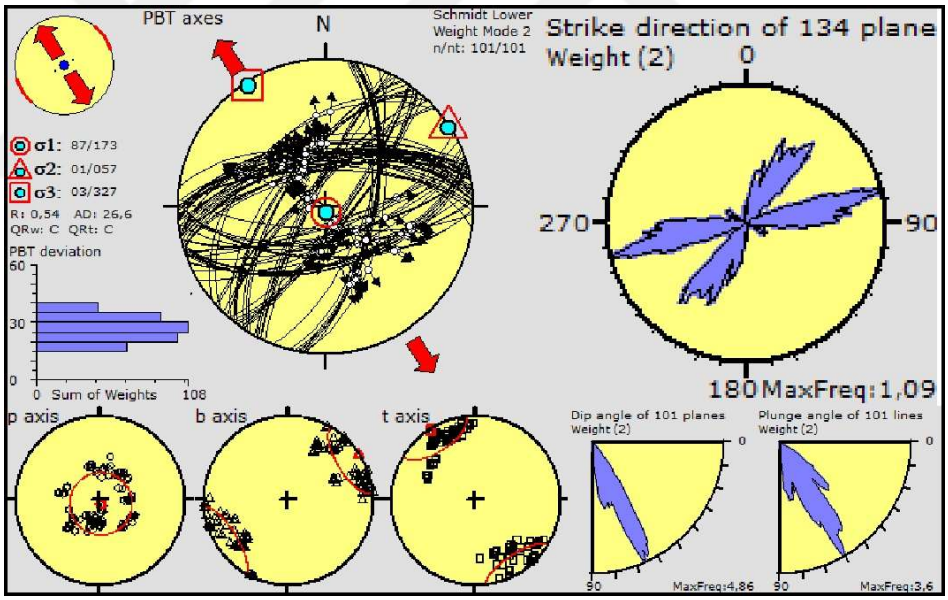

Figure 4.2. Stereoplots of fault planes, principle stress axes; roseplots of predominant fault strikes, dip amounts of fault planes and striations from phase-1. (Small arrows on arcs indicate slip senses).

According to the result of processed slip vector data, principle stress axes revealed as 07°/173° for σ1, 01°/057° for σ2 and 02°/227° for σ3. Considering the nearly vertical orientation of σ1 and horizontal orientation of σ3, related tectonic phase can be evaluated as dominantly extensional (Figure 4.2).

4.1.2. NNE-SSW extensional phase (phase-2)

Kinematic analyses of 257 measurements on fault plane attitude and slip vector data during the regional-scale works show that the faults related to NW-SE extensional phase predominate at 4 directions; (1) N50°-60°E, (2) N70°-90°E and (3) N40°-50°W (Figure 4.3). The sites, resultant orientations of resultant principle stress axes and rock ages related to this phase given in Table 4.2.

Of the predominant faults, those that trend generally in N50°-60°E have steeply (70°-80°) to gently dipping (15°-20°) geometries and dominantly have dextral-normal oblique sense of movement while N70°-90°E trending moderately to steeply dipping (60°-80°) faults have dominantly normal sense of movement (see small arrows on fault plane arcs on Figure 4.3). The last predominant sets of faults in N40°-50°W generally are steeply dipping (65°-80°) sinistral-normal oblique faults.

Table 4.2. List of measurement sites, resultant principle stress orientations and lithology ages related to phase-2 (R= Ratio of principle stress differences, n/nt= working/total data)

Sites	Principle Stress Orientations (plunge/trend)			R	n/nt	Lithology Age
	σ1	σ2	σ3			
1	66°/322°	14°/085°	19°/180°	0,50	5/5	Eocene
2	57°/307°	27°/090°	17°/189°	0,47	6/6	Oligocene
4	71°/088°	19°/273°	01°/182°	0,50	7/7	Oligocene
5-2	61°/243°	24°/098°	15°/002°	0,50	28/28	Oligocene
9-1	57°/289°	24°/061°	22°/161°	0,50	5/5	Oligocene
11	81°/168°	01°/263°	09°/354°	0,50	5/5	Oligocene
12	42°/284°	47°/088°	08°/186°	0,50	5/5	Oligocene
14	58°/276°	30°/071°	11°/168°	0,50	5/5	Oligocene
17	45°/283°	45°/112°	05°/017°	0,50	5/5	Oligocene
19-2	68°/315°	16°/090°	14°/185°	0,48	66/70	Eocene
20-2	46°/284°	41°/078°	13°/180°	0,50	5/5	Oligocene
21	64°/309°	23°/099°	12°/194°	0,50	5/5	Oligocene
22-2	47°/267°	43°/091°	02°/359°	0,48	45/45	Oligocene
23	49°/268°	36°/120°	16°/017°	0,51	15/15	Oligocene
24	80°/033°	02°/289°	10°/199°	0,50	18/18	Oligocene
29	59°/099°	31°/265°	06°/359°	0,50	4/4	Oligocene
30	71°/144°	13°/275°	14°/008°	0,47	5/5	Oligocene
31	86°/202°	02°/093°	04°/002°	0,50	5/5	Oligocene
32-1	70°/316°	14°/090°	14°/184°	0,50	15/15	Oligocene
Phase-2 (NNE-SSW Extension)	69°/286°	21°/093°	04°/185°	0,54	253/257	

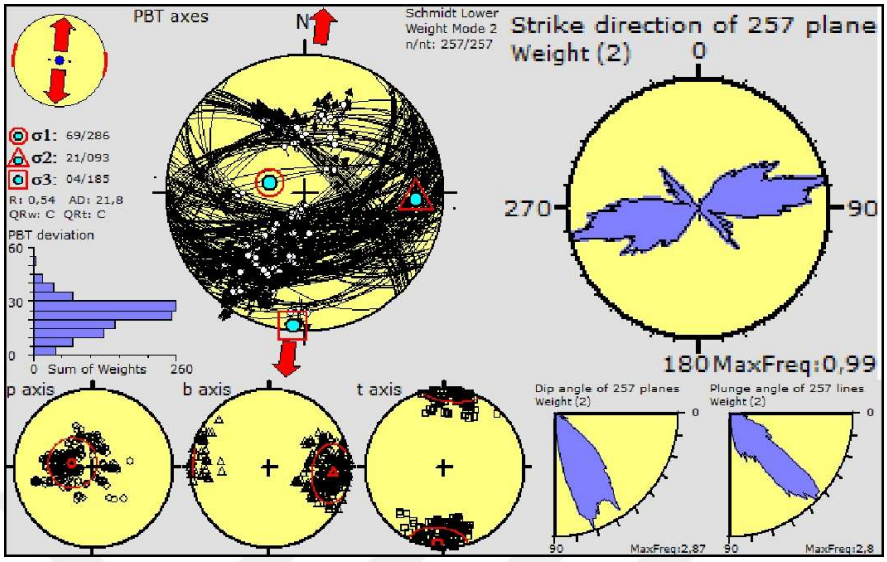

Figure 4.3. Stereoplots of fault planes, principle stress axes; roseplots of predominant fault strikes, dip amounts of fault planes and striations from phase-2. (Small arrows on arcs indicate slip senses)

Based on principle stress axes with their nearly vertical σ1 (86°/267°), and horizontal σ3 (02°/138°) orientations, the faults are likely to have extensional characteristics.

4.1.3. NE-SW extension phase (phase-3)

Kinematic analyses of 151 measurements on fault plane attitude and slip vector data during the regional-scale works reveal a NE-SW extensional kinematic characteristics based on p-t axes, principle stress directions and fault geometry configuration (Figure 4.4). The sites, resultant orientations of resultant principle stress axes and rock ages related to this phase given in Table 4.2. Considering the results, it is possible to determine 4 predominant trends for the faults (Figure 4.4) as (1) N60°-70°E, (2) N80°-90°E, (3) N60°-70°W and (4) N15°-25°W. All predominant fault groups example steeply dipping geometry (70°-90°).

Table 4.3. List of measurement sites, resultant principle stress orientations and lithology ages related to phase-3 (R= Ratio of principle stress differences, n/nt= working/total data)

Sites	Principle Stress Orientations (plunge/trend)			R	n/nt	Lithology Age
	σ1	σ2	σ3			
3	17°/120°	73°/297°	01°/030°	0,50	5/5	Oligocene
5-1	41°/303°	44°/091°	16°/198°	0,54	13/13	Oligocene
6	41°/303°	47°/103°	10°/204°	0,50	5/5	Oligocene
8	42°/322°	30°/082°	34°/194°	0,49	11/11	Oligocene
9-2	13°/106°	75°/311°	06°/197°	0,50	5/5	Oligocene
10	36°/330°	54°/149°	00°/240°	0,48	32/32	Quaternary
15	32°/103°	58°/276°	03°/011°	0,50	9/9	Oligocene
19-3	22°/301°	67°/145°	09°/034°	0,50	10/10	Eocene
22-3	40°/311°	49°/119°	06°/206°	0,50	8/8	Quaternary
25-1	52°/302°	37°/107°	07°/202°	0,53	14/14	Oligocene
26	32°/117°	55°/272°	12°/020°	0,50	3/3	Miocene
27	33°/115°	56°/275°	09°/000°	0,50	3/3	Oligocene
28-2	46°/309°	35°/085°	23°/192°	0,50	2/2	Oligocene
32-2	63°/303°	27°/135°	05°/042°	0,50	6/6	Quaternary
Phase-3 (NE-SW Extension)	32°/306°	56°/106°	09°/211°	0,6	151/151	

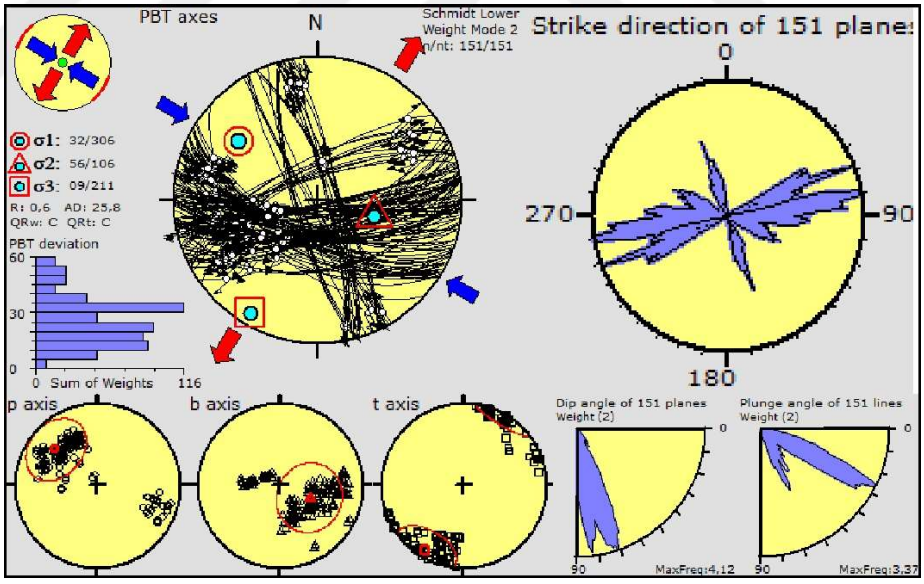

Figure 4.4. Stereoplots of fault planes, principle stress axes; roseplots of predominant fault strikes, dip amounts of fault planes and striations from phase-3. (Small arrows on arcs indicate slip senses)

Based on slip vectors presented on stereoplots N80°-90°E and N60°-70°E trending faults example dextral-strike-slip characteristics. Slip vectors of N15°-25°W and N60°-70°W trending faults indicate respectively sinistral and normal-slip characteristics. According to the result of processed slip vector data, principle stress

axes revealed as 32°/306° for σ1, 56°/106° for σ2 and 09°/211° for σ3. Considering the subhorizontal-horizontal orientation of σ1 and σ3 and sub-vertical orientation of σ2, subhorizontal slip vectors and steeply dipping fault geometries, related tectonic phase can be evaluated as dominantly strike-slip.

4.1.4. Spatio-temporal distribution of tectonic phases and related faults

As mentioned above, three different tectonic phases were differentiated based on the collected and processed fault orientation and slip sense data from the regional-scale works in the central Biga Peninsula where Neogene volcano-plutonic units dominate. Spatio-temporal relations between the phases were established with respect to locations, general outcrop orientations and ages of currently known lithologies and geodynamic history of Biga Peninsula during syn- and post collisional extension related to Neotethyan geodynamic evolution. Collected data, field observations and available literature within the regional-scale area have enabled the distinction of three tectonic phases from older to younger as (1) NW-SE extension (Phase-1), (2) NNE-SSW extension (Phase-2), and (3) NE-SW extension (Phase-3).

Biga Peninsula has a complex Neogene tectonic history related to syn-/post collisional extension subsequent to closure of Neotethys (Delaloye and Bingöl, 2000; Okay and Satır, 2000a; Yılmaz and Karacık, 2001; Dilek and Altunkaynak ,2007; Altunkaynak, 2007; Beccaletto et al., 2005; Beccaletto et al, 2007; Kaymakcı et al., 2007; Karacık et al., 2008; Altunkaynak and Genç, 2008; Brun and Faccenna, 2008; Cavazza et al., 2009; Ring et al, 2010; Jolivet and Brun, 2010; Altunkaynak et al., 2012; Sözbilir et al., 2016; Sanchez et al., 2016; Ersoy et al., 2017; Kuşcu et al., 2019; Aydın et al., 2019; Erenoğlu et al., 2020; Aslan et al., ;2020; Schaarschmidt et al., 2021; Gürer et al., 2021; Koçyiğit, 2023; Gülyüz et al., 2024). Based on published kinematic features related to exhumation of basement units, spatial distribution of magmatics with specific ages and spatial relation of basement and cover units and recent morphology, it seems that the faults formed by successive tectonic phases become younger and from north to south, in time. Following the beginning of post-collisional extension during the early Eocene, northern Biga Peninsula were occupied by widespread andesitic to dacitic volcanism (lavas and pyroclastics) (Yılmaz, 1990; Ercan et.al.,1995; Dönmez et.al.2005; Altunkaynak and Genç, 2008; Sanchez et.al.,2016). Prior to determined

phases of this study a NE-SW extension, reveals itself in ductile-brittle kinematic indicators of Kemer Micaschists (Beccaletto, 2007; Beccaletto et al., 2007) (Figure 4.5A,B). Within northern and central part in Biga Peninsula, Eocene-Oligocene volcanic cover is exposed in NW-SE trending belt between Çamlıca Metamorphics and Kemer Micaschists and juxtaposes with metamorphic basesment along same trend (Okay, 1991; Siyako and Bürkan, 1991; Beccaletto et al., 2007; Bonev and Beccaletto, 2007; Aygül et al.,2012) (Figure 4.5A). Kinematic measurements of previous (Beccaletto et al., 2007) studies of mineral lineations and shear senses from Kemer Micaschists describes a NE-SW syn-/post-collisional extension during Paleocene-early Eocene within northern Biga Peninsula.

The major faults formed by the NW-SE extensional tectonic phase (phase-1) are characterized by two major trends as nearly ENE-WNW and NE-SW respectively with extension dominant slip sense and dextral-normal oblique slip sense. Related kinematic indicators were generally observed within middle-late Eocene – early Oligocene aged volcano-plutonic rocks formed within northern and central Biga Peninsula, (Fig. 4.1A and B). The ENE-WSW trending fault surfaces of this phase, contain striations indicating kinematics of both due to NW-SE extension and NNE-SSW extensions indicating that the same fractures should have been used or the faults were re-activated by subsequent tectonic phases (Figure 4.1B).

Spatial distribution of kinematic solutions from measurement sites indicate that the NNE-SSW extensional tectonic regime (Phase-2) effects nearly all regional-scale area and measured from middle-late Oligocene to Eocene aged volcano-plutonic rocks. (Figure 4.1A,B). Oligo-Miocene in the Biga Peninsula correspond to the initiation of core complex exhumation of Kazdağ by detachment faults. Subsequent NNE-SSW extension share similar extensional trends (Figure 4.9A,C and Figure 4.3) within the western part of Kazdağ Core Complex (Okay and Satır, 2000a; Beccaletto et al.,2007; Bonev and Beccaletto, 2007). Also Oligo-Miocene episode is marked by formation of Half-graben basins, increased half graben subsidence and southward migration of magmatism (Sanchez et al., 2016;Ersoy et al., 2017; Kuşcu et al., 2019). Major trends of the faults with the kinematic features of this regime strongly resembles that of the recent ENE-WSW trending horst-graben morphology of Biga Peninsula (Figure 4.5A). This suggests that this tectonic regime played a major role for the development of recent morphology of the Biga Peninsula.

Related kinematic indicators to NE-SW extension (Phase-3) were generally observed within middle-late Eocene – Quaternary aged volcano-plutonic and sedimentary rocks formed within the Biga Peninsula, (Fig. 4.1.A and B). It is well known that dextral strike-slip tectonic regime also effects the region since Mio-Pliocene (Kaymakcı et al., 2007; Gürer et al., 2016; Gürer et al., 2021; Sanchez et al., 2016; Şengör et al., 2005, Şengör, el al.,1995). In Kaymakcı et al. (2007), an illustrated roseplot diagram showing major trends of faults related to late Miocene to recent transtensional tectonic regime indicates nearly the same major trends with the resultant plots of Phase-3 (Figure 4.4)

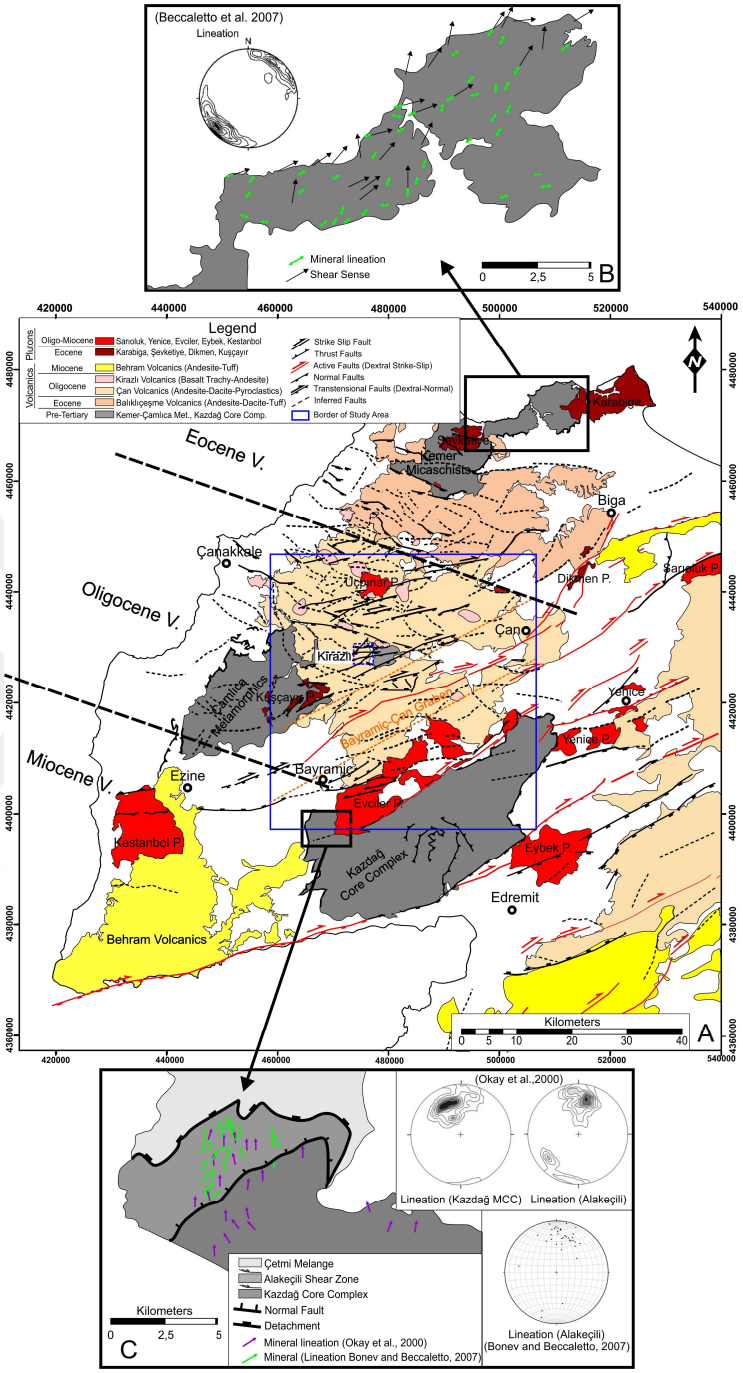

Figure 4.5. (A) Spatial distribution of basemen and volcano-plutonic rocks of Biga Peninsula based on predominant directions. (B) Contour diagram of kinematic data indicating NE-SW extension and spatial distribution of shear-senses within Kemer Micaschists (Beccaletto et al.,2007), (C) Contour diagrams of kinematic data indicating NNE-SSW extension and spatial distribution of shear-senses within Northwestern margin of Kazdağ Core Complex and Alakeçili Shear Zone (Okay et al, 2000; Beccaletto et al.,2007).

4.2. Kinematic Properties and Fault Types of Kirazlı Deposit

Fault orientation and kinematic indicator measurements within district-scale work area (deposit-scale) was conducted on 51 fault planes. Each measurement site, measured fault orientations and resultant kinematic axes illustrated in Figure 4.10. Dominant fault geometries were determined by common kinematic features. All measured fault planes were not shown for every measurement site on the map because not every fault had a lateral extension that could be plotted on the map and some faults represented wider deformation zones than a single fault plane. However, regardless of the lateral extension of the fault surface, each measurement is taken into account and shown on the map (Figure 4.10A). At the majority of sites, the crosscutting relationships between the major fault trends in response to different kinematic phases were not identified due to the intense argillic alteration superimposing on earlier porphyry-Cu and HS-epithermal Au style alterations in the deposit. Besides, existence of multiple sets of slickenlines with different orientations on individual fault planes, indicate that the pre-existing faults were re-activated (reworking) by subsequent kinematic phases or at least endured multiple tectonic phases. Reactivation of pre-existing faults or deformation zones also makes it difficult to interpret crosscutting relationships that allow to build temporal order between major trends. For this reason, the tectonic phases identified in the regional-scale work area were compared with the data obtained in the deposit-scale area. The sites, resultant orientations of resultant principle stress axes and rock ages related to determined phases listed in Table 4.4, 4.5 and 4.6.

Table 4.4. List of measurement sites, resultant principle stress orientations and lithology ages related to Phase-1 (R= Ratio of principle stress differences, n/nt= working/total data)

Sites	Principle Stress Orientations (plunge/trend)			R	n/nt	Lithology Age
	σ1	σ2	σ3			
35	51°/061°	26°/213°	14°/313°	0,50	5/5	Early Oligocene
36	62°/282°	20°/089°	04°/180°	0,50	5/5	Middle Eocene
41	57°/030°	27°/247°	17°/148°	0,50	5/5	Late Eocene
42	54°/072°	35°/237°	07°/332°	0,50	5/5	Late Eocene
46	59°/217°	14°/102°	27°/005°	0,50	9/9	Late Eocene
47	54°/283°	21°/045°	28°/147°	0,50	9/9	Late Eocene
49	58°/080°	32°/249°	05°/342°	0,50	9/9	Late Eocene
Phase-1	70°/029°	16°/245°	11°/152°	0,52	39/47	

Table 4.5. List of measurement sites, resultant principle stress orientations and lithology ages related to Phase-2 (R= Ratio of principle stress differences, n/nt= working/total data)

Sites	Principle Stress Orientations (plunge/trend)			R	n/nt	Lithology Age
	σ1	σ2	σ3			
4	66°/332°	10°/085°	22°/179°	0,50	5/5	Late Oligocene
6	54°/339°	09°/082°	35°/179°	0,50	5/5	Late Oligocene
7	10°/280°	80°/087°	02°/190°	0,50	5/5	Late Oligocene
8	67°/330°	10°/086°	22°/180°	0,50	5/5	Late Oligocene
11-12	28°/280°	62°/109°	04°/012°	0,50	9/9	Early Oligocene
18	58°/290°	32°/117°	03°/025°	0,49	9/9	Early Oligocene
19	55°/227°	19°/108°	29°/007°	0,50	4/4	Early Oligocene
21-29	37°/292°	53°/108°	02°/200°	0,48	43/48	Early Oligocene
39	35°/265°	53°/063°	11°/167°	0,50	5/5	Early Oligocene
40	65°/288°	24°/090°	07°/183°	0,50	5/5	Early Oligocene
43	39°/255°	49°/060°	08°/159°	0,50	5/5	Late Eocene
44	69°/282°	20°/089°	04°/180°	0,50	5/5	Early Oligocene
45	42°/271°	46°/111°	10°/011°	0,50	5/5	Early Oligocene
48	49°/265°	36°/119°	17°/015°	0,50	5/5	Early Oligocene
50	57°/266°	33°/090°	02°/359°	0,50	5/5	Early Oligocene
Phase-2	45°/284°	45°/100°	02°/192°	0,52	120/125	

Table 4.6. List of measurement sites, resultant principle stress orientations and lithology ages related to Phase-3 (R= Ratio of principle stress differences, n/nt= working/total data)

Sites	Principle Stress Orientations (plunge/trend)			R	n/nt	Lithology Age
	σ1	σ2	σ3			
1	04/146	71/043	18/238	0,50	4/4	Late Oligocene
2	15/129	72/274	10/036	0,38	9/9	Late Oligocene
3	44/130	44/333	12/231	0,50	4/4	Late Oligocene
5	10/299	80/114	01/209	0,50	9/9	Late Oligocene
9	10/280	80/87	02/190	0,50	5/5	Late Oligocene
10	23/114	55/240	25/013	0,50	5/5	Late Oligocene
13	14/134	75/284	07/042	0,49	4/4	Early Oligocene
14	19/310	67/095	12/216	0,50	6/6	Early Oligocene
15	28/280	62/109	04/012	0,50	7/9	Early Oligocene
16	37/343	52/146	09/247	0,50	4/4	Early Oligocene
17	41/349	43/132	20/241	0,50	6/6	Early Oligocene
20	01/312	76/046	14/222	0,51	7/10	Early Oligocene
30	20/309	67/097	11/215	0,50	2/5	Early Oligocene
31-34	21/308	69/140	04/040	0,71	31/33	Late Oligocene
37	24/146	64/350	09/241	0,50	5/5	Middle Eocene
38	32/312	49/086	23/206	0,50	5/5	Early Oligocene
51	12/320	60/207	26/056	0,50	7/7	Early Oligocene
Phase-3	11/309	79/132	01/039	0,58	123/140	

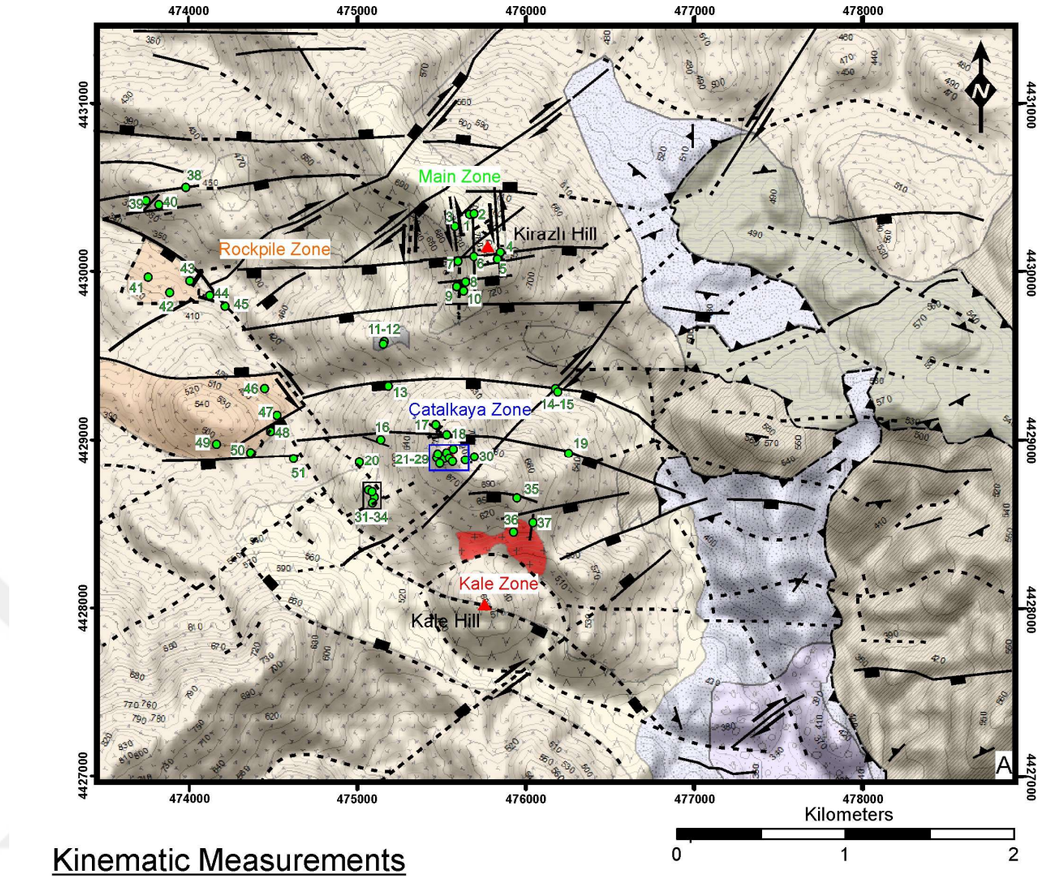

Kinematic Measurements

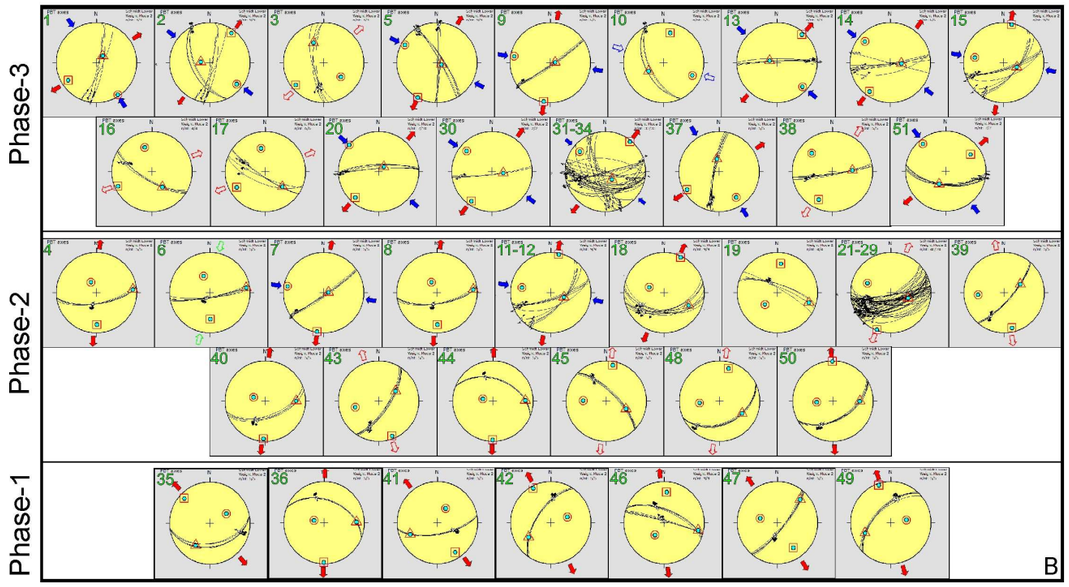

Kinematic Phases

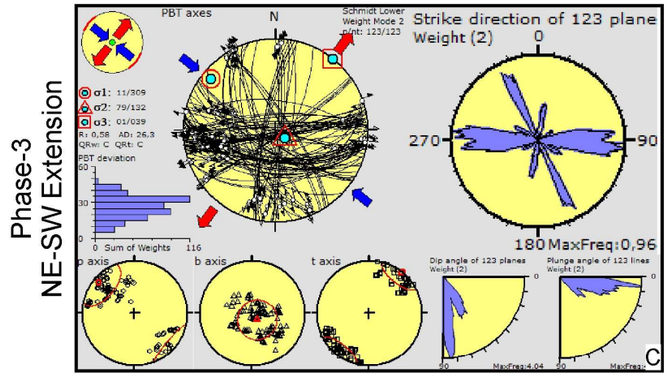

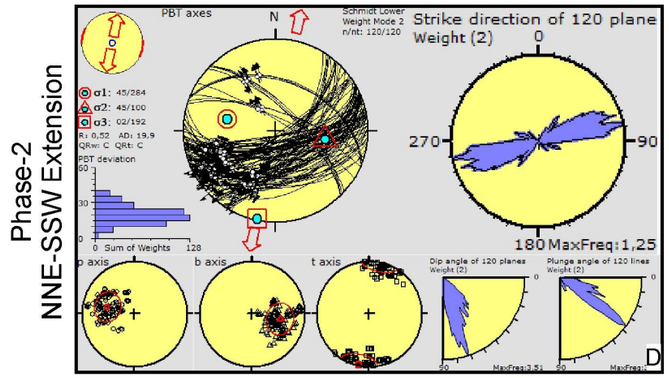

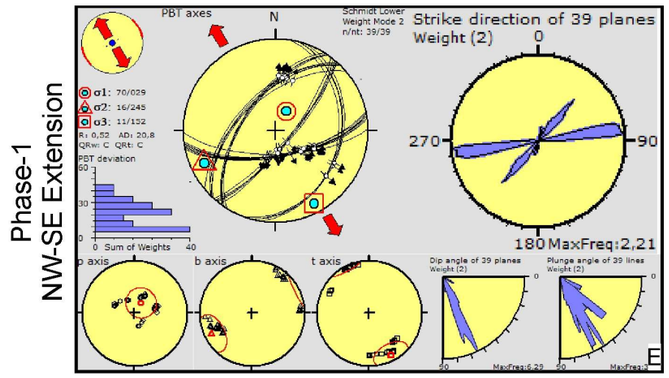

Figure 4.6. (A) Lithological-structural map of district-scale study area and locations of kinematic measurement sites, (B) Stereoplots of measured faults and p-t axes of measurement sites, (C),(D),(E),(F) Stereoplots of fault planes, principle stress axes; roseplots of predominant fault strikes, dip amounts of fault planes and striations from determined tectonic phases. (Lithologies are same as in the Figure 3.1.)

As the result of analysis, three basic kinematic characters have been identified within the Kirazlı Deposit, similar to the results of regional scale studies as (1)NW-SE, (2)NNE-SSW, and (3)NE-SW extensions (Figure 4.6C-E and Figure 4.7). Major fault trends for each phase within the district, slightly differ from the regional scale major trends. However, the extension axes and the principle stress orientations obtained as a result of local measurements strongly resemble the regional results and comparation is presented in Figure 4.7.

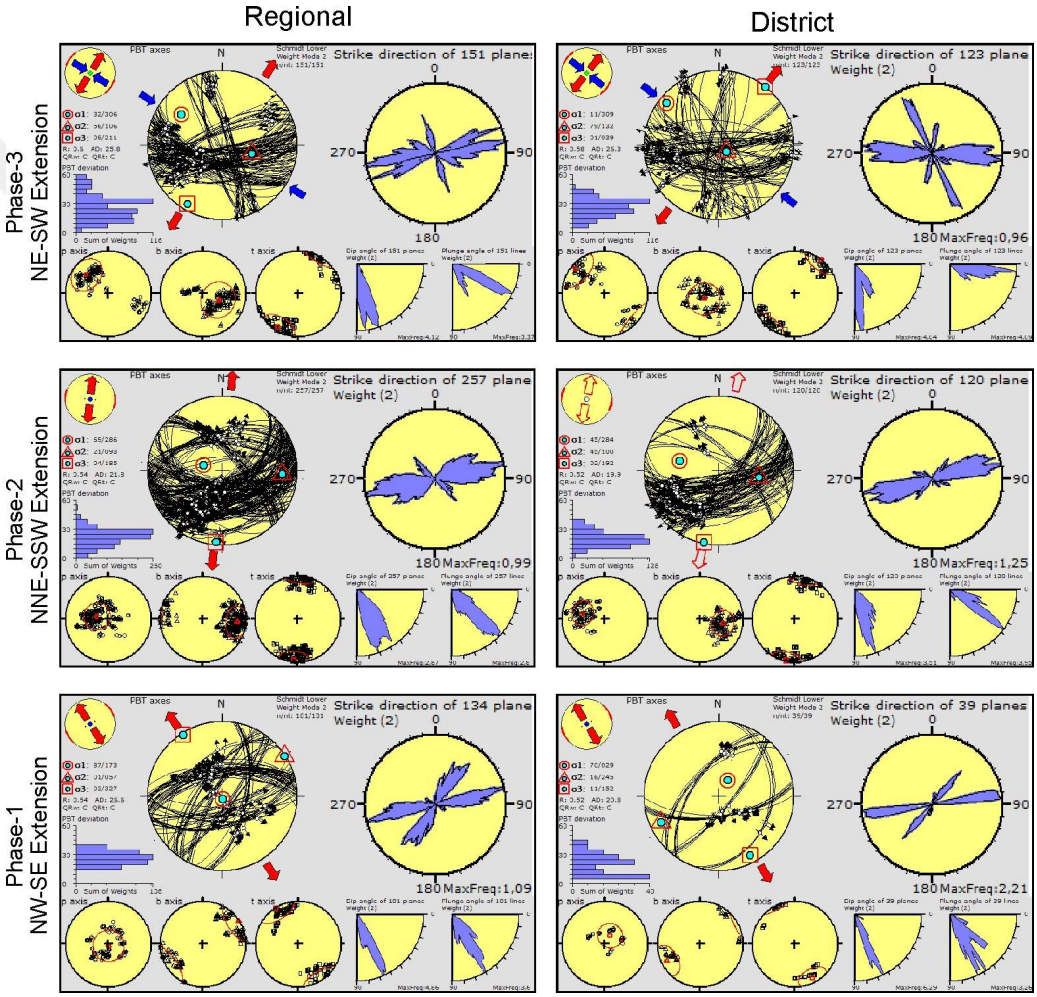

Figure 4.7. Geometric correlations of regional and district scale tectonic phases based on predominant fault orientations, principle stress orientations, p-t axes and related shear models.

The prepared local geology map includes faults with certain lateral extension within the Kirazlı Deposit (Figure 4.6A). When the distributions of these faults, the morphology of the district and the distributions of volcanic units are examined, it can be realized that the lithological boundaries between different volcanic sequences and recent morphology correspond to certain trends.

The district include previously identified cenozoic volcanic units from bottom to top, namely plagioclase-phyric andesite lava, basaltic andesite lava flow and tufficious levels. Within the district three major fault trend with certain lateral extends emerged as NW-SE, E-W and NE-SW. When the morphology is examined, taking these main trends into consideration, it is observed that NW-SE trending faults from a boundary between the western and central parts of the mineralization area. The same trend also can be observed in the southeastern part of the mineralization area, crosscutting volcanics and metamorphics In the central part, mineralization hosting hills from north to south with approximately NW-SE trending ranges, namely Kirazlı and Çataklaya, separated by E-W trending extensional and oblique fault. Faults with similar trends determine the formation of a stepped morphology descending from north to south. NE-SW trending faults generally truncate and crosscut previously mentioned faults. Yet all mentioned trends present a complex relative temporal order based on crosscutting relations related to reactivation of previously formed deformation zones. As a different fault set, approximately N-S striking moderately/steeply dipping faults were detected on Kirazlı hill, exception from other three dominant trends. These faults are generally observed as short segments truncated by/between E-W and NW-SE oriented faults indicating that faults with N-S trend, generally pre-dates the other faults. Besides the morphology, the NW-SE fault limits the late Eocene Plagioclase-phyric andesite to the western part of the district. This unit does not crop out in the central and eastern parts of the study area and juxtaposes with the early Oligocene basaltic andesite along both NW-SE trending and nearly E-W trending extensional faults in the western part of district (Figure 4.10A).

5. ALTERATION-MINERALIZTION AND VEINS

Both field and laboratory studies were conducted to determine the features related to mineralization and the spatio-temporal relationships of these features with structural elements within the Kirazlı district. For this purpose, physical characteristics, predominant geometries and crosscutting relations of observable veins on the surface were examined and recorded. Besides, oriented sampling was carried out along pre-defined traverses approximately perpendicular/sub-perpendicular to deformational zones within the zones in the district (Figure 5.14). Thin sections those were prepared from oriented samples have been used to determine the geometric, spatial and relative temporals relations of the veins/veinlets.

In addition to field studies, drill-core samples of pre-selected drill holes and drill logs were examined to determine vertical extension of fault zones mapped on the surface, structural and mineralization textures, and vein-veinlet relations.

5.1. Alteration-Mineralization Pattern

The Kirazlı deposit located at the central Biga Peninsula include previously described porphyry and epithermal mineralizations. The high sulfidation epithermal mineralization has a reserve of 33.86 Mt at 0.69 g/t Au, 9.42 g/t Ag, and a resource of 3.056 Mt at 0.43 g/t Au, 2.71 g/t Ag (Cormier et al. 2017). The exploration works by the company “Alamos Gold Inc.” revealed the existence of prophyry type mineralization at the southern part of district. No alteration mapping was done during the field works. The alteration map by Aluc et al. (2023) was used instead.

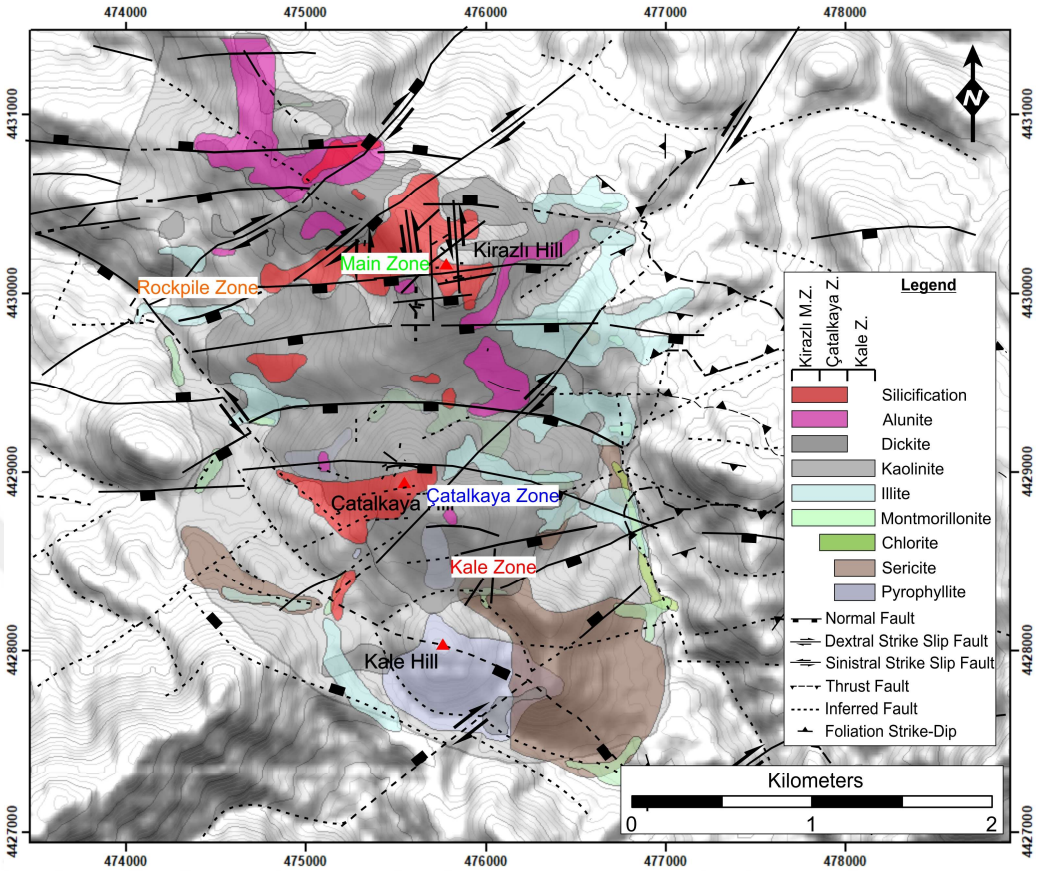

Figure 5.1. The alteration map showing the main alteration types (after Aluç et al. 2023) and structures mapped during this study.

Mineralizations from north to south occurs in main , çatalkaya and kale zones within the district (Figure 5.1). These zones are mainly exposed at the Kirazlı , Çatalkaya and Kale Hills. The HS-epithermal Au alterations and mineralization are exposed at Kirazlı and Çatalkaya Hills while the porphyry Cu alterations and mineralization are hosted by Kale and southern part of Çatalkaya hills (Figure 5.1).

Nine different mineral-based alteration zones were described by Aluç et al. (2023) as silicification, alunite, kaolinite, dickite, illite, pyrophyllite, chlorite, sericite and montmorillonite (Figure 5.1). The silicification is located at the Kirazlı and Çatalkaya hills forming the center of alteration zones with a widespread kaolinite-dickite alteration envelope. The dickite alteration is limited to southern margin of Çatalkaya Hill, and is not exposed at the Kale hill where porphyry-Cu alterations predominate (Figure 5.2A). Alunite alteration dominates NW and SE cliffs of the Kirazlı Main zone collectively forming a NW-SE trend (Figure 5.2A). As expected from a HS-epithermal system, illite, montmorillonite and chlorite-altered areas form ourter

envelope of the silicicifed and alunite-altered areas (Figure 5.2B) (Aluç et al., 2023). While the montmorillonite alteration is limited to Kale Hill, the sericite alteration neighbors the montmorillonite alteration at the east and other montmorillonite-altered rocks are generally located at western and eastern margins of mineralized area between Çatalkaya and Kale hills (Figure 5.2C).

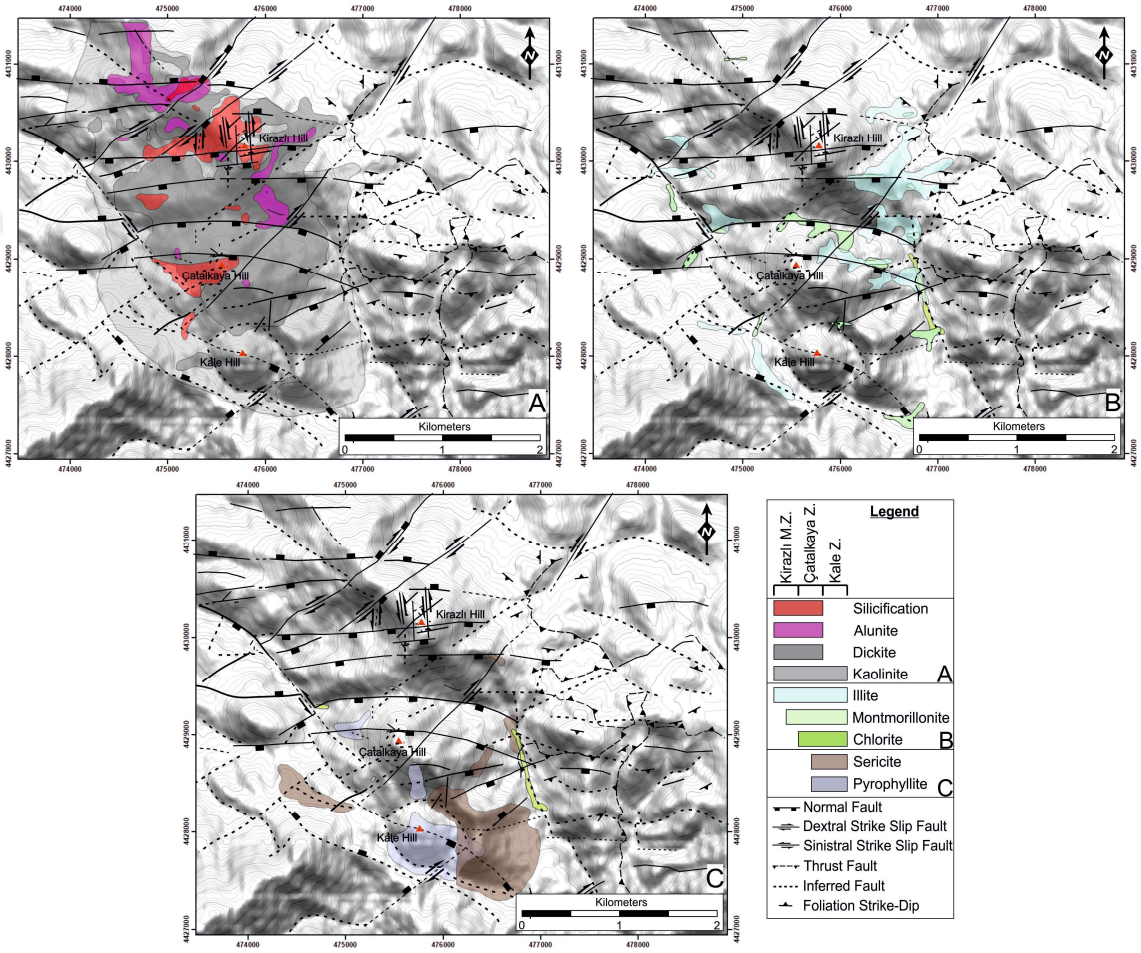

Figure 5.2. (A) and (B) The spatial distribution of HS-epithermal-style, and (C) porphyry Cu style alterations in the Kirazlı district (after Aluç et al., 2023)

5.2. Vein and Veinlets

This study has focused on the orientation, geometry and spatio-temporal asociations of the veins within the epithermal Au and porphyry Cu-style systems in the Kirazlı district. The genetic classification and association with the epithermal Au and porphyry Cu systems are commonly adapted from Aluç et al. (2023). Therefore, no

study on their genetic classification has been made in the the present study. This chapter mainly focuses on understanding of the spatial and geometric characteristics of the veins with their temporal and spatial association with the structures in the Kirazlı district. The types and nature of the veins have been investigated by (1) inspection of drill-core samples, (2) field observations and (3) petrography of vein-bearing oriented samples collected from the field. The works on the drill core samples were carried out to establish the type and temporal association between different types of vein. Since drill cores have not been oriented by the company, the orientation and geometry of the veins on the drill core remain unknown. Their orientation with the core axis is not helpful in determining their spatial association with the structures in the district. Therefore, the observations on the drill cores are mainly for the identification of types and temporal association of veins in the Kirazlı district. The field works were directed to (1) collect oriented surface samples, (2) identify the type and physical characteristics, and (3) determine orientation/predominant directions of the veins exposed at the surface. The mineralogical characteristics of the different veins were obtained from the oriented surface samples. Then, data obtained by the field and petrographical works were used to correlate the spatial and geometric association between veins and structures in the district.

5.2.1. Veins in the drill core samples

The total of 270 drill core samples were collected and examined from 18 drillholes 14 of are collared on the main zone for HS-epithermal Au mineralization and 4 of which collared on Kale zone for porphyry Cu-type mineralization . There were only 3 drill holes collared on the Çatalkaya zone, and these were drilled for the identification of the porphyry Cu system at depth. None of these intercepted both epithermal Au and porphry Cu-style alterations at the Çatalkaya zone. Therefore, no drill hole and core samples were available to test transition from epithermal to porphyry-style systems. Consequently, these 3 drillholes from "Çatalkaya" zone discarded from sampling program in the district. Likewise, the studies deciphering the distinguishing features of the style and basic characteristics of veins from epithermal Au and porphyry Cu-style systems were conducted on drill core samples from the Main and Kale zones. Locations of drillholes for sampling are presented in Figure 5.3.

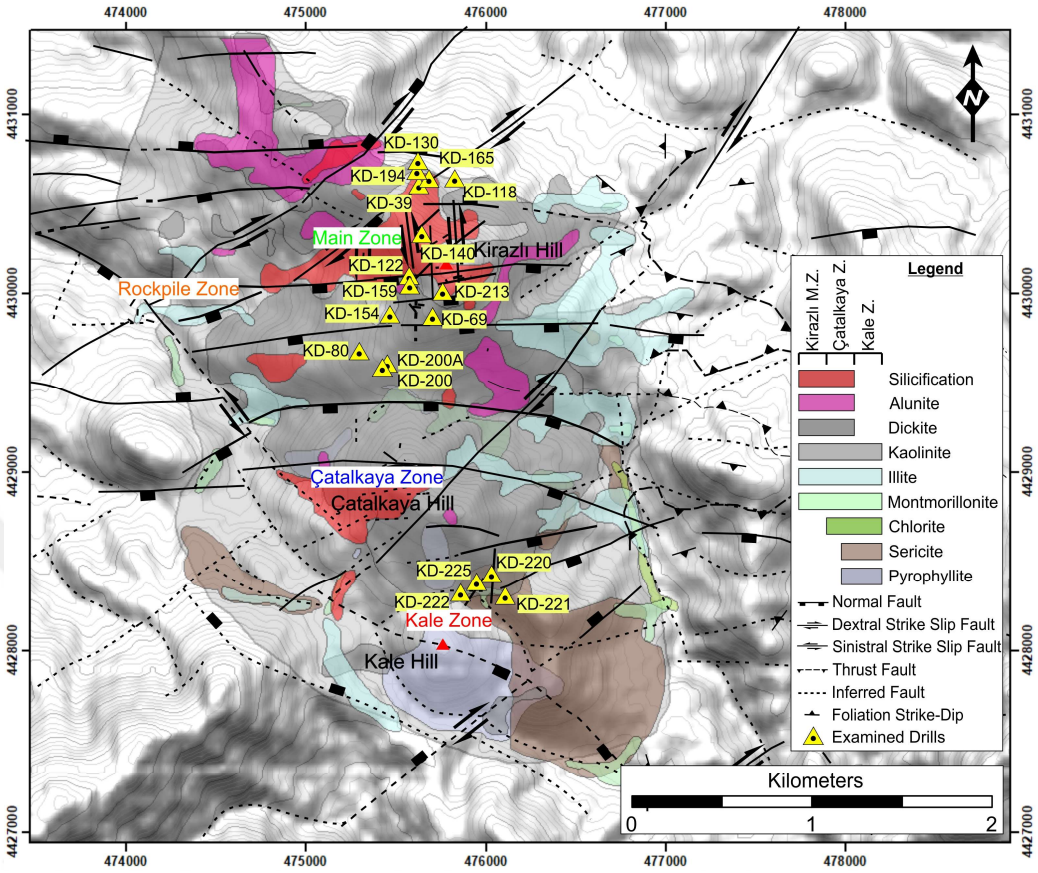

Figure 5.3. Topography map with alterations and structures also showing the locations and hole ID of the drill holes for core sampling in this study (alteration map after Aluç et al.,2023)

5.2.1.1. Porphyry Cu-style veins

The mineralogical assemblage, textural and crosscutting relations of the veins in the drillcores enabled the identification of four types of vein/veinlets in the porphyry Cu-style mineralization. These include early-stage quartz-only veins, main porphyry stage quartz-sulfide veins, sulfide-only veins and late stage carboanate veins.

Early stage quartz-only veins are classified as A-veins (Aluç et al. 2023) and generally dominate in core samples collected from deeper intercepts of the drillholes intersecting the porphyry Cu-style alteration. The quartz-only veins are generally thick (1-2 cm), wormy, parallel to subparallel or stockwork vein arrays without any sulfide centerline or margin (Figure 5.4A-B). These veins are offset by fractures normal to margins and filled with sulfide minerals (Figure 5.4B). The early quartz-only veins are traversed (cut) by quartz-sulfide and sulfide-only veins (Figure 5.4B). According to Aluç et al. (2023) subsequent quartz-sulfide and sulfide-only veins are classified as B-veins and

D-veins, respectively. These subsequent veins are considered as the veins in main porphyry Cu mineralization phase. The Quartz-sulfide veins present a straight, sheet-like to parallel/subparallel vein arrays with sulfide centerline (Figure 5.5A-D). Halos of secondary biotite and/or K-feldspar typically enveloping the A- and B-veins, were not recognized in the core samples.

The sulfide-only veins with quartz-sericite halo (envelope), post-date the quartz-only and quartz-sulfide veins (Figure 5.6A-B), and are formed by filling a subsequent fractures truncating the previous vein phases (Figure 5.5E,F). These typically form cross cutting network of vein arrays forming stockwork vein pattern (Figure 5.6B), and are classified as D-veins within the phyllic alteration zone of the Kirazlı porphyry Cu system (Aluç et al. 2023). (Figure 5.6). Late stage carbonate veins are composed of calcite. They occur as truncating all earlier vein phases emplaced in both subsequently formed fractures and re-opened sulfide-bearing veins (Figure 5.7). Relatively thick carbonate veins are commonly barren with calcite-only nature (Figure 5.7A and B whereas relatively thinner and straight ones accompanied by pyrite or oxidized pyrite (Figure 5.7C,D).

Figure 5.4. Drill cores with early-stage A-veins (A) arrays of veins and (B) offset by micro faults

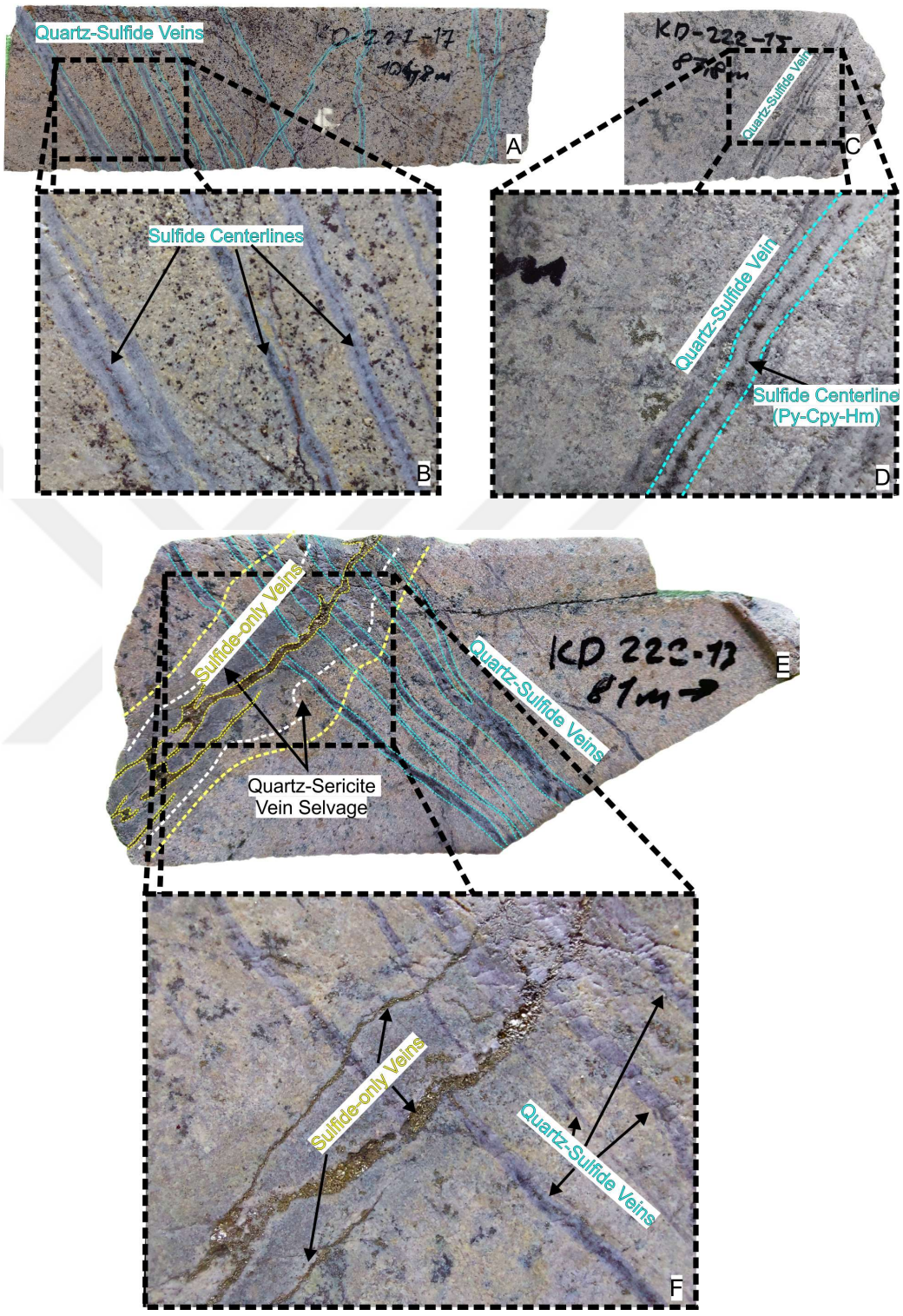

Figure 5.5. Drill core samples showing (A) to (D) quartz- sulfide, and (E) and (F) sulfide only veins post-dating the quartz-sulfide veins.

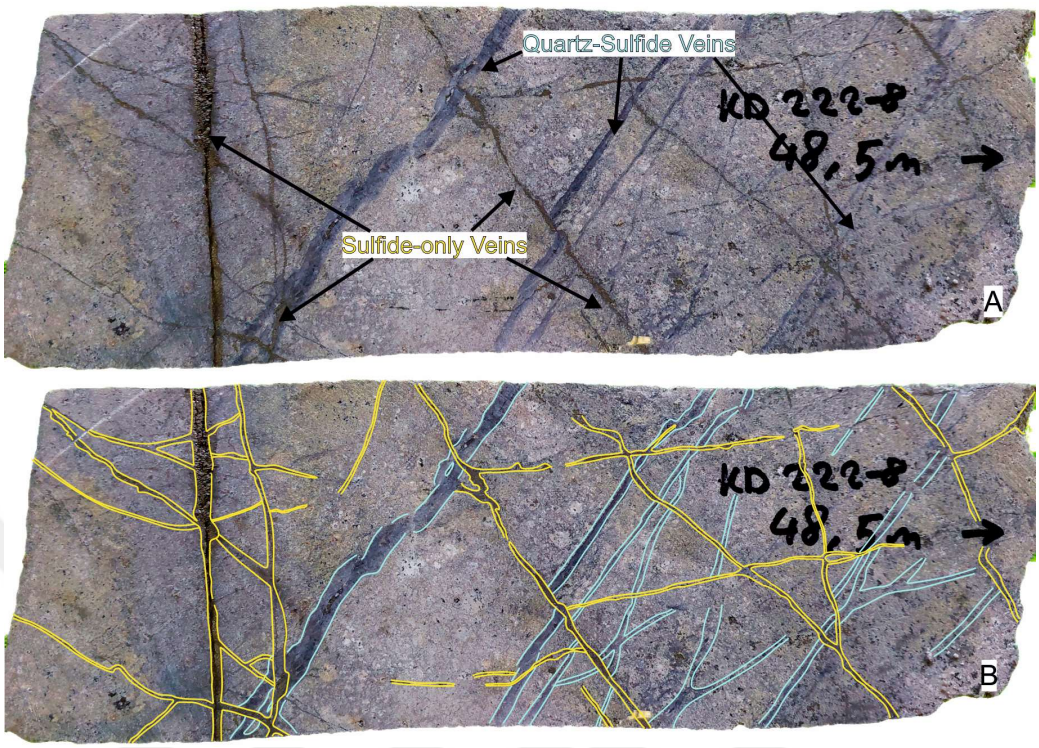

Figure 5.6. Drill cores showing (A) sulfide only veins, and (B) stockwork veins post-dating the quartz-sulfide veins

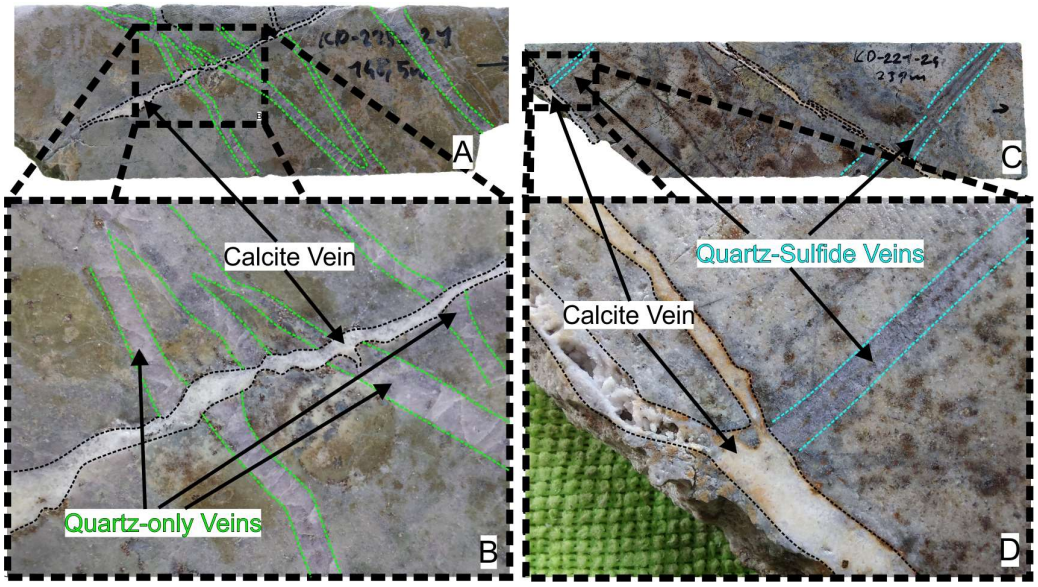

Figure 5.7. Drill cores showing (A) calcite-only late carbonate vein, (B) close-up view of A, (C) pyrite-bearing late carbonate vein and (D) close up view of C

5.2.1.2. HS-epithermal Au-style veins

The veins within the HS-Epithermal Au-style alterations are scarce, and limited number of veins have been identified only in few drill holes intercepting the Main Zone at the Kirazlı Hill (Figure 5.3). The HS Epithermal Au-style system is composed of the main body of silicification composed entirely of vuggy textured quartz (Figure 5.8), and residual to massive quartz. They are hosted by phreatic breccia, and form the core zone of the HS epithermal Au system. The available veins in the epithermal Au system are mostly hosted either by silicified phreatic breccia and cross-cutting pyrite-rich quartz veins.

The silicified phreatic breccia is the main body of silicification, and is almost a vertical and trends in N-S direction. The silicification in the phreatic breccia is by generation of massive gray quartz accompanied by sulfides cementing the clasts (Figure 5.9). It is generally accompanied by hydrothermal vein breccia and crackle breccia (Figure 5.10) indicative of fluid assisted brecciation and hydrolic fracturing. This phase is mostly observed at upper and middle portions of the HS epithermal Au system, and appears to be background for various types of subsequently truncating veins.

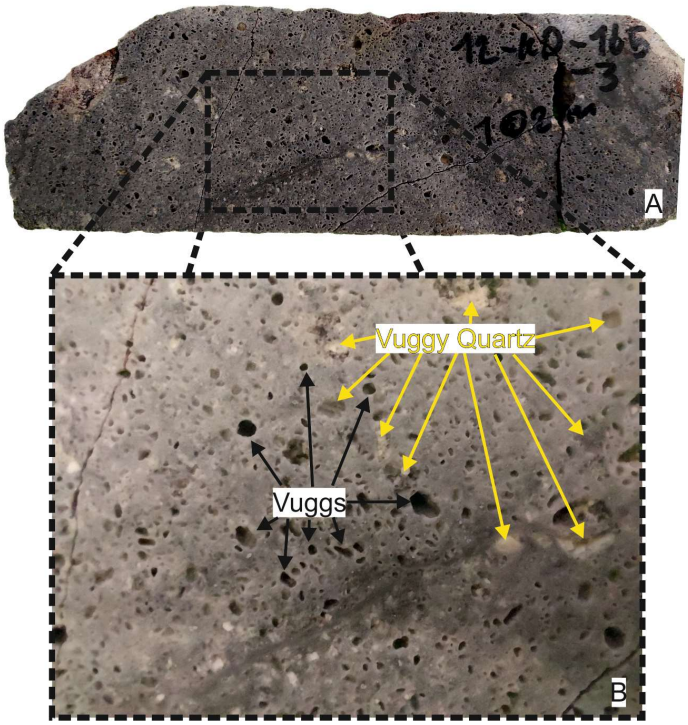

Figure 5.8. (A)Vuggy-textured quartz from the drill cores within the HS epithermal Au system and (B) close-up view of A.

The veins in the order of their formation in the epithermal Au system include (1) quartz-sulfide veins accompanied by milky-white quartz center frequently, (2) straight gray-quartz veins crosscutting the quartz-sulfide veins and, (3) white quartz phase mostly along straight, extensional fracture arrays truncating the earlier vein phases. The abundance and type of the cross-cutting quartz or quartz-sulfide veins changes with depth in the drill holes.

Figure 5.9. Drill core showing the dark-gray quartz-sulfides cementing the breccia.

The quartz-sulfide veins are of straight veins hosting mostly pyrite±chalcopyrite. These veins mostly have a massive-sulfide margin with or without white-quartz center (Figure 5.10 and 5.11) in deeper portions of the main zone. The difference between veins from different depth may indicate transitition from hydraulic to stress-dominated fracturing regime.

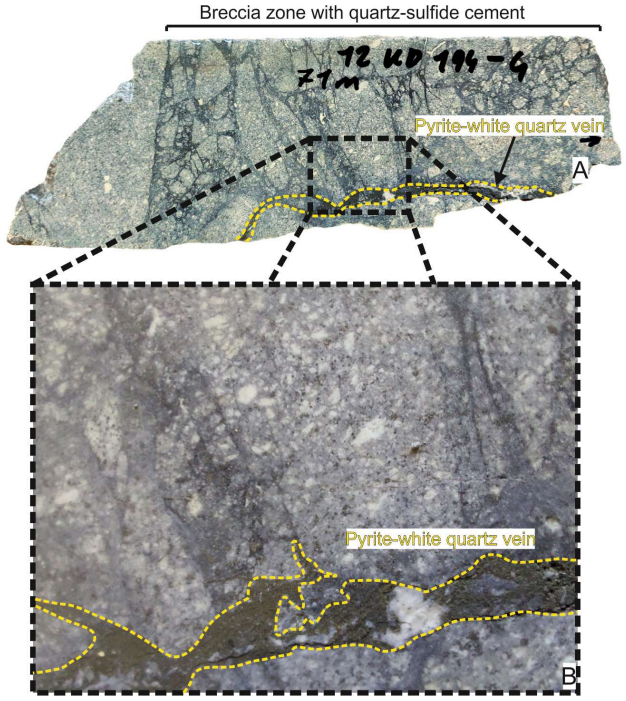

Figure 5.10. Drill core (A) showing dark grey quartz cement, vein breccia and (B) cross cutting quartz-sulfide veins

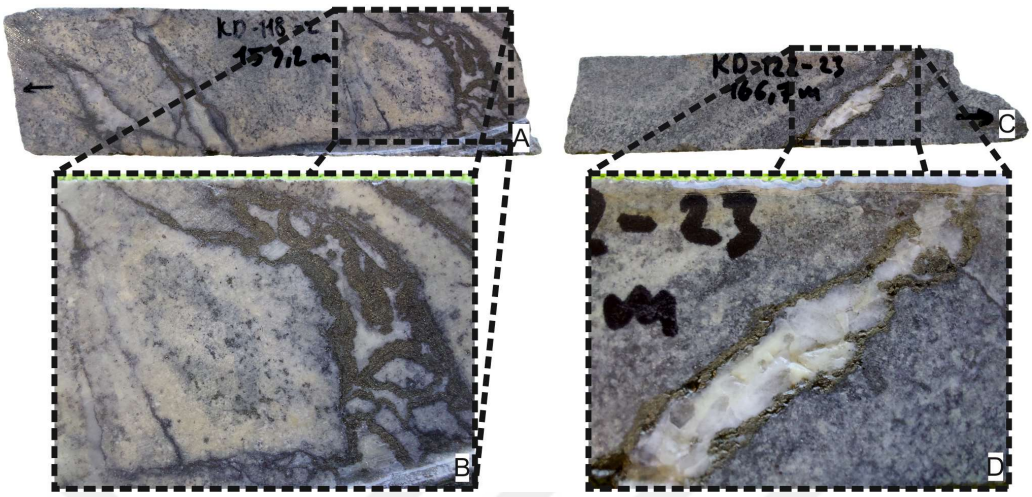

Figure 5.11. A,C) Drill cores showing quartz-sulfide veins, (B) close view of A and (D) close view of C

Unlike to quartz-sulfide veins, the straigth gray quartz veins do not contain sulfide minerals, and post date the massive gray quartz cement in the phreatic breccia and quartz-sulfide veins in the epithermal system (Figure 5.12A-B). These veins differ from the earlier phases by their micro-crystalline quartz (Figure 5.12B) and smaller relatively rounded vein filling clasts (Figure 5.12A).

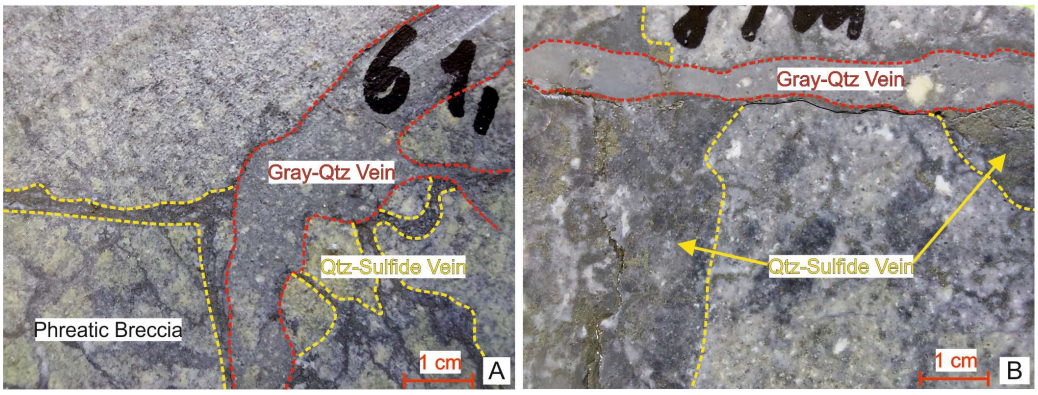

Figure 5.12. (A) and (B) gray quartz vein crosscutting phreatic breccia and quartz-sulfide veins.

The latest white quartz veins mostly occur as straight and extensional fracture arrays truncating the quartz-sulfide and gray-quartz veins(Figure 5.13A-B). They do not contain sulfide minerals unlike the earlier quartz-sulfide veins. New extensional fracture formation and contiuous extension of previously formed veins may be the evident of continuous syn-mineral regional extension during the last phase.

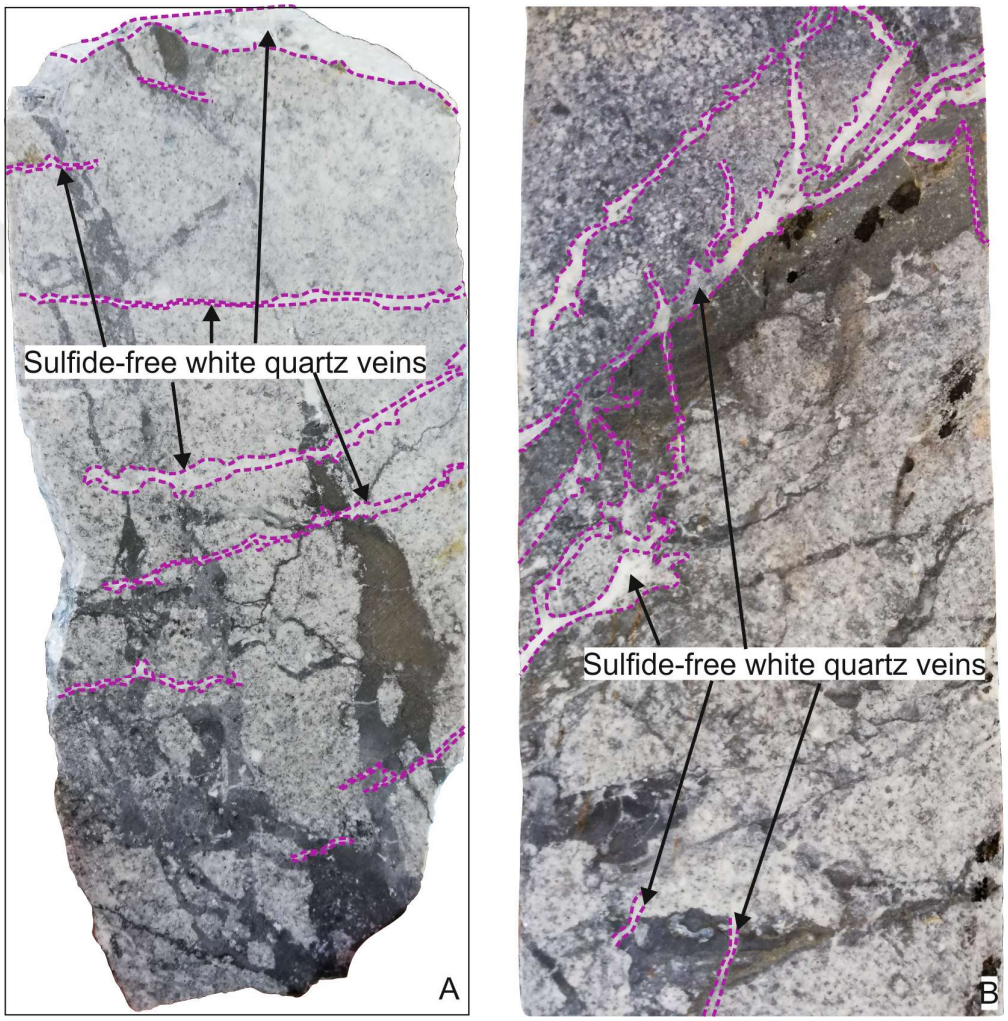

Figure 5.13. Drill cores showing white sulfide-free quartz veins truncating (A) gray quartz vein and (B) quartz-sulfide veins.

5.2.2. Veins on surface and predominant vein orientations

The vein types and predominant vein direction were identified during the field works and petrographical analysis of the oriented surface samples. The strike and dip of the veins identified on the surface exposures were measured. The strike and dip of the micro veins/veinlets not observable by the naked eye were measured by petrographical examination of the oriented samples. The oriented-sampling was conducted along 6 lines traversing the Main, Çatalkaya and Kale zones (Figure 5.14). Of the, 125 oriented surface samples, 103 was sawed to form chip samples for thin-sectioning for petrographical analysis. The petrographical analysis and measurements enabled the identification of predominant vein orientation and relative timing of different vein types on the surface samples.

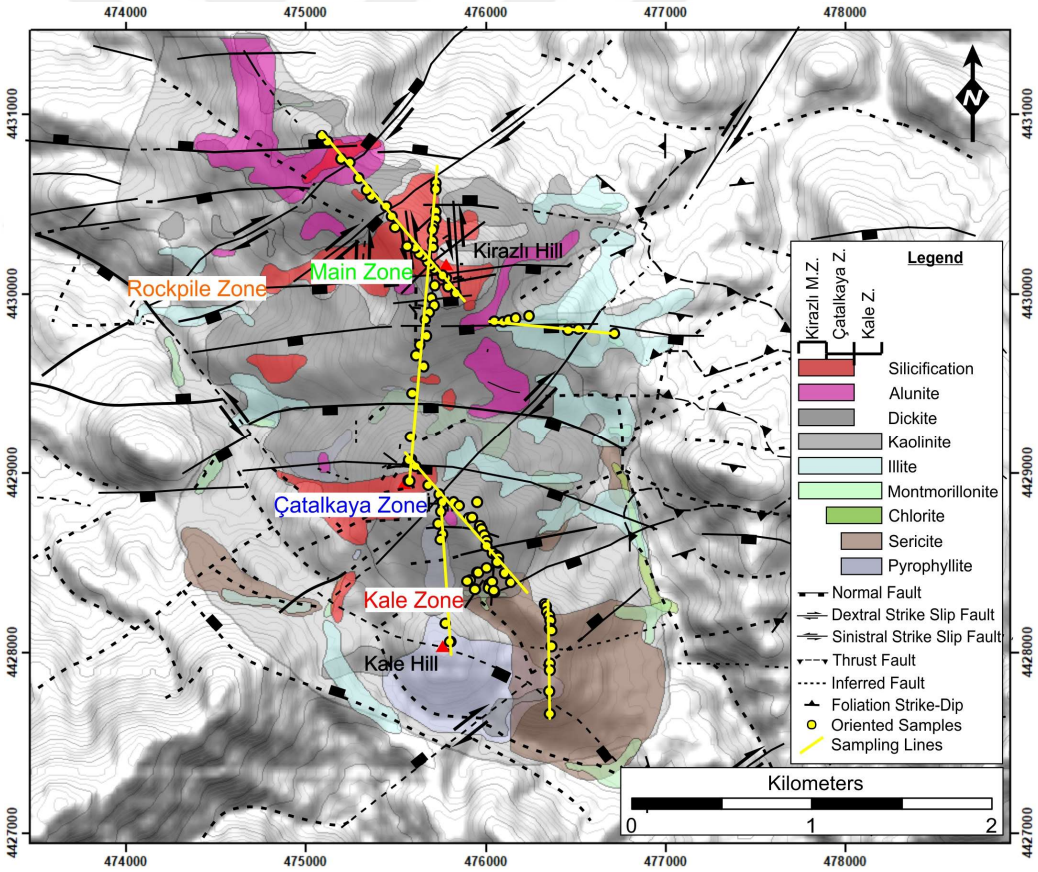

Figure 5.14. Topography map with alterations, structures, sampling lines and locations of oriented samples (alteration map after Aluç et al.,2023)

5.2.2.1. Porphyry Cu-style veins/veinlets

For the determination of predominant vein/veinlet orientation within porphyry Cu mineralized area, strike and dip of 100 veins/veinlets from 40 chip samples have been measured (Appendix-A). Rose plot, stereographic projection and contour diagram from poles of vein planes have been plotted (Figure 5.15). These plots revealed two preferred orientation of veins; s striking in N65°-85°E and N25°-35°W and dipping towards ENE-WSW with dip amount of 55°-65° due northwest and vertical. Majority of NW-SE veins nearly have vertical orientations besides the ones dipping due southwest between 65°-70°(Figure 5.15).

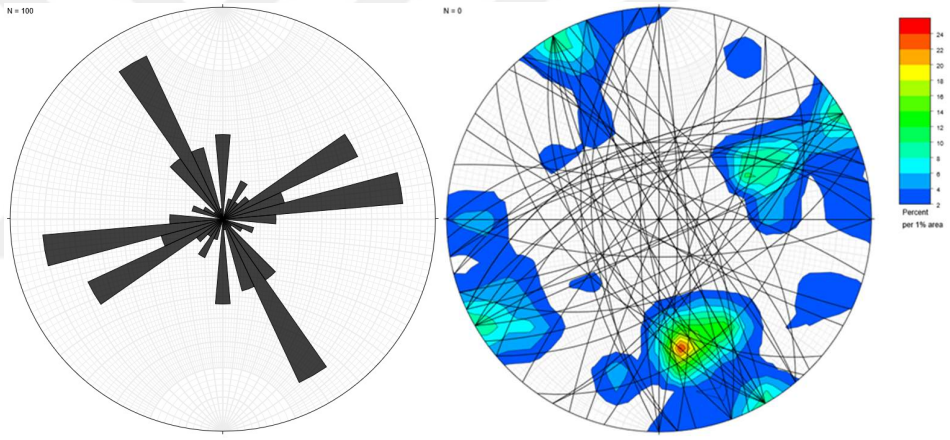

Figure 5.15. Stereographic projection and contour diagram from poles of vein planes measured from chip samples

Since the intense clay alteration and oxidation obliterated most of the veins at the surface, it has not been possible to identify all vein types defined by drillcore examination. Most of the straight B-type (quartz-sulfide veins) and stockwork type D-veins (sulfide-only veins) were oxidized to form quartz-goethite veins (Figure 5.16A-D), and the measurements were conducted on these veins. The predominant strike direction of these veins are N°15-35°W, N80°-85°E for B-veins and N35°-45°E, N30°-50°W, N-S for D-veins (Figure 5.17A,B).

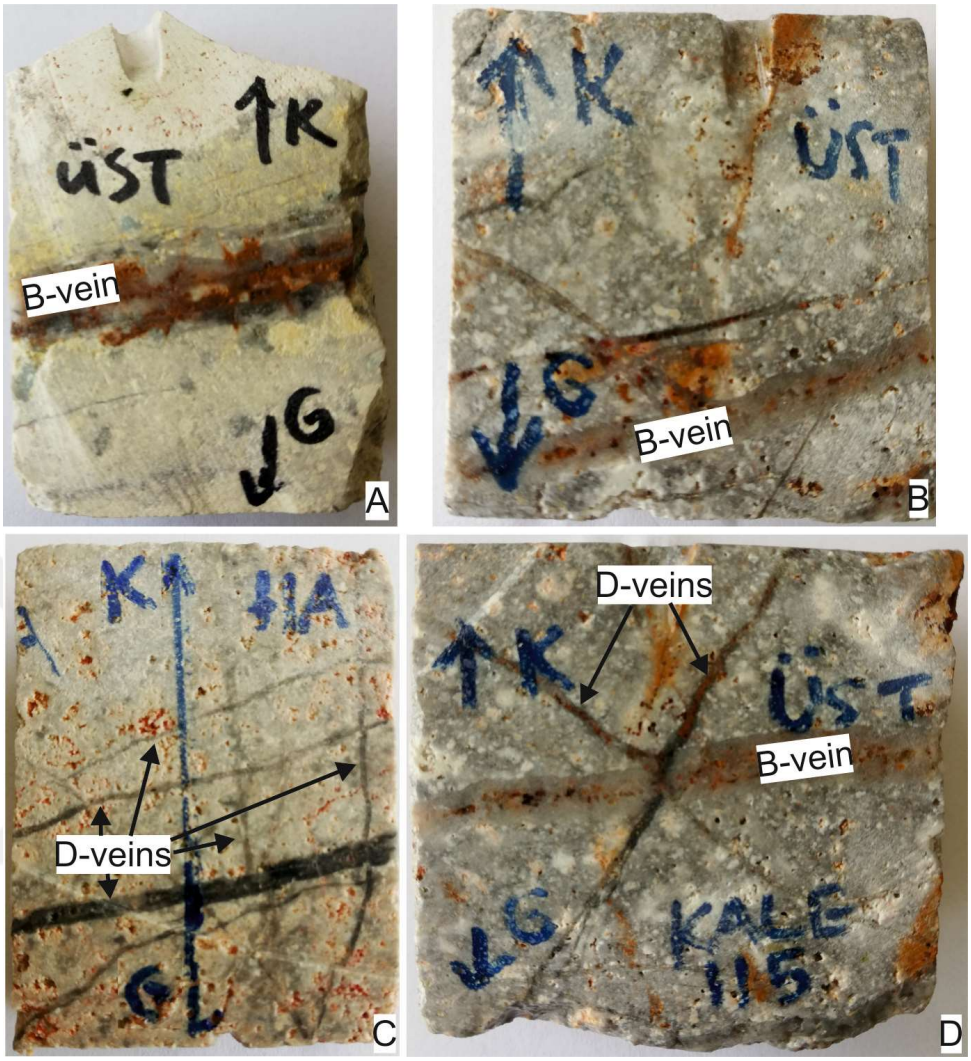

Figure 5.16. Oriented samples showing (A) and (B) Oxidized B-type (quartz-sulfide veins) and (C) and (D) stockwork type D-veins, note that the N and S are shown as "K" and S", respectively on the samples.

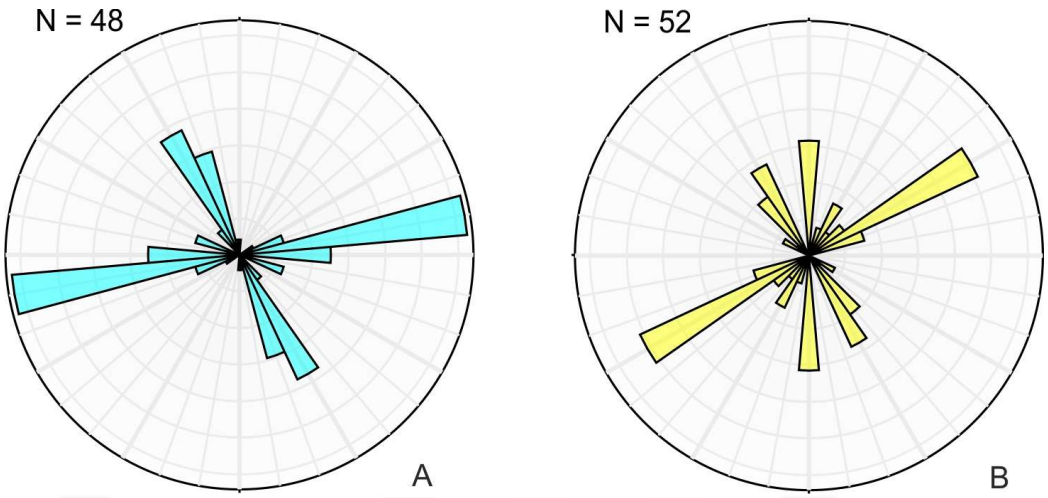

Figure 5.17. (A) The predominant strike direction of B-veins and (B) D-veins from chip samples.

The petrographical examination of the oriented thin-sections from chip-samples revealed that the vein/veinlets predominantly strike in N°15-35°W, N80°-85°E and N35°-45°E for the quartz veins. Quartz crystals within these veins are commonly blocky-elongated crystals (Figure5.18A-F). The elongated quartz crystals are formed perpendicular and subperpendicular to vein margins (Figure5.18A-F). Most of the elongated quartz crystals are identified as stretched blocky crystals (Figure 5.18E and F). Streched crystals, multi-phase vein texture and subperpendicular elongated crystals are indicative of syn-tectonic mineralization and multiple crack-seal events (Figure 5.18E-F). Additionally, the veins also contain centerline oxidized opaque minerals, mostly goethite, fine-grained quartz crystals and clay patches (Figure 5.18A-B). Approximate elongation direction of quartz crystals within the veins generally indicate a NW-SE directed extension (Figure 5.18A-D and F).

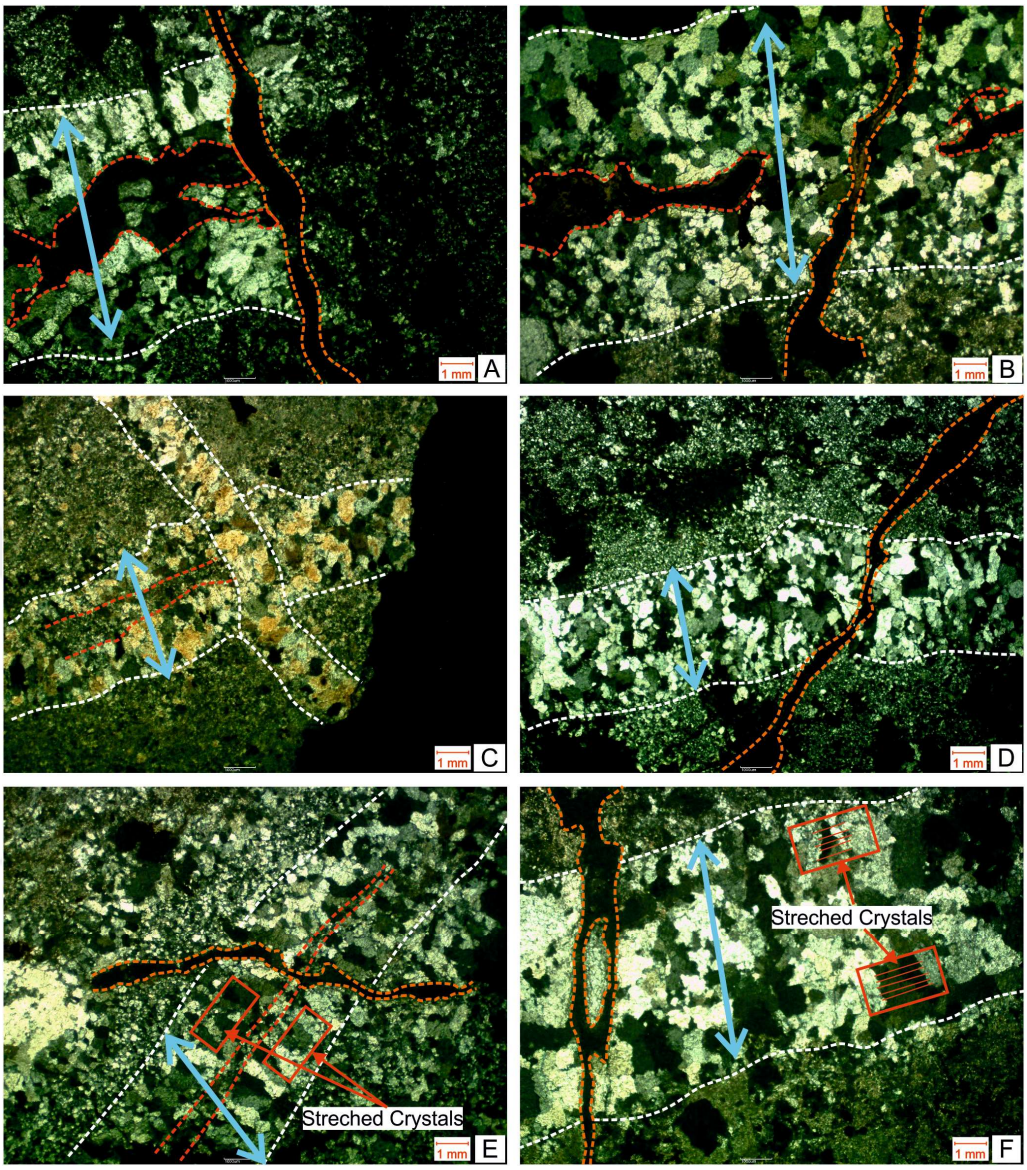

Figure 5.18. Photomicrographs illustrating (A) to (F), quartz veinlets from oriented thin sections, elongated and stretched quartz minerals within veins. Note that blue arrows showing extension directions based on elongation axes of quartz minerals.

5.2.2.2. Epithermal veins/veinlets

The intense oxidation on the surface in Main Zone prevents the identification of vein/veinlet phase from oriented samples. Despite the difficulties in finding suitable veins on the oriented samples to measure the orientation of the veins within the main zone and HS epithermal Au system, a limited measurement were able to be taken from

some the fractures where quartz veins/veinlets are hosted. However, silicified vein breccias were observed in samples from the margins of the main silicification zone.

Various type of breccia textures were recognized both on the oriented chip-samples and petrographical analysis of them (Figure 5.19A-C). The breccias commonly contain angular clasts with variable clast size and high clast/matrix ratio indicating the fluid-assisted brecciation in earlier stages (Figure 5.19A and, Figure 5.20B,C). Towards later stages, the clast/matrix ratio drops (Figure 5.19B) or clast are observed as milled (Figures 5.19C and 5.20D) indicating that brecciation occured under a more effective tectonic contribution. Yet it is reported by Jebrak (1997) that fluid-assisted brecciation generally prefer to occur within pre-existing weak zones formed by increasing regional stress. The quartz textures on the thin sections, chip samples and drillcores suggests that the silica core include vuggy-quartz texture (Figure 5.20A), hydrothermal breccia veins and subsequently formed veins with decreasing clast/matrix ratio may indicate increasing tectonic contribution. Petrographical analyses on the hydrothermal veins generally suggest that the HS-epithermal mineralization formed under a NNE-SSW extension (Figure 5.20C-F).

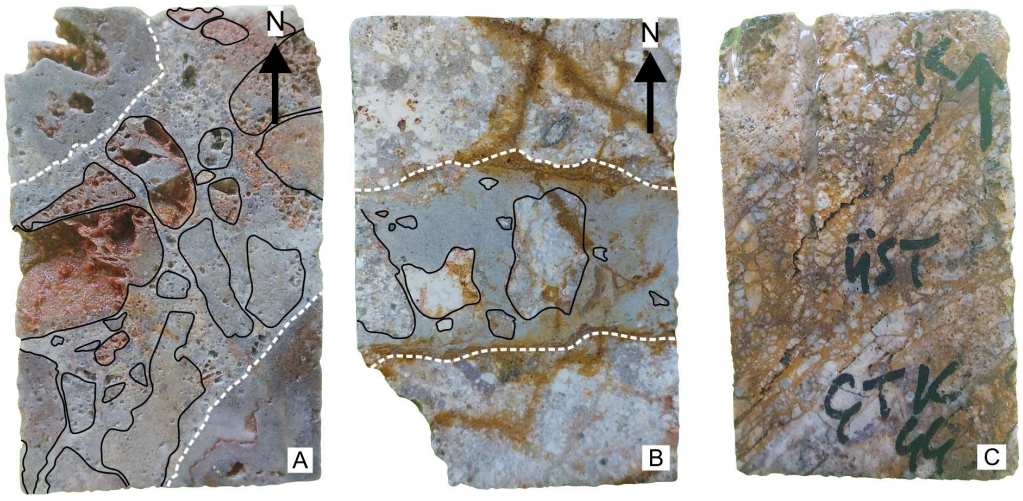

Figure 5.19. Chip samples showing various types of silicified breccia (A) vein containing silicified angular vein breccia with high clast/matrix ratio, (B) vein with low clast/matrix ratio, and (C) oxidized vein array with milled clasts formed under tectonic contribution. Note the direction of North is marked on the samples.

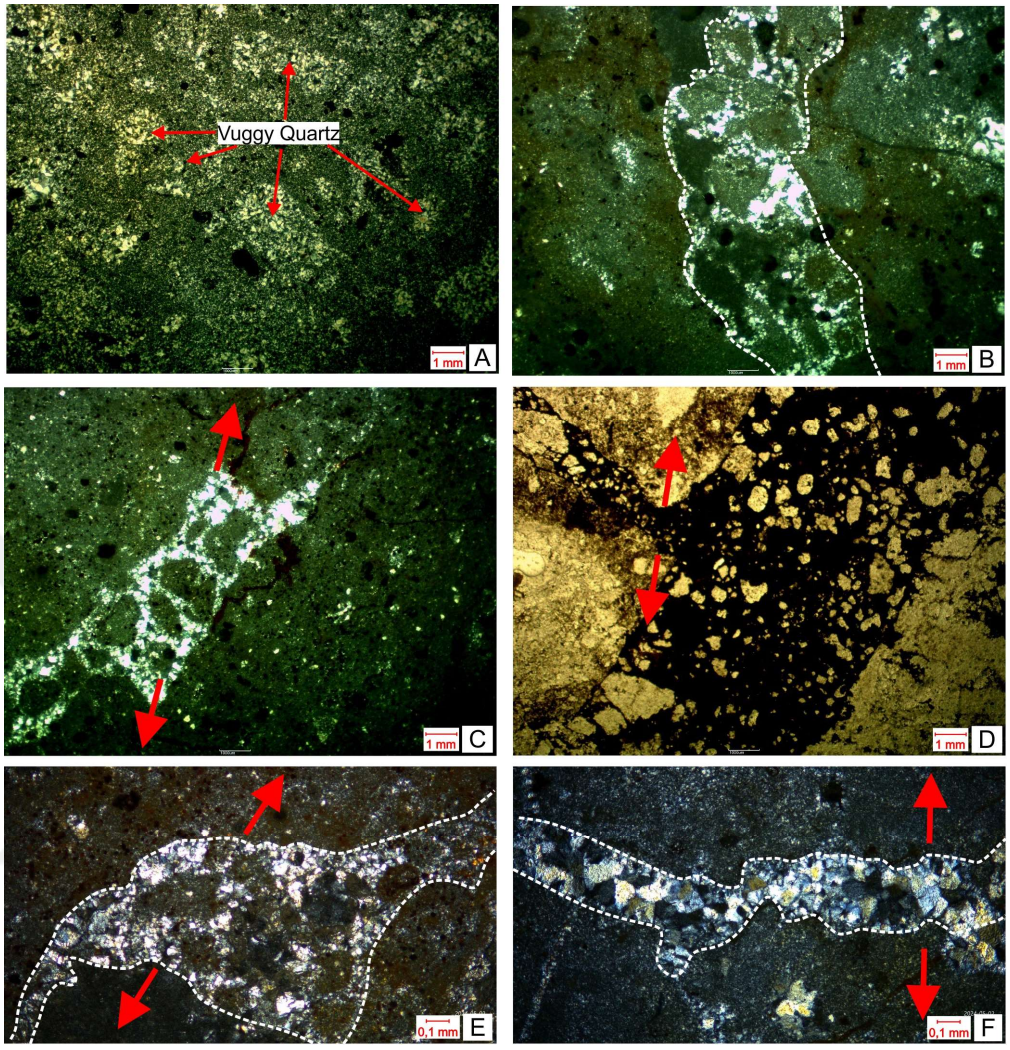

Figure 5.20. Photomicrograph illustrating (A) vuggy-quartz from silica core, (B) and (C) hydrothermal-breccia veinlets, (D) oxidized vein with milled breccia clasts, (E), (F) quartz veinlets exampling NE-SW and N-S extension. Note that red arrows pointing direction of extension.

5.2.2.3. Surface measurements of vein orientations

The surface measurement aiming the determination of predominant orientation of porphyry Cu and epithermal Au-style vein/veinlets include 429 (Appendix-A) measurements from 41 outcrops covering Main, Çatalkaya and Kale Zones, Selected locations are presented in Figure 5.21. The strike and dip of the veins were plot on the rose diagrams. The rose-plots were grouped into 23 zones (Figure 5.21) based on spatial distribution of examined outcrops.

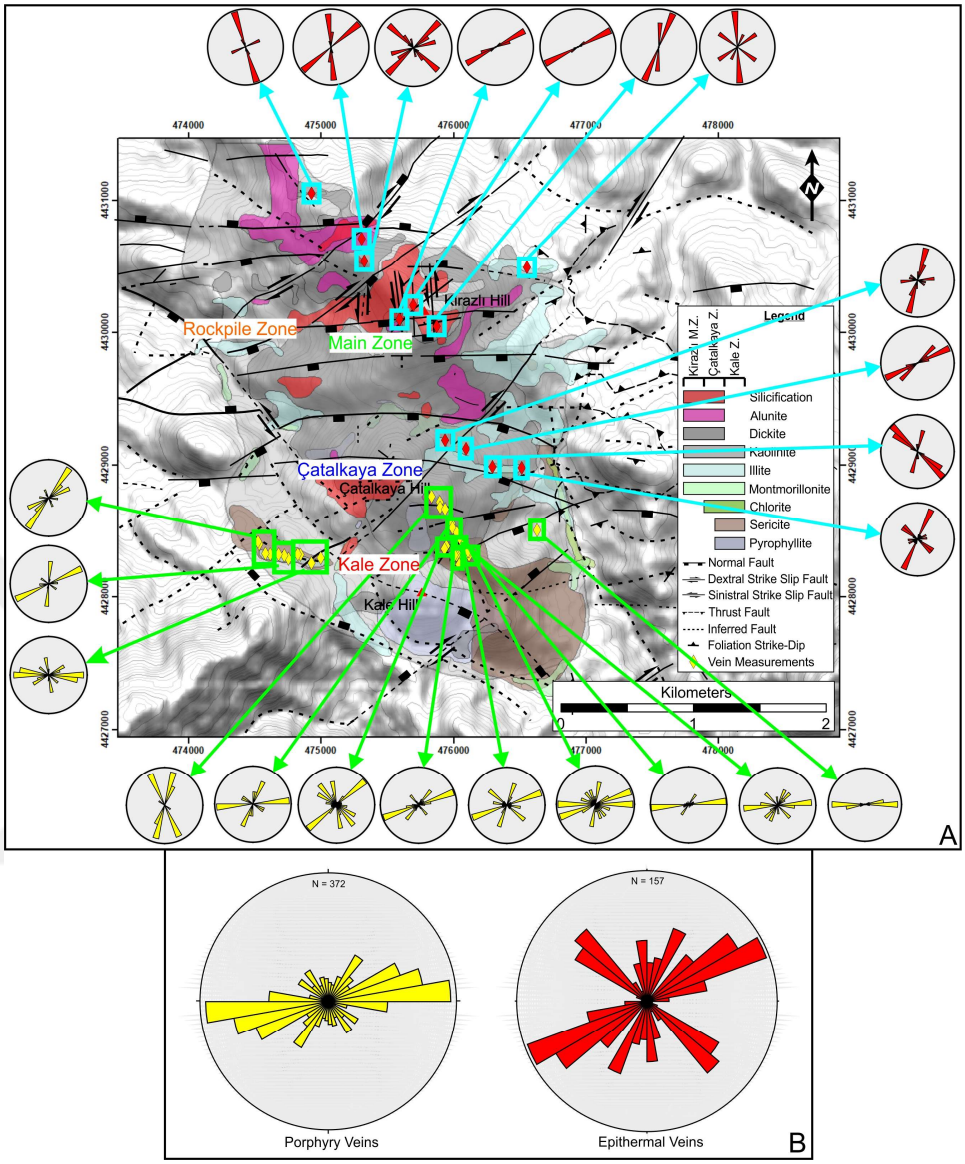

Figure 5.21. (A) Geological map with alterations (after Aluç et al. 2023) and observation points where vein orientations are measured at the field, and (B) predominant strike orientation of the porphyry Cu and epithermal Au-style alteration (yellow colored rose plots for the measurement on porphyry Cu-style and red for the epithermal Au-style veins)

Pervasive oxidation and supergene clay alteration masked and destructed the hypogene alterations and veins at the surface. Therefore, type, characteristics, geometry and attitude of most veins have not been adequately measured. However, a few spots where these features for porphyry Cu and epithermal Au-style systems are still preserved, were available (Figure 5.22A). The textural features and type of the veins including quartz-sulfide B-veins and sulfide-only D-veins from the porphyry Cu (Figure 5.22A-D), and vein breccias in the epithermal Au system (Figure 5.23A,B) were identified.

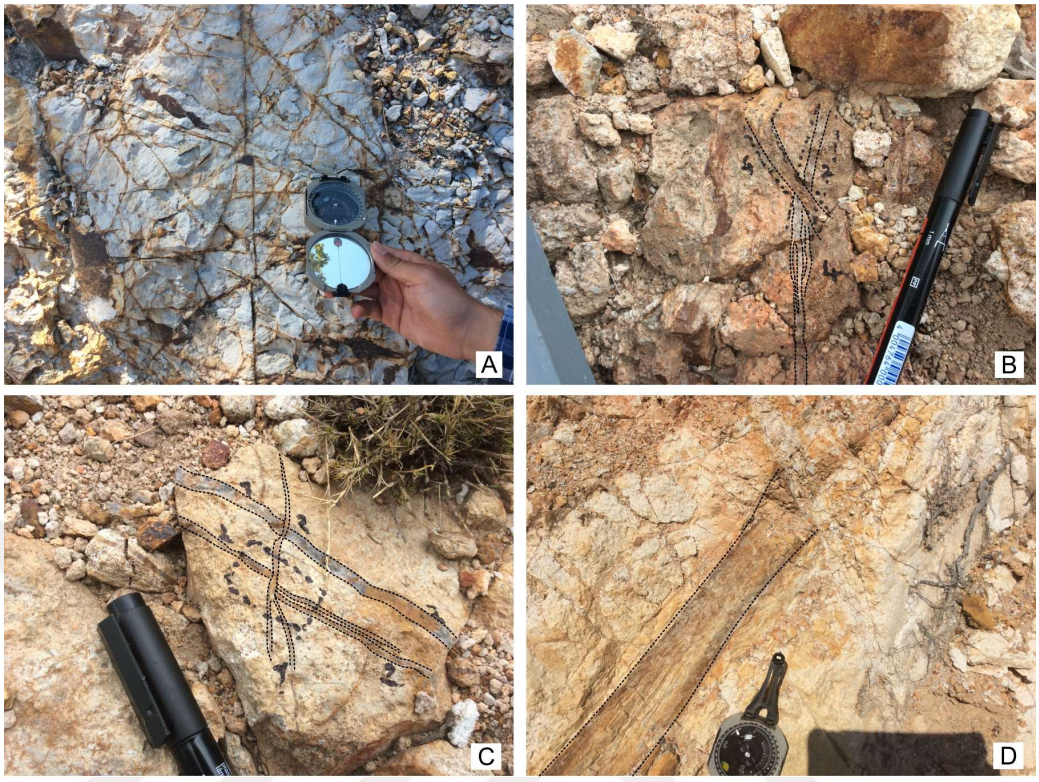

Figure 5.22. Field photos showing (A) stockwork veins within the epithermal Au exposure, (B), (C) and (D) quartz-sulfide (B-veins)

The recognition of the stockwork and B-type veins on the surface is indicative of exhumation and erosion/oxidation of the intermediate (phyllic alteration) and deeper levels (potassic alteration) of the porphyry Cu system.

The stockwork veins (phyllic alteration level) are exposed at smoothly sloping ridge between the Çatalkaya and Kale Hills to east and west (Figure 5.21). The B-veins are especially exposed at the area to the northwest of Kale Hill where they occur as 5-10 cm thick veins or vein zones. Unlike the veins observed within the other locations elsewhere (Figure 5.21B,C) these veins have relatively larger along strike extension (Figure 5.21D).

The mesasurements on the porphyry Cu-style alteration rose-plots based on strike orientation of veins/veinlets within the porphyry Cu style alteration, indicate the strike directions ranging between N75°-85°E, N45°-55°W and N40°-50°E (Figure 5.21B). The most prodominent vein orientation of N75°-85°E direction refer to the predominant direction of the B-veins while strike directions of N45°-55°W and N40°-50°E show the predominant orientation of stockwork and D veins.

Measurements on orientation of the veins within the epithermal Au-style alteration were conducted on vein breccia and vein/veinlets exposed on smooth to moderately sloping ridges on the SE and NW sectors of the main zone. These locations refer to a transition from the residual-quartz core and enveloping quartz-alunite alteration zones of main zone and dickite alteration zone northwest of Çatalkaya zone (Figure 5.21A). The vein breccia is the most common vein type at the main zone (residual quartz core and quartz-alunite alteration zone), and generally reflect the fluid-assisted breccia texture with high clast/matrix ratio and no or slightly re-oriented clasts (Figure 5.23A and B). They are generally of 5-8 cm thick quartz-cemented or oxidized sulfide-cemented type. The veins/veinlets are commonly exposed at dickite alteration (marginal zones), and are of relatively thin (0.5-1.0 cm) breccia-free quartz veins. Based on the rose-plots prepared from measured vein/veinlets orientations, three predominant strike directions have been identified as as N50°-70°E, N40°-60°W and N20°-30°E (Figure 5.21B). There are also veins striking in and N5°-10°W.

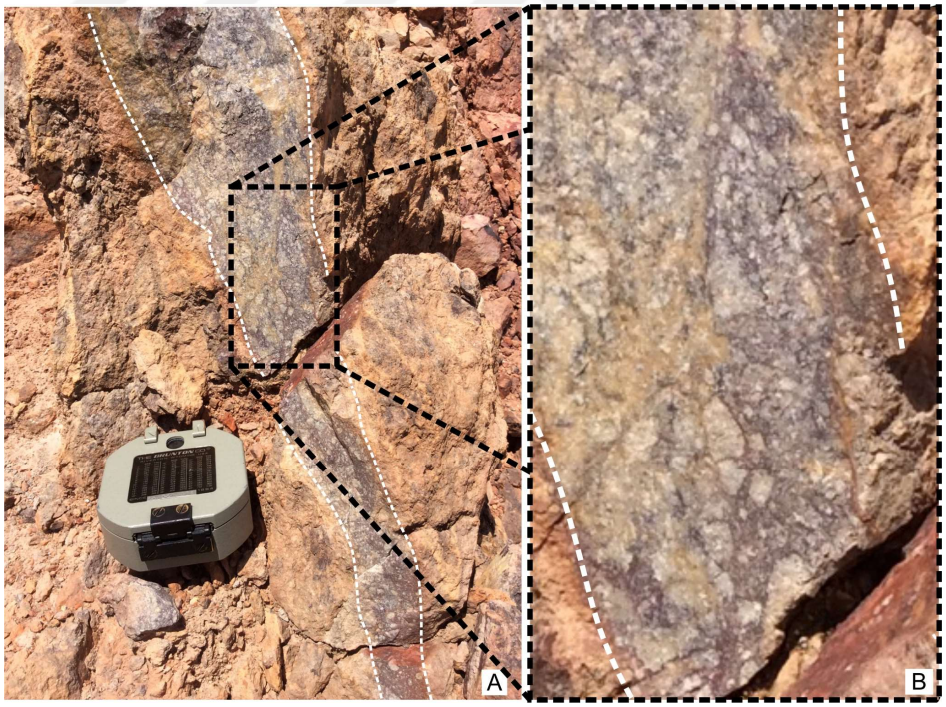

Figure 5.23. Photo showing the, (A) veins breccias from the epithermal Au system and (B) close up view of A.

5.3. Association of Au-Grade

The association of gold grade and vein type/texture with depth throughout the drill holes are determined by assay data provided by company. The assay data include gold grades from 240 drill holes within the mineralized area. The gold grade of 1.5-3.0 ppm were taken as high grade ore zones and were determined by Leapfrog-Geo (Bentley-Seequent) software. The great majority of the high gold grade zone comes from the holes intersecting the thicker zones of HS epithermal Au-style mineralization. As the drill holes intersecting the porphyry Cu-style alterations are limited in number, it is not sufficient to make a characterization of gold mineralization and gold grade in this type. However a schematic cross-section including successive alterations and ore zone is presented based on the data from few drill holes. (Figure 5.24B,F) The available assay data revaled that the high grade gold dominate within a N-S trending body hosted by main zone between the elevations of 450 and 750 meters (Figure 5.24A-E). The drill core observations on the type and characteristics of the veins in this study showed that high gold grade zone overlap mostly with N-S trending and vertically oriented phreatic- breccia zone and residual quartz core of the system (Figure 5.24D,E). The distribution of high grade zones indicate that the mineralization acccompanied to high permeability zones originated from volcanic breccia-lithic tuff layers, phreatic breccia bodies and hydrothermal breccia zones. Yet, the high gold grade also exhibits an overall layer-parallel nature limited mostly within the lithologic boundary of the volcanic breccia and lithic tuff layers in the volcanic-volcaniclastic rocks of the district (Figure 5.24B,D). This may also indicate the stratabond nature of gold mineralization implying a lithologic control on the gold mineralization.

The temporal association of veins and their textural characteristics within the drill cores and assay data suggest that the primary permeability was lithologically controlled and fluid flow should have focused along volcanic breccia and lithic tuff layers and inter-connected fracture arrays. Subsequent acid leaching and residual to vuggy textured quartz generation should have promoted the secondary permeability and early Au-Ag mineralization alongside the residual-vuggy quartz core of the system. Subsequent vertical phreatic zone coincide with the high Au grades accompanied by significant increase in base metal concentration.

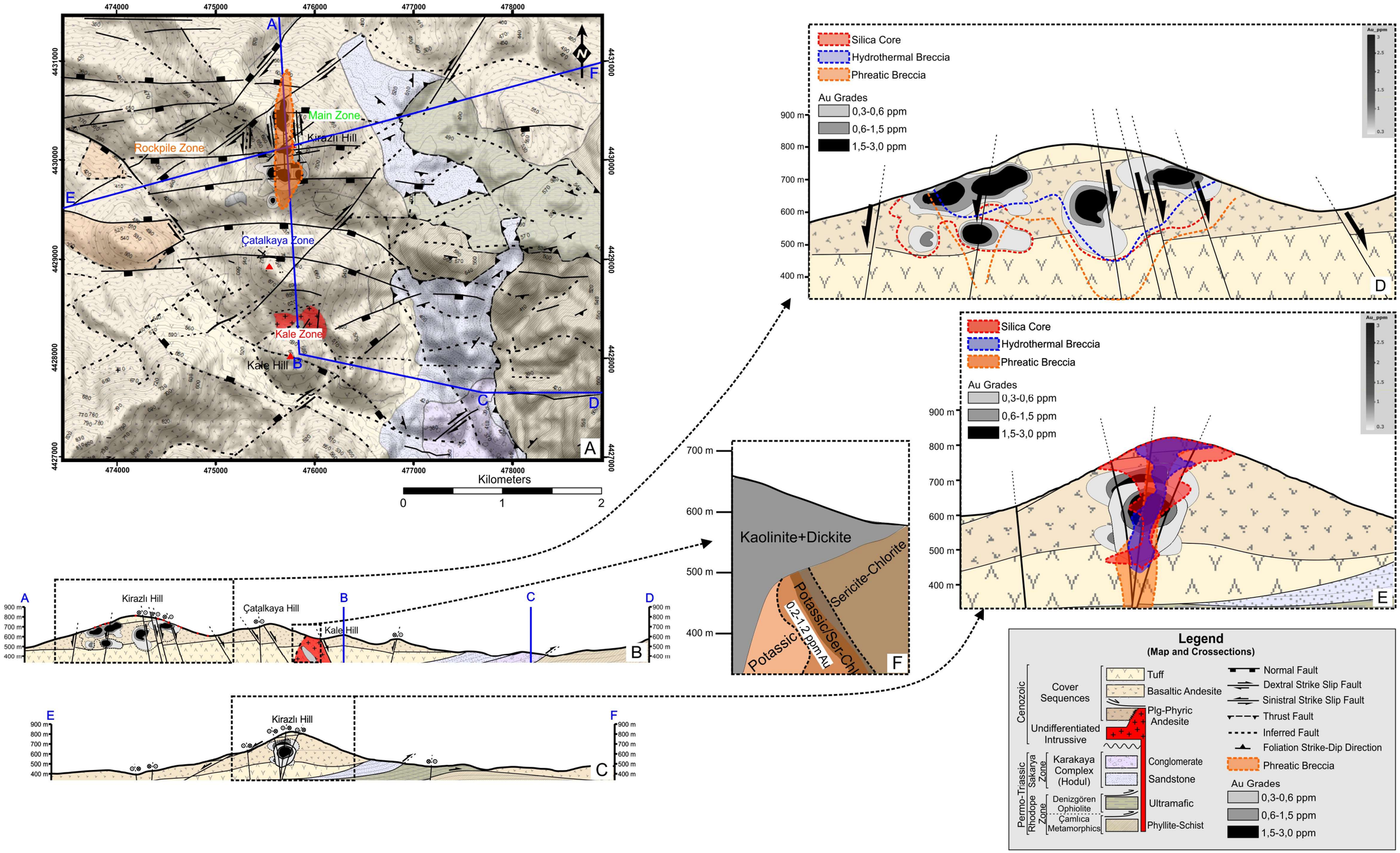

Figure 5.24. (A) Geological map of Kirazlı District and map distribution of Au grades, (B) A-B-C-D composite cross-section and vertical distribution of Au grades, (C) E-F cross-section and vertical distribution of Au grades, (D) and (E) close-up views of distribution of Au grades from cross-sections in B and C, (F) alteration types and Au grade in porphyry styale mineralization.

6. DISCUSSION

6.1. Tectonic Phases and Their Spatio-Temporal Association

According to the findings based on the kinematic data, predominant fault orientation, and available data, four successive tectonic phases have been identified in the Kirazlı district. They are mainly successive phases of extensional tectonics, and are Phase-1 with NW-SE extension, Phase-2 with NNE-SSW extension and Phase-3 for NE-SW extension (Figure 4.1).

The orientation of principal stress directions for the faults in the NW-SE extensional phase-1 is dominated by vertical σ1 and horizontal σ2 and σ3 principal stress orientation within an extensional system (Figure 4.2). Plunges of slip data on fault planes slip vectors on different fault sets identified in this phase are suggestive of both dextral-normal oblique system and sinistral-normal oblque slip with more dominant dip-slip characteristics. Phase-1 related kinematic indicators were generally observed within middle-late Eocene – early Oligocene aged volcano-plutonic rocks formed within northern and central Biga Peninsula, (Fig. 4.1A and B, Table 4.1.). The ENE-WSW trending fault surfaces of this phase, contain striations indicating kinematics of both due to NNE-SSW extension and NE-SW extensions indicating that the same fractures should have been used or the faults were re-activated by subsequent tectonic phases (Figure 4.1B)

The most prominent strike directions of faults in the Phase-2 resemble the general trend of detachment faults bordering the Kazdağ Core Complex and general trend of half-graben system at central Biga Peninsula. This phase coincides temporally with the Oligo-Miocene extension marked by the initiation of core complex exhumation of ENE-WSW trending Kazdağ metamorphics by detachment faults. Besides, the extension axis for the Oligo-Miocene extensional period in the Biga Peninsula shares similarities with prominent fault orientation and extension direction of the phase-2. The extension trends based on kinematic analysis (Okay and Satır, 2000; Beccaletto et

al.,2007; Bonev and Beccaletto, 2007) indicate approximately NNE-SSW extension direction, similar to Phase-2 identified in this study.

The field works on the fault planes for both Phase-2 and Phase-3 show that ENE-WSW and NE-SW predominant strike directions are shared by both phases. This may indicate that Phase-3 tectonic regime appears to have reactivated the earlier Phase-2 faults. The Phase-3 share kinematic and geometric features similar to the well known transtensional NE-SW and strike-slip tectonics in the Biga Peninsula (Kaymakcı et al., 2007). The Biga Peninsula is traversed by ENE-WNW and NE-SW trending dextral fault segments accepted as in the southern splay of north Anatolian fault zone (NAFZ). The roseplot for the faults formed during the phase-3 indicate that they are conformable with the orientation strike-slip faults were generated during the recent tectonic era represented by combination of both ongoing Aegean extension and successive dextral deformation by southern splay of NAFZ.

Brunetti (2016) documented a temporal order of tectonic phases similar to temporal order identified in this study and the ENE-WSW and NE-SW trending faults are also present within the Halilağa deposit formed at the northern margin of Kazdağ Core Complex (to southeast of Kirazlı deposit). Brunetti (2016) also revealed that these faults were formed due to a NW-SE extension during middle Eocene (Phase-1 in this study) and reactivated as dextral-normal oblique faults during the Mio-Pliocene.

6.2. Correlation Between Regional and District Scale Faults

The data on (1) kinematic axes, (2) predominant fault orientations, (3) slip senses, (4) slickenline plunges and (5) roseplot/stereoplots for the faults mapped in the regional and district-scale works (Figure 4.7) show comparable tectonic phases except for minor differences. For example, although the extension directions of each phase strongly resemble to each other, the principal stress axes except the sigma-3 and predominant fault orientations of Phase-2 and Phase-3 point to slightly different orientations (Figure 4.7). This is because some predominant trends that exist on a regional scale analyses could not be included in the analyses of the district-scale works since they do not contain any recognizable slickenlines. The absence of slickenlines related to the specific fault trends within the district-scale works, may imply that such

faults were preferred by hydrothermal fluids, and traces of kinematic data was obliterated by intense alteration and vein filling minerals.

6.3. Spatio-Temporal Association Between Mineralizations and Tectonic Phases

Porphyry Cu and HS epithermal Au occurrences in the Biga Peninsula are temporally and spatially associated with the magmatism resulted by syn- to post collisional Cenozoic magmatism during the closure of NeoTethys Ocean. Porphyry Cu systems are hosted by 42.6 to 18.2 Ma andesite porphyry and diorite to granite intrusions (Kuşcu et al., 2019), and are spatially aligned along NE-SW trending intrusive belts generally bounded by extensional fault systems that were considered to be loci for the emplacement of the intrusive bodies (Yiğit, 2012; Sanchez et al.,2016; Kuşcu et al., 2019). The available data show that porphyry Cu deposits were generated during time intervals of 42-35 Ma and 30-18, at northern and southern Biga Peninsula, respectively (Kuşcu et al., 2019). The HS-epithermal Au deposits are hosted commonly by the Oligocene volcanic rocks of the central Biga Peninsula (Dededağı, Bodurlar, Dedeler, Doğancılar, Sarpdağ, Kartaldağ, TV-Tower, Çaltıkara, Hamatepe, Seyrattepe, Halilağa-north, Pirentepe, Ağıdağı, Çamyurt, Karıncalı) and southeastern Biga Peninsula (İkizce, Saz, Gök, Sapdağ). These deposits within the central Biga Peninsula at north of Kazdağ Core Complex are roughly aligned along the structures trending in NW-SE direction (Figure 2.3). This direction was considered to represent the faults with arc-parallel orientation (Sanchez, 2012), and was described as earliest structural trend predating the E-W faults (Yılmaz and Karacık, 2001). This NW-SE structural trend was also pronounced as a significant pathway for the hydrothermal fluids and ore precipitation (Sanchez, 2012; Brunetti, 2016). As emphasized earlier, the same trend is also comparable to structures along which Eocene volcanic rocks are juxtaposed to the basement rocks (Kemer Micaschists-Çamlıca Metamorphics). Therefore, the faults in this trend may represent the early structures that resulted in the generation of basin over the metamorphic basement within the biga Peninsula.

The porphyry Cu and HS epithermal Au style deposits may occur as telescoping systems with cogenetic origin that coexist in space and time. However, telescoping systems are very scarce in the world. Besides, the coexistence of porphyry Cu and HS

epithermal Au style deposits in the same deposit area may not necessarily be cogenetic and telescoping. However, for the HS-Epithermal Au deposits within the Biga Peninsula it is stated that "*abundant epithermal deposits presumably are related to deeper* ***unexposed porphyry systems***" (Kuşcu et al, 2019) and "*hydrothermal fluids responsible for lithocap formation are inferred to have been fed by steeply dipping extensional faults and associated fractures above* ***concealed and inferred plutons***" (Sanchez et al., 2016). The coexistence of both porphyry Cu and HS epithermal Au mineralization in the Kirazlı district is matter of discussion by Aluç et.al. (2023). Based on the geochemical characteristics and geochronologic age on the magmatism and mineralization events in the Kirazlı deposit they showed that porphyry Cu and HS-epithermal Au mineralization are "spatially associated but genetically disconnected" (Aluc et al.,2023). According to available data the porphyry style mineralization is hosted by middle-late Ecoene volcano-plutonic (undifferentiated intrusive rocks: 40.47 ± 0.33 to 41.20 ± 0.45 Ma, and plagioclase-phyric andesite: 37.88 ± 0.26 to 38.40 ± 0.25 Ma; Aluc et al., 2023) rocks and HS-epithermal style mineralization is hosted by Oligocene volcanic rocks (basaltic-andesite lava flow and volcanoclastics: 31.93 ± 0.54 to 32.69 ± 0.26 Ma; Aluc et al., 2023). Besides, the geochronologic data on the alteration minerals for the porphyry Cu and HS epithermal Au systems indicate that the timing of porphyry Cu event is 36.68 ± 0.39 Ma (main porphyry) - 33.62 ± 0.17 Ma. (molybdenite event) and timing of the epithermal Au event is 30.7±1.5 Ma - 25.3 ± 0.4 Ma. These ages in their error limits suggest that they could not be part of the same magmatic hydrothermal system (i.e they are not cogenetic). However, Aluç et. al. (2023) also documented that the epithermal system overlies the porphyry Cu system at the deposit similar to cogenetic telescoping systems. As their ages are different and epithermal system post-dates the porphyry Cu system, their spatial overlap should be due to some other factors.

The field/structural mapping studies in this study, and alteration zones mapped by Aluç et al. (2023) at the western part of district revealed that the boundary between Eocene and Oligocene volcanics is not stratigraphic but tectonic. They are juxtaposed to each other along extensional faults (Figure 3.1). Also alteration map by Aluç et al. (2023) show that alteration zones of porphyry Cu and epithermal Au style deposits are approximately exposed at isolated parts of the district (Figure 5.1). For instance, the pyrophyllite and sericite allteration zones defining the alterations for the porphyry Cu

style deposit, crop at the southern part of district between Çatalkaya and Kale hill. Besides, the B-/D-type veins that form typical veins associated with the potassic and sericitic alteration zones of a typical porphyry Cu system respectively, crop out specificly within sericite altered zones. Whereas the massive silicified bodies representing the HS epithermal Au system overlie the alterations and veins of the porphyry Cu style system. They occur more or less massive sub-horizontal bodies forming the peaks of the Kirazlı and Çatalkaya Hills while quartz-alunite alteration of the epithermal Au system specifically crop out forming a NW-SE trending zone close to Kirazlı Hill. It is delimited from south and north by the normal and strike-slip faults around the Kirazlı Hill (Figure 5.2). Considering the combined map distribution of silicification/quartz-alunite alteration and mapped faults on the map, the silicification and quartz-alunite alteration zones present a sliced and bordered pattern by E-W and NE-SW trending faults (Figure 5.2A). The marginal montmorillonite-illite dominated zones in the HS-epithermal Au style mineralization show orientation parallel to E-W trending extensional faults (Figure 5.2C). Although porphyry Cu and HS epithermal Au mineral alterations are limited to certain parts of the study area, no sharp or deformational boundary between porphyry Cu and epithermal Au-specific alteration zones have been observed during field studies. Besides, as there were limited number of drill holes intersecting both epithermal Au and porphyry Cu related alterations in the Kirazlı deposit, the nature of transition between the two and if there is structural disturbance leading to juxtaposition of two systems are not clearly documented.

6.4. Spatio-Temporal Associations Between High-Permeability Zones and Structural Elements within the District

6.4.1. Porphyry-Cu style mineralization

The fracture producing events related to formation of porphyry Cu vein and veinlets may result from both stress states during emplacement of porphyry stock or governing tectonic regime (Tosdal and Richards, 2001). While concentric and radial vein arrays reflect the uniaxial stress conditions of magmatic processes, linear vein arrays show influence of tectonic regime (Tosdal and Richards, 2001). A-veins representing the early stage of porphyry Cu mineralization generally form under the high-

pressure/temperature conditions resulting more ductile deformation and wormy A-vein formation (Tosdal and Richards, 2001; Sillitoe, 2010). Subsequent B-veins with more straight vein walls and more linear geometry indicate lower temperature conditions while the formation of D-type veins post-dating A- and B-veins form under more brittle environment (Tosdal and Richards, 2001).

For the determination of spatio-temporal association between the preferred orientation of porphyry Cu veins and tectonic phases and structural features it seems more suitable to examine the B-type and D-type veins together (Tosdal and Richards, 2001). Combined preferred orientations of B-/D-type vein/veinlet of porphyry Cu type mineralization were obtained from the field and oriented chip samples. The average preferred orientation of 100 B-/D-type vein/veinlets from oriented chip samples range between N65°-85°E and N25°-35°W (Figure 5.15A) while the 372 field measurements on the same type of veins from the sericite altered zones of porphyry Cu mineralization result in directions N75°-85°E, N45°-55°W and N40°-50°E (Figure 5.21). The most prominent vein orientation common for both types indicates a ENE-WSW trend. ENE-WSW trend for the veinlets from oriented thin-sections prepared from oriented chip samples is favor of NW-SE and NNW-SSE extension based on elongation of stretched quartz crystals within the veins (Figure 5.17) consistent with the NW-SE extension axis and the predominant regional fault orientations of tectonic Phase-1 dominated during late Eocene to early Oligocene. The ENE-WSW fault orientation of tectonic Phase-1 at Kale zone was observed rarely during district-scale measurements (Figure 4.6). This is most probably due to erase of the slickenlines and kinematic indicators once available on the fault planes by intense and syn-tectonic alteration and mineralization or may be due to the reactivation of faults possibly obliterated the necessary kinematic data related to the tectonic Phase-1.

6.4.2. HS-epithermal style mineralization

HS-epithermal Au deposits tend to be formed in contractional and neutral stress states related to arc environments or settings where transitition from contraction to extension is recorded in some districts (Rhys et al.,2020). The latter represents post-subduction/-collision environment. The Biga Peninsula is one of the few places (Oligo-Miocene Anatolia and Rhodope belt; Rhys et al. 2020 and references therein) where epithermal

Au mineralization is accompanied andesitic magmatism in transtensional and extensional environments (Rhys et al.,2020). District-scale zones in HS epithermal Au systems are often generated controlled by lithological, hydrothermal and structural features (Rhys et al.,2020). The hydrothermal fluid flows resulting in the HS epithermal Au ore formation may be localized along pre- or syn-volcanic, arc-oblique or parallel structural zones that are overprinted or accompanied by phreatic-phreatomagmatic breccia bodies (Arribas, 1995; Hedenquist and Taran, 2013; Rhys et al.,2020). Vertical/subvertical tabular geometry of HS epithermal Au ore bodies may be related to the orientation of mineral-hosting phreatic/hydrothermal breccia zones formed as the result of successive tectonism and brecciation events. Also, structural comminution during late-stage mineralization may govern preferred orientation of veins and lateral extension of marginal alteration zones.

The primary permeability of HS epithermal Au deposits is generally governed by permeable volcanoclastic horizons (lithic tuff, unvelded tuff, etc) and increased porosity by acid leaching of relatively pre-existing volcanic minerals (vuggy zones). Interplay between phreatic/hydrothermal brecciation and faulting events under regional stress state promotes the vertical secondary permeability along tabular shaped vertical up-flow zones under a horizontal/subhorizontal lithocap (Dilles and John, 2020; Rhys et al.,2020). The drill logs and core assay data, drillcore examination and distribution of mineral-based alterations (Aluc et al., 2023) show that main ore body of HS epithermal Au style mineralization is hosted by a NNW-SSE trending vertical/subvertical and tabular phreatic/hydrothermal breccia body. The vertical/subvertical-tabular geometry of the HS epithermal system in Kirazlı deposit may suggestive of fluids channelized along permeable and porous breccia body formed along a pre-/syn-mineral structural trend (Dilles and John, 2020; Rhys et al.,2020). However, as the kinematic indicators related to NNW-SSE structural trend is obliterated by most probably by subsequent brecciation and mineralization events at the Kirazlı Hill, discontinuous short segments of NNW-SSE and N-S striking vertical/subvertical faults remain recognizable on field and plotted on the map (Figure 5.1 and 5.20). NNW-SSE and N-S faults are generally post-dated and bisected by E-W and NE-SW striking fault sets. Alunite alteration around the phreatic/hydrothermal breccia body has a NW-SE oriented lateral distribution and has a sliced and bordered appearance by E-W and NE-SW oriented faults (Figure 5.2C).

The veins belonging to the HS epithermal Au mineralization are generally recorded around residual-silica core (silicification zone) enveloped by quartz-alunite zones at the Main zone and dickite alteration zone at the northwest of Çatalkaya zone (Figure 5.2A). The veins around the Main zone generally contain the fluid-assisted breccia texture with high clast/matrix ratio and no or slightly re-oriented clasts indicating hydraulic assisted fracturing (Figure 5.18A-B) while the veins from illite-montmorillonite zones are relatively thin (0.5-1.0 cm) breccia-free quartz veins referring the increased tectonic contribution. Based on the rose-plots prepared from vein/veinlets orientations at the field, the predominant strikes emerge as N50°-70°E, N40°-60°W and N20°-30°E and N5°-10°W (Figure 5.21B). Recognized extension directions from quartz veins/veinlets from oriented thin sections resemble with the extension during tectonic Phase-2. However, extension direction may change between early- and late-stage mineralization. Examined micro-veins from oriented thin-sections indicate a NNE-SSW and N-S extension pattern (Figure 5.20).

6.5. Summary of Temporal Relations Between Tectonism and Mineralization Within District

According to the available data, the oldest magmatic units are undifferentiated intrusive and plagioclace-phyric andesite within the district. The published geochronologic ages of 40.47-41.20 Ma and 37.88-38.40 Ma are suggestive of emplacement of these magmatic units at the northern part of Biga Peninsula during post-collisional era. Porphyry Cu-related intrusions generally favour arc-oblique/parallel transtensional or strike-slip deformation zones working as crustal-scale pathways for ascending magma within arc/backarc settings. Sanchez et al. (2016) relates the emplacement of Eocene intrusives of northern part of Biga Peninsula along the arc-parallel structures. Formation of middle-late Eocene magmatics followed by a NW-SE extension providing the necessary stress relaxation appeart to have favoured by porphyry type mineralization. The NW-SE directed extension and ENE-WSW and NE-SW directed preferred orientation of porphyry Cu-related B- and D-veins are example of the similar features with the regional tectonic Phase-1 identified in this study (Figure 4.1 and 5.21B). According to available ages of early Oligocene basaltic andesite and pyroclastic rocks (31.93-32.69 Ma; Aluc et al.,2023), it seems that they

post-date the formation of porphyry Cu type mineralization (36.68 ± 0.39 Ma; Aluc et al.,2023) and related to a subsequent phase of magmatism within Biga Peninsula (Altunkaynak and genç, 2008; Sanchez et al.,2016; Kuşcu et al.,2019; Aluc et al.,2023). It is clearly recognized that Eocene and Oligocene volcanic sequences are juxtaposed by approximately E-W striking faults at the western part of Kirazlı district implying that formation of Oligocene volcanic units was followed by an extensional tectonism. Sanchez et al. (2016) proposed a NNW tilting of the volcanic sequences in the Biga Peninsula, and this was ascribed to same extension and prior to HS epihermal Au mineralization. In addition, Gülyüz et al. (2024) documented northward tilting of the Eocene porphyry Cu mineralized system at the Halilağa prospect in the Çan (Çanakkale), and juxtaposition of HS epithermal and porphyry Cu systems along the low angle normal faults that also tilted the porphyry Cu body. The geometry and spatial distribution of silicification (silica core) and surrounding pyrite-vein dominated areas within HS epithermal Au mineralization are conformable to NNW-SSE trending and vertical/subvertical phreatic/hydrothermal breccia that also exhibit geometry different from preferred orientations of veins in the porphyry Cu type mineralization. This breccia body spatially coincide with short and bisected vertical-subvertical N-S/NNW-SSE striking faults at Kirazlı Hill. These faults provide almost no recognizable kinematic data that may indicate interplay between successive faulting and brecciation events and intense alteration that obliterated necessary evidence for kinematic characteristics. Enveloping quartz-alunite alteration favours a NW-SE trending spatial distribution (Figure 5.2C). Silica core and enveloping quartz-alunite alteration are sliced and bordered by approximately E-W and NE-SW striking faults. Quartz-alunite alteration is limited from south by a approximately E-W striking south-dipping extensional fault and stays limited to Main at Kirazlı Hill (Figure 5.2C). Map-view distribution of illite-dominated marginal alteration zones show comparable geometric and spatial relation to intersections of E-W and NE-SW trending fault zones indicating that marginal alterations of the HS epithermal Au mineralization may temporally coincide with structures related to regional tectonic Phase-2. Also, extensional direction of late stage quartz veinlets cross-cutting veins associated silica core and alunite zone from oriented thin-sections are conformable to extensions with the tectonic Phase-2 (Figure 5.20). Figure 6.1 presents the temporal relation between mineralization and tectonic phases based on published literature and findings of this study.

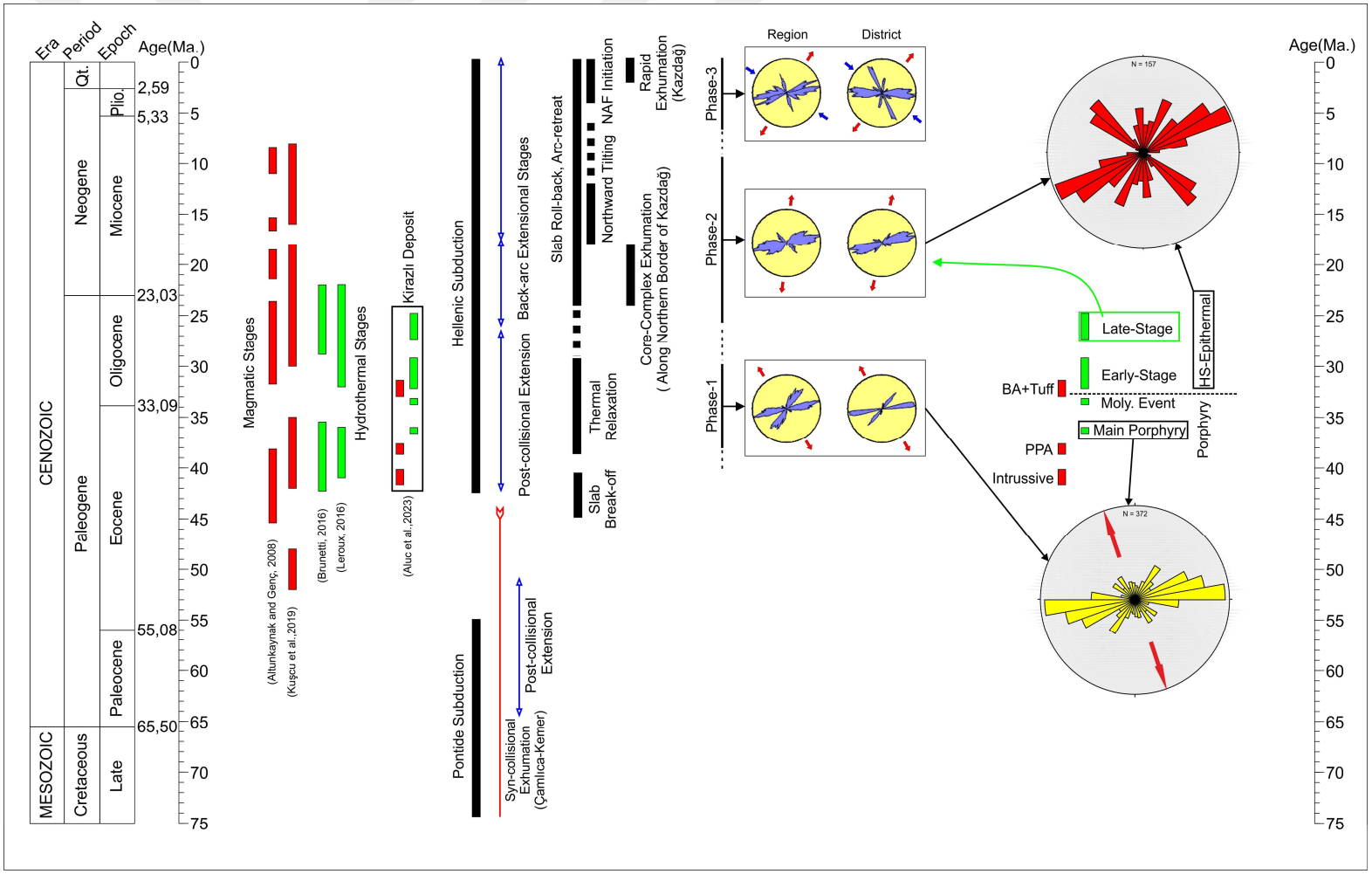

Figure 6.1. Regional and district scale temporal relations between tectonic, magmatic and hydrothermal events. (Regional Magmatic stages = Altunkaynak and Genç, 2008; Kuşcu et al, 2019; Regional Hydrothermal stages = Brunetti, 2016; Leroux, 2016; Kuşcu et al, 2019; Regional Tectonic history = Brun and Sokoutis, 2007; Brun and Faccenna, 2008; Agostini et al, 2010; Jolivet and Brun, 2010; Sanchez et al, 2016; Kuşcu et al. 2019; Schaarschmidt et al.2021; Gülyüz et al., 2024; District scale magmatic and hydrothermal chronology = Aluc et al.,2023)

7. CONCLUSION

The main conclusions rised from this thesis are summerized as follows:

- The Kirazlı porphyry Cu and HS-epithermal style mineralizations are hosted respectively by middle-late Eocene volcano-plutonic rocks and early Oligocene volcanic-volcanoclastic rocks at the central Biga Peninsula during the post-collisional/back-arc extension governing the Cenozoic tectono-magmatic evolution of northwestern Türkiye.
- The paleostress findings based on analysis of structural data from regional and district-scale studies area revealed four different tectonic phases indicating unique extension directions principle stress orientations. These tectonic phases and principle stress axes include (1) NW-SE extension (Phase-1: σ1=87°/173°, σ2=01°/057°, σ3=03°/327°), (2) NNE-SSW extension (Phase-2: σ1=69°/286°, σ2=21°/093°, σ3=04°/185°) and (3) NE-SW extension (Phase-3: σ1=32°/306°, σ2=56°/106°, σ3=09°/211°). The predominant fault orientations of each tectonic phases from both district and regional scale closely resemble each other .
- Based on published geochronology ages (Aluc et al.,2023) mineralization hosting volcano plutonic rocks formed during two different episode in middle-late Eocene and early Oligocene. It is clearly recognized that Eocene and Oligocene volcanic sequences are juxtaposed by approximately E-W striking faults at the western part of Kirazlı district implying that formation of Oligocene volcanic units was followed by an extensional tectonism. However no sharp or deformational boundary between porphyry Cu (hosted by Eocene undifferentiated intrussive) and epithermal Au-specific alteration zones (hosted by oligocene volcanic/volcanoclastic sequence) have been observed during field studies.
- Porphyry-Cu style mineralization consist of four successive hydrothermal vein phases identified as quartz-only A-veins, quartz-sulfide B-veins, sulfide-only D-veins and late stage calcite-only carbonate veins. Vein orientation measurements at the field and oriented chip samples revealed that the most prominent preferred

orientation of straight B-veins and D-veins are in ENE-WSW direction. The petrographic examinations of thin-sections revealed that growth direction of stretched quartz crystals of B-veins indicate NW-SE extension and multiple crack-seal events indicating a syn-mineral tectonism. The preferred orientation of B-/D-veins resemble the the predominant direction of the structures and extension axis of Phase-1 tectonism identified by the regional-scale works.

- The silicified core of HS-epithermal style mineralization is hosted by approximately N-S trending vertical/subvertical phreatic breccia body accompanied by hydrothermal vein breccia and crackle breccia indicative of fluid assisted brecciation and hydraulic fracturing and appears to be background for various types of subsequently truncating veins. The veins in the order of their formation in the HS epithermal Au system include (1) quartz-sulfide veins accompanied by milky-white quartz , (2) straight gray-quartz veins crosscutting the quartz-sulfide veins and, (3) white quartz veins mostly along straight, extensional fracture arrays truncating the earlier vein phases. Vein orientations are generally recorded around the residual-silica core enveloped by quartz-alunite zones at the Main and dickite alteration zone at the northwest of Çatalkaya zone and three preffered orientation determined as N50°-70°E, N40°-60°W and N20°-30°E. The veins around the Main zone generally contain the fluid-assisted breccia texture with high clast/matrix ratio and no or slightly re-oriented clasts indicating hydraulic assisted fracturing while the veins from illite-montmorillonite zones are relatively thin breccia-free quartz veins referring the increased tectonic contribution. Petrographical analyses of the hydrothermal veins in oriented thin sections, generally suggest that the late stage quartz veins formed under a NNE-SSW extension resembling the same extension axis of Phase-2 tectonism.

- Silica core and enveloping quartz-alunite alteration of HS epithermal Au mineralization is sliced and bordered by approximately E-W and NE-SW striking faults while illite-dominated marginal alteration zones show comparable geometric and spatial relation to intersections of E-W and NE-SW trending fault zones indicating that marginal alterations of the HS epithermal Au mineralization temporally coincide with structures governed by Phase-2.

- The published data and findings in this study revealed that the porphyry-Cu style mineralization and HS-epithermal Au mineralization within Kirazlı district formed along permeable zones resulted by different tectonic phases and an extensional tectonism juxtaposing the Eocene volcano-plutonic and Oligocene volcanic/volcanoclastic sequences along approximately E-W trending faults occurred prior to formation of HS-epithermal Au mineralization implying that the both styles of mineralizations were not temporally linked mineralization systems.

REFERENCES

Agostini, S., Doglioni, C., Innocenti, F., Manetti, P., & Tonarini, S. (2010) On the geodynamics of the Aegean rift, *Tectonophysics*, 488(1-4), 7-21

Aldanmaz, E., Pearce, J. A., Thirlwall, M. F., & Mitchell, J. G. (2000) Petrogenetic evolution of late Cenozoic, post-collision volcanism in western Anatolia, Turkey,. *Journal of volcanology and geothermal research*, 102(1-2), 67-95

Altunkaynak, Ş. (2007) Collision-driven slab breakoff magmatism in northwestern Anatolia, Turkey, *The Journal of Geology*, 115(1), 63-82

Altunkaynak, S., & Dilek, Y. (2006) Timing and nature of post-collisional volcanism in western Anatolia and geodynamic implications, *Special Papers - Geological Society of America*, 409, 321

Altunkaynak, Ş., Dilek, Y., Genç, C.Ş., Sunal, G., Gertisser, R., Furnes, H., Foland, K.A. and Yang, J., (2012) Spatial, temporal and geochemical evolution of Oligo–Miocene granitoid magmatism in western Anatolia, Turkey, *Gondwana Research*, 21(4), 961-986

Altunkaynak, Ş., & Genç, Ş. C. (2008) Petrogenesis and time-progressive evolution of the Cenozoic continental volcanism in the Biga Peninsula, NW Anatolia (Turkey), *Lithos*, 102(1-2), 316-340

Aluç, A., Kuşcu, İ., Ulyanov, A., Selby, D., Antoine, C., Spikings, R., & Moritz, R. (2023) Protracted metallogenic and magmatic evolution of the Kirazlı epithermal Au-Ag and porphyry Cu deposits, Biga Peninsula, NW Turkey: evidence from zircon U-Pb, muscovite 40Ar/39Ar, and molybdenite Re-Os geochronology, *Mineralium Deposita*, 1-21

Arribas Jr., A., (1995) Characteristics of high-sulfidation epithermal deposits, and their relation to magmatic fluid. In: Thompson, J.F.H. (Ed.), Magmas, fluids, and ore deposits: *Mineralogical Association of Canada Short Course*, 23, pp. 419–454

Aslan, Z., Demir, H., & Altın, İ. (2020) U–Pb zircon geochronology and petrology of the early Miocene Göloba and Şaroluk plutons in the Biga Peninsula, NW Turkey: Implications for post-collisional magmatism and geodynamic evolution, *Journal of African Earth Sciences*, 172, 103998

Aydın, Ü., Şen, P., Özmen, Ö., & Şen, E. (2019) Petrological and geochemical features of Biga Peninsula granitoids, NW Anatolia, Turkey, *Bulletin of the Mineral Research and Exploration*, 160(160), 81-115

Aygül, M., Topuz, G., Okay, A., Satir, M. and Meyer, H. P. (2012). The kemer metamorphic complex (NW Turkey): a subducted continental margin of the Sakarya zone, *Turkish Journal of Earth Sciences*, 21(1), 19-35

Beccaletto, L., Bartolini, A. C., Martini, R., Hochuli, P. A., & Kozur, H. (2005) Biostratigraphic data from the Çetmi Melange, northwest Turkey: palaeogeographic and tectonic implications, *Palaeogeography, Palaeoclimatology, Palaeoecology*, 221(3-4), 215-244

Beccaletto, L., & Jenny, C. (2004) Geology and correlation of the Ezine Zone: a Rhodope fragment in NW Turkey?, *Turkish Journal of Earth Sciences*, 13(2), 145-176

Bingöl, E. (1976) Bati Anadolu'nun jeotektonik evrimi, *Bulletin of the Mineral Research and Exploration*, 86(86), 14-34

Black, K. N., Catlos, E. J., Oyman, T., and Demirbilek, M. (2013) Timing Aegean extension: evidence from in situ U–Pb geochronology and cathodoluminescence imaging of granitoids from NW Turkey, *Lithos*, 180: 92-108

Bonev, N., & Beccaletto, L. (2007) From syn-to post-orogenic Tertiary extension in the north Aegean region: constraints on the kinematics in the eastern Rhodope–Thrace, Bulgaria–Greece and the Biga Peninsula, NW Turkey, *Geological Society, London, Special Publications*, 291(1), 113-142

Bonev, N., Beccaletto, L., Robyr, M., & Monié, P. (2009) Metamorphic and age constraints on the Alakeçi shear zone: implications for the extensional exhumation history of the northern Kazdağ Massif, NW Turkey, *Lithos*, 113(1-2), 331-345

Bonev, N., Marchev, P., Moritz, R., & Collings, D. (2015) Jurassic subduction zone tectonics of the Rhodope Massif in the Thrace region (NE Greece) as

revealed by new U–Pb and 40Ar/39Ar geochronology of the Evros ophiolite and high-grade basement rocks, *Gondwana Research*, 27(2), 760-775

Brun, J. P., & Faccenna, C. (2008) Exhumation of high-pressure rocks driven by slab rollback, *Earth and Planetary Science Letters*, 272(1-2), 1-7

Brun, J. P., & Sokoutis, D. (2007) Kinematics of the southern Rhodope core complex (North Greece), *International Journal of Earth Sciences*, 96, 1079-1099

Brunetti, P. (2016) Magmatic-hydrothermal evolution and post-ore modifications of the Halilağa porphyry cu-au deposit, NW Turkey, Ph.D. Thesis University of British Columbia, Vancouver, 272

Cavazza, W., Okay, A. I., & Zattin, M. (2009) Rapid early-middle Miocene exhumation of the Kazdağ Massif (western Anatolia), *International Journal of Earth Sciences*, 98, 1935-1947

Connolly, P., & Cosgrove, J. (1999) Prediction of fracture-induced permeability and fluid flow in the crust using experimental stress data. *AAPG bulletin*, 83(5), 757-777

Cooke, D. R., Hollings, P., & Walshe, J. L. (2005) Giant porphyry deposits: characteristics, distribution, and tectonic controls, *Economic Geology*, 100(5), 801-818

Cooke, D.R., Simmons, S.F., (2000) Characteristics and genesis of epithermal gold deposits. In: Hagemann, S.G., Brown, P.E. (Eds.), Gold in 2000. *Society of Economic Geologists, Reviews in Economic Geology*, 221–244

Cormier, A., Jutras, M., Welhener, H., Minard, T., Chiaramello, P., Cremeens, J. (2017) NI 43-101 Technical Report Feasibility Study Technical Report on the Kirazlı Project, Çanakkale Province, Turkey, 420

Cox, S.F., (2005) Coupling between deformation, fluid pressures, and fluid flow in ore-producing hydrothermal systems at depth in the crust. In: Hedenquist, J.W., Thompson, J.F.H., Goldfarb, R.J., Richards, J.P. (Eds.), *Economic Geology One Hundredth Anniversary Volume. Society of Economic Geologists*, pp. 39-76

Cunningham-Dunlop I.R., Lee, C. (2007) Technical Report on Kirazli Gold Property, Çanakkale Province, Turkey, 78

Çiftçi, N. B., & Bozkurt, E. (2009) Pattern of normal faulting in the Gediz Graben, SW Turkey, *Tectonophysics*, 473(1-2), 234-260

Delaloye, M., & Bingöl, E. (2000) Granitoids from western and northwestern Anatolia: geochemistry and modeling of geodynamic evolution, *International Geology Review*, 42(3), 241-268

Dewey, J. F. (1988) Extensional collapse of orogens, *Tectonics*, 7(6), 1123-1139

Dewey, J. F., & Şengör, A.M.C. (1979) Aegean and surrounding regions: complex multiplate and continuum tectonics in a convergent zone, *Geological Society of America Bulletin*, 90(1), 84-92

Dilek, Y., & Altunkaynak, Ş. (2007) Cenozoic crustal evolution and mantle dynamics of post-collisional magmatism in western Anatolia, *International Geology Review*, 49(5), 431-453

Dilek, Y., & Altunkaynak, Ş. (2009) Geochemical and temporal evolution of Cenozoic magmatism in western Turkey: mantle response to collision, slab break-off, and lithospheric tearing in an orogenic belt, *Geological Society of London, Special Publications*, 311(1), 213-233

Duru, M., Dönmez, M., Ilgar, A., Pehlivan, Ş., and Akçay, A. E., (2012) Geological map of the Biga Peninsula: Ankara, Turkey", *General Directorate of Mineral Research and Exploration of Turkey (MTA) Publications*, 1:250,000 scale, MTA, Ankara

Duru, M., Pehlivan, Ş., Şentürk, Y., Yavaş, F., & Kar, H. (2004) New results on the lithostratigraphy of the Kazdağ Massif in northwest Turkey, *Turkish Journal of Earth Sciences*, 13(2), 177-186

Erenoglu, O., Bozcu, M., & Billor, M. Z. (2022) Age and petrology of Eocene-Oligocene calc-alkaline volcanism in Biga Peninsula (NW Turkey): Implications for magma origin and geodynamic evolution, *Journal of African Earth Sciences*, 192, 104559

Ersoy, E. Y., Palmer, M. R., Genç, Ş. C., Prelević, D., Akal, C., & Uysal, İ. (2017). Chemo-probe into the mantle origin of the NW Anatolia Eocene to Miocene volcanic rocks: Implications for the role of, crustal accretion, subduction, slab roll-back and slab break-off processes in genesis of post-collisional magmatism, *Lithos*, 288, 55-71

Federici, I., Cavazza, W., Okay, A., Beyssac, O., Zattin, M., Corrado, S., & Dellisanti, F. (2010) Thermal evolution of the Permo− Triassic Karakaya subduction-accretion complex between the Biga Peninsula and the Tokat Massif (Anatolia), *Turkish Journal of Earth Sciences*, 19(4), 409-429

Gülyüz, N., Gülyüz, E., Karaoğlan, F., & Kuşcu, İ. (2024) Low temperature thermochronology reveals tilting of crystalline bodies, Halilaga porphyry Cu-Au deposit, NW Anatolia: Implications for exploration of porphyry copper deposits and interpretation of low-temperature thermochronology data for regional tectonics, *Ore Geology Reviews*, 105958

Gülyüz, N., Shipton, Z. K., Kuşcu, İ., Lord, R. A., Kaymakcı, N., Gülyüz, E., & Gladwell, D. R. (2018) Repeated reactivation of clogged permeable pathways in epithermal gold deposits: Kestanelik epithermal vein system, NW Turkey, *Journal of the Geological Society*, 175(3), 509-524

Gürer, Ö. F., Sanğu, E., Gürer, A., & Akın, M. (2021) Late Cenozoic shift from extension to strike-slip stress regime in the west of the Biga Peninsula, NW Turkey, *Journal of Structural Geology*, 148, 104348

Gürer, Ö. F., Sangu, E., Özburan, M., Gürbüz, A., Gürer, A., & Sinir, H. (2016) Plio-Quaternary kinematic development and paleostress pattern of the Edremit Basin, western Turkey, *Tectonophysics*, 679, 199-210

Helvacı, C., Ersoy, E. Y., Sözbilir, H., Erkül, F., Sümer, Ö., & Uzel, B. (2009) Geochemistry and 40Ar/39Ar geochronology of Miocene volcanic rocks from the Karaburun Peninsula: Implications for amphibole-bearing lithospheric mantle source, Western Anatolia, *Journal of Volcanology and Geothermal Research*, 185(3), 181-202

Hou, Z., & Cook, N. J. (2009). Metallogenesis of the Tibetan collisional orogen: A review and introduction to the special issue, *Ore Geology Reviews*, 36(1-3), 2-24

Hou, Z., Zhang, H., Pan, X., & Yang, Z. (2011) Porphyry Cu (–Mo–Au) deposits related to melting of thickened mafic lower crust: examples from the eastern Tethyan metallogenic domain, *Ore Geology Reviews*, 39(1-2), 21-45

Innocenti, F., Agostini, S., Doglioni, C., Manetti, P., & Tonarini, S. (2010) Geodynamic evolution of the Aegean: constraints from the Plio-Pleistocene volcanism of the Volos–Evia area, *Journal of the Geological Society*, 167(3), 475-489

Jackson, J., & McKenzie, D. (1988) The relationship between plate motions and seismic moment tensors, and the rates of active deformation in the Mediterranean and Middle East, *Geophysical Journal International*, 93(1), 45-73

Jébrak, M. (1997) Hydrothermal breccias in vein-type ore deposits: a review of mechanisms, morphology and size distribution, *Ore geology reviews*, 12(3), 111-134

Jolivet, L., & Brun, J. P. (2010) Cenozoic geodynamic evolution of the Aegean, *International Journal of Earth Sciences*, 99, 109-138

Karacık, Z., Yılmaz, Y., Pearce, J. A., & Ece, Ö. I. (2008) Petrochemistry of the south Marmara granitoids, northwest Anatolia, Turkey, *International Journal of Earth Sciences*, 97, 1181-1200

Kaymakci, N., Aldanmaz, E., Langereis, C., Spell, T.L., Gurer, O.F., Zanetti, K.A., (2007) Late Miocene transcurrent tectonics in NW Turkey:evidence from paleomagnetism and 40Ar–39Ar dating of alkaline volcanic rocks. *Geological Magazine*. 144 (2), 379–392

Koçyiğit, A. (2023) Neotectonics of the Sarıköy-İnova and Çan-Bayramiç-Ezine fault zones: basin formation, age and slip rates, NW Anatolia-Türkiye, *Bulletin of the Mineral Research and Exploration*, 172(172), 119-140

Kuşcu, İ., Tosdal, R. M., & Gençalioğlu-Kuşcu, G. (2019) Episodic porphyry Cu (-Mo-Au) formation and associated magmatic evolution in Turkish Tethyan collage, *Ore Geology Reviews*, 107, 119-154

Leroux, G.M. (2016) Stratigraphic and petrographic characterization of HS epithermal Au-Ag mineralization at the TV Tower district, Biga Peninsula, NW Turkey, M.Sc. Thesis, University of British Columbia, Vancouver, 198

McKenzie, D. (1978) Active tectonics of the Alpine—Himalayan belt: the Aegean Sea and surrounding regions, *Geophysical Journal International*, 55(1), 217-254

Meulenkamp, J. E., Van der Zwaan, G. J., & Van Wamel, W. A. (1994) On Late Miocene to recent vertical motions in the Cretan segment of the Hellenic arc, *Tectonophysics*, 234(1-2), 53-72

Micklethwaite, S., & Cox, S. F. (2004) Fault-segment rupture, aftershock-zone fluid flow, and mineralization, *Geology*, 32(9), 813-816

Micklethwaite, S., Sheldon, H. A., & Baker, T. (2010) Active fault and shear processes and their implications for mineral deposit formation and discovery, *Journal of Structural Geology*, 32(2), 151-165

Okay, A. I., & Altiner, D. (2004) Uppermost Triassic limestone in the Karakaya Complex-stratigraphic and tectonic significance, *Turkish Journal of Earth Sciences*, 13(2), 187-199

Okay, A. I., & Göncüoğlu, M. C. (2004) The Karakaya Complex: a review of data and concepts, *Turkish Journal of Earth Sciences*, 13(2), 75-95

Okay, A. I., & Mostler, H. (1994) Carboniferous and Permian radiolarite blocks from the Karakaya Complex in northwest Turkey, *Turkish Journal of Earth Sciences*, 3, 23–28

Okay, A. I., & Satir, M. (2000a) Coeval plutonism and metamorphism in a latest Oligocene metamorphic core complex in northwest Turkey, *Geological Magazine*, 137(5), 495-516

Okay, A. İ., & Satır, M. (2000b) Upper Cretaceous eclogite-facies metamorphic rocks from the Biga Peninsula, Northwest Turkey, *Turkish Journal of Earth Sciences*, 9(2), 47-56

Okay AI, Satir M, Maluski H, Siyako M, Monie P, Metzger R, Akyüz S (1996) Paleo- and Neo-Tethyan events in northwestern Turkey: geologic and geochronologic constraints. In: Yin A, Harrison TM (eds) The tectonic evolution of Asia. *Cambridge University Press*, Cambridge, 420–441

Okay, A., Siyako, M., & Burkan, K. A. (1991) Geology and tectonic evolution of the Biga Peninsula, northwest Turkey. *Bulletin-Technical University of Istanbul*, 44

Oliver, J. (1986) Fluids expelled tectonically from orogenic belts: Their role in hydrocarbon migration and other geologic phenomena, *Geology*, 14 (2): 99-102

Oyman, T. (2010) Geochemistry, mineralogy and genesis of the Ayazmant Fe–Cu skarn deposit in Ayvalik,(Balikesir), Turkey, *Ore Geology Reviews*, 37(3-4), 175-201.

Pickett, E. A., & Robertson, A. H. (1996) Formation of the Late Palaeozoic–Early Mesozoic Karakaya Complex and related ophiolites in NW Turkey by Palaeotethyan subduction–accretion, *Journal of the Geological Society*, 153(6), 995-1009

Pickett, E. A., & Robertson, A. H. (2004) Significance of the volcanogenic Nilüfer Unit and related components of the Triassic Karakaya Complex for Tethyan subduction/accretion processes in NW Turkey, *Turkish Journal of Earth Sciences*, 13(2), 97-143

Reid, R. R., Caddey, S. W., and Rankin, J. W. (1975) Primary refraction control of ore shoots, with examples from the Coeur d'Alene District, Idaho, *Economic Geology*, 70 (6): 1050-1061

Rhys, D. A., Lewis, P. D., & Rowland, J. V. (2020) Structural controls on ore localization in epithermal gold-silver deposits: A mineral system approach. In J. V. Rowland & D. A. Rhys (Eds.), Applied structural geology of ore-forming hydrothermal systems. *Society of Economic Geologists ,Review in Economic Geology*. 83–145

Richards, J. P. (2003) Tectono-magmatic precursors for porphyry Cu-(Mo-Au) deposit formation, *Economic geology*, 98(8), 1515-1533

Richards, J. P. (2009) Postsubduction porphyry Cu-Au and epithermal Au deposits: Products of remelting of subduction-modified lithosphere, *Geology*, 37(3), 247-250

Ring, U., Glodny, J., Will, T., & Thomson, S. (2010), The Hellenic subduction system: high-pressure metamorphism, exhumation, normal faulting, and large-scale extension, *Annual Review of Earth and Planetary Sciences*, 38, 45-76

Rojay, B. and Sözen, M.L. (2010) "Geological Report on the Kirazlı Prospect, Çanakkale", *Golder Associates (Golder)*

Rolland, Y., Perincek, D., Kaymakci, N., Sosson, M., Barrier, E., & Avagyan, A. (2012) Evidence for~ 80–75 Ma subduction jump during Anatolide–Tauride–Armenian block accretion and~ 48 Ma Arabia–Eurasia collision in lesser caucasus–East Anatolia, *Journal of Geodynamics*, 56, 76-85

Sánchez, M.G., McClay, K.R., King, A.R., Wijbrams, J.R. (2016) Cenozoic crustal extension and its relationship to porphyry Cu-Au-(Mo) and epithermal Au-(Ag) mineralization in the Biga Peninsula, northwestern Turkey, *Society of Economical Geologists Special Publications*, pp. 113–156

Schaarschmidt, A., Haase, K. M., Voudouris, P. C., Melfos, V., & Klemd, R. (2021) Migration of arc magmatism above mantle wedge diapirs with variable sediment contribution in the Aegean, *Geochemistry, Geophysics, Geosystems*, 22(6), e2020GC009565

Seedorff, E., Dilles, J.H., Proffett Jr., J.M., Einaudi, M.T., Zurcher, L., Stavast, W.J.A., Johnson, D.A., Barton, M.D., (2005) Porphyry deposits: characteristics and origin of hypogene features, *Economic Geology 100th Anniversary Volume*, 251–298

Seyítoğlu, G., & Scott, B. C. (1996) The cause of NS extensional tectonics in western Turkey: tectonic escape vs back-arc spreading vs orogenic collapse, *Journal of Geodynamics*, 22(1-2), 145-153

Sibson, R. H. (1987) Earthquake rupturing as a mineralizing agent in hydrothermal systems, *Geology*, 15(8), 701-704

Sibson, R. H., Robert, F., & Poulsen, K. H. (1988) High-angle reverse faults, fluid-pressure cycling, and mesothermal gold-quartz deposits, *Geology*, 16(6), 551-555

Sillitoe, R. H. (2010) Porphyry copper systems, *Economic geology*, 105(1), 3-41

Sillitoe, R.H., Hedenquist, J.W., (2003) Linkages between volcanotectonic settings, ore fluid compositions, and epithermal precious-metal deposits, *Economical Geology Special Pubications*, 10, 315–343

Simmons, S.F., White, N.C., John, D.A., (2005) Geological characteristics of epithermal precious and base metal deposits, *Economic Geology 100th Anniversary volume*, 485–522

Sözbilir, H., Sümer, Ö., Özkaymak, Ç., Uzel, B., Güler, T., & Eski, S. (2016) Kinematic analysis and palaeoseismology of the Edremit Fault Zone: evidence for past earthquakes in the southern branch of the North Anatolian Fault Zone, Biga Peninsula, NW Turkey, *Geodinamica Acta*, 28(4), 273-294

Şengör, A.M.C. (1987) Cross-faults and differential stretching of hanging walls in regions of low-angle normal faulting: examples from western Turkey, *Geological Society London, Special Publications*, 28(1), 575-589

Şengör, A.M.C., & Canitez, N. (1982) The North Anatolian Fault. Alpine-Mediterranean Geodynamics, 7, 205-216 North AnatolianFault. *In: Alpine-Mediterranean Geodynamics, American. Geophysical Union., Geodynamics Series*, 7, 205-216

Şengör, A.M.C., & Kidd, W.S.F. (1979) Post-collisional tectonics of the Turkish-Iranian plateau and a comparison with Tibet, *Tectonophysics*, 55(3-4), 361-376

Şengör, A.M.C., Tüysüz, O., Imren, C., Sakınç, M., Eyidoğan, H., Görür, N., Le Pichon, X. and Rangin, C., (2005) The North Anatolian fault: A new look, *Annual Review of Earth Planetary Sciences*, 33, 37-112

Şengün, F., Yiğitbaş, E., & Tunc, I. O. (2011) Geology and tectonic emplacement of eclogite and blueschists, Biga peninsula, northwest Turkey, *Turkish Journal of Earth Sciences*, 20(3), 273-285

Tosdal, R. M., & Richards, J. P. (2001) Magmatic and structural controls on the development of porphyry Cu±Mo±Au deposits, *Structural controls on ore genesis*, 14, 157-181

Tosdal, R. M., Dilles, J. H., & Cooke, D. R. (2009), From source to sinks in auriferous magmatic-hydrothermal porphyry and epithermal deposits, *Elements*, 5(5), 289-295

Tunc, I. O., Yiğitbaş, E., Şengün, F., Wazeck, J., Hofmann, M., & Linnemann, U. (2012) U-Pb zircon geochronology of northern metamorphic massifs in the Biga Peninsula (NW Anatolia-Turkey): new data and a new approach to

understand the tectonostratigraphy of the region, *Geodinamica Acta*, 25(3-4), 202-225

Yigit, Ö. (2009) Mineral deposits of Turkey in relation to Tethyan metallogeny: implications for future mineral exploration, *Economic Geology*, 104(1), 19-51

Yigit, Ö. (2012) A prospective sector in the Tethyan Metallogenic Belt: Geology and geochronology of mineral deposits in the Biga Peninsula, NW Turkey, *Ore Geology Reviews*, 46, 118-148

Yılmaz, Y., Genç, Ş. C., Karacık, Z., & Altunkaynak, Ş. (2001) Two contrasting magmatic associations of NW Anatolia and their tectonic significance, *Journal of Geodynamics*, 31(3), 243-271

Yılmaz, Y., & Karacık, Z. (2001) Geology of the northern side of the Gulf of Edremit and its tectonic significance for the development of the Aegean grabens, *Geodinamica Acta*, 14(1-3), 31-43

,

APPENDICES

Appendix-A. Measurements of Vein Strikes

B-Veins (Chip Samples)								
No.	Strike	Dip	Dip Quad		No.	Strike	Dip	Dip Quad
1	163	60	W		25	70	80	S
2	162	65	W		26	260	88	N
3	159	63	W		27	260	88	N
4	90	90	S		28	65	78	S
5	340	80	E		29	320	80	E
6	255	50	N		30	150	78	W
7	259	61	N		31	330	90	E
8	260	65	N		32	330	89	E
9	263	60	N		33	328	90	E
10	262	64	N		34	245	50	N
11	258	65	N		35	150	65	W
12	256	62	N		36	145	65	W
13	264	60	N		37	90	70	S
14	261	58	N		38	152	45	W
15	260	65	N		39	150	54	W
16	170	82	W		40	146	50	W
17	255	56	N		41	150	50	W
18	252	58	N		42	60	90	S
19	255	65	N		43	150	55	W
20	160	80	W		44	270	54	N
21	340	65	E		45	266	50	N
22	320	45	E		46	244	58	N
23	285	74	N		47	242	62	N
24	290	70	N		48	238	60	N

D-Veins (Chip Samples)								
No.	Strike	Dip	Dip Quad		No.	Strike	Dip	Dip Quad
1	20	90	E		27	15	70	E
2	240	72	N		28	355	75	E
3	60	80	S		29	130	45	S
4	175	55	W		30	115	80	S
5	172	51	W		31	50	50	S
6	205	78	W		32	180	60	W
7	204	79	W		33	330	90	E
8	70	50	S		34	245	50	N
9	230	60	N		35	360	80	E
10	232	61	N		36	360	80	E
11	330	74	E		37	150	65	W
12	220	78	W		38	330	90	E
13	320	75	E		39	60	65	S
14	245	65	N		40	137	55	W
15	150	70	W		41	150	50	W
16	175	50	W		42	63	90	S
17	335	75	E		43	61	90	S
18	320	80	E		44	60	86	S
19	180	90	W		45	58	90	S
20	120	81	S		46	30	55	E
21	55	58	S		47	180	80	W
22	265	55	N		48	240	61	N
23	30	60	E		49	244	58	N
24	315	70	N		50	240	64	N
25	260	60	N		51	242	62	N
26	35	30	E		52	238	60	N

Porphyry B-veins and D-veins (Field Measurements)												
No.	Strike	Dip	Dip Quad		No.	Strike	Dip	Dip Quad		No.	Strike	Dip	Dip Quad
0	200	65	W		148	255	75	N		295	40	72	E
1	199	65	W		149	250	70	N		296	40	72	E
2	203	65	W		150	256	80	N		297	55	78	S
3	205	65	W		151	245	85	N		298	0	55	E
4	337	75	E		152	250	80	N		299	10	60	E
5	300	75	N		153	257	83	N		300	356	67	E
6	190	65	W		154	250	75	N		301	305	50	N
7	191	66	W		155	240	80	N		302	300	50	N
8	192	60	W		156	260	65	N		303	298	54	N
9	190	66	W		157	250	80	N		304	300	60	N
10	330	80	E		158	245	60	N		305	15	65	E
11	330	81	E		159	65	78	S		306	15	65	E
12	331	80	E		160	68	80	S		307	315	55	N
13	150	85	W		161	60	78	S		308	310	60	N
14	205	65	W		162	68	83	S		309	315	70	N
15	205	65	W		163	70	82	S		310	304	70	N
16	80	65	S		164	70	80	S		311	315	50	N
17	80	67	S		165	75	76	S		312	315	60	N
18	81	66	S		166	69	87	S		313	200	53	W
19	290	67	N		167	70	82	S		314	205	50	W
20	190	85	W		168	70	87	S		315	200	54	W
21	185	70	W		169	140	68	W		316	210	50	W
22	120	75	S		170	320	30	E		317	200	50	W
23	185	75	W		171	320	40	E		318	199	45	W
24	185	85	W		172	145	70	W		319	200	55	W
25	165	80	W		173	320	40	E		320	240	75	N
26	185	75	W		174	145	70	W		321	240	80	N
27	340	85	E		175	320	80	E		322	235	70	N
28	80	75	S		176	32	33	E		323	315	35	N
29	65	87	S		177	45	83	E		324	315	40	N
30	66	89	S		178	215	45	W		325	313	39	N
31	70	87	S		179	215	44	W		326	200	85	W
32	70	80	S		180	215	40	W		327	200	85	W

33	64	87	S		181	222	50	W		328	300	87	N		
34	60	80	S		182	210	40	W		329	310	85	N		
35	90	55	S		183	213	45	W		330	300	78	N		
36	91	55	S		184	215	45	W		331	300	85	N		
37	89	54	S		185	215	54	W		332	302	80	N		
38	87	60	S		186	215	40	W		333	297	70	N		
39	94	50	S		187	218	42	W		334	260	55	N		
40	300	70	N		188	220	40	W		335	260	55	N		
41	330	60	E		189	250	80	N		336	90	65	S		
42	320	70	E		190	245	76	N		337	91	58	S		
43	163	70	W		191	250	70	N		338	90	61	S		
44	250	65	N		192	255	75	N		339	94	56	S		
45	290	85	N		193	252	81	N		340	90	67	S		
46	175	76	W		194	250	87	N		341	95	58	S		
47	315	70	N		195	250	78	N		342	90	66	S		
48	105	85	S		196	240	80	N		343	86	60	S		
49	160	80	W		197	250	74	N		344	75	70	S		
50	285	70	N		198	250	80	N		345	80	73	S		
51	80	75	S		199	270	85	N		346	70	70	S		
52	81	75	S		200	200	60	W		347	76	76	S		
53	82	75	S		201	200	63	W		348	75	70	S		
54	79	74	S		202	198	73	W		349	260	80	N		
55	81	70	S		203	203	65	W		350	261	83	N		
56	80	75	S		204	205	65	W		351	257	78	N		
57	80	75	S		205	205	60	W		352	256	85	N		
58	84	78	S		206	200	54	W		353	260	80	N		
59	80	76	S		207	300	45	N		354	270	80	N		
60	85	80	S		208	305	45	N		355	269	79	N		
61	78	76	S		209	315	75	N		356	265	80	N		
62	80	69	S		210	310	73	N		357	265	78	N		
63	83	75	S		211	311	78	N		358	267	78	N		
64	88	67	S		212	280	87	N		359	258	85	N		
65	80	75	S		213	280	80	N		360	260	80	N		
66	240	73	N		214	276	88	N		361	250	76	N		
67	240	65	N		215	130	87	S		362	250	71	N		
68	240	85	N		216	130	85	S		363	255	83	N		
69	240	72	N		217	170	85	W		364	255	80	N		
70	340	90	E		218	160	80	W		365	260	75	N		
71	275	65	N		219	160	80	W		366	260	60	N		
72	275	80	N		220	160	80	W		367	260	87	N		
73	87	83	S		221	160	80	W		368	255	80	N		
74	87	84	S		222	5	90	E		369	250	60	N		
75	87	85	S		223	345	75	E		370	255	85	N		
76	87	86	S		224	345	75	E		371	259	80	N		
77	125	80	S		225	345	75	E		372	260	80	N		
78	35	75	E		226	275	75	N		373	261	82	N		

79	35	75	E		227	280	70	N		374	264	87	N		
80	35	75	E		228	300	90	N		375	260	89	N		
81	35	75	E		229	300	87	N		376	270	80	N		
82	35	75	E		230	299	80	N		377	255	70	N		
83	260	67	N		231	230	80	N		378	253	81	N		
84	295	80	N		232	170	70	W		379	90	60	S		
85	123	80	S		233	170	75	W		380	93	58	S		
86	30	90	E		234	260	75	N		381	88	58	S		
87	30	90	E		235	320	75	E		382	92	56	S		
88	28	90	E		236	320	82	E		383	94	65	S		
89	30	90	E		237	45	83	E		384	170	80	W		
90	230	55	N		238	45	83	E		385	171	83	W		
91	335	90	E		239	45	83	E		386	175	78	W		
92	280	90	N		240	45	83	E		387	95	55	S		
93	250	70	N		241	170	70	W		388	96	50	S		
94	265	70	N		242	170	70	W		389	100	60	S		
95	265	70	N		243	260	75	N		390	93	72	S		
96	265	70	N		244	300	70	N		391	60	62	S		
97	265	70	N		245	300	79	N		392	60	60	S		
98	265	70	N		246	300	78	N		393	68	56	S		
99	265	70	N		247	304	80	N		394	65	60	S		
100	260	75	N		248	305	68	N		395	60	65	S		
101	255	80	N		249	300	70	N		396	350	80	E		
102	264	75	N		250	305	68	N		397	100	50	S		
103	260	70	N		251	40	80	E		398	100	50	S		
104	270	65	N		252	40	80	E		399	310	80	N		
105	264	80	N		253	40	80	E		400	310	80	N		
106	170	50	W		254	40	80	E		401	125	60	S		
107	265	60	N		255	240	85	N		402	125	60	S		
108	270	65	N		256	20	90	E		403	5	87	E		
109	267	60	N		257	345	90	E		404	6	78	E		
110	262	65	N		258	245	85	N		405	10	80	E		
111	265	70	N		259	245	85	N		406	5	80	E		
112	275	75	N		260	275	75	N		407	80	40	S		
113	135	48	S		261	275	75	N		408	85	39	S		
114	135	48	S		262	285	70	N		409	78	45	S		
115	210	33	W		263	320	72	E		410	60	65	S		
116	201	33	W		264	320	72	E		411	60	64	S		
117	220	80	W		265	320	72	E		412	65	60	S		
118	22	80	E		266	50	80	S		413	61	59	S		
119	50	90	S		267	50	80	S		414	60	55	S		
120	40	30	E		268	50	80	S		415	60	70	S		
121	170	50	W		269	50	80	S		416	60	75	S		
122	265	60	N		270	320	80	E		417	60	68	S		
123	270	65	N		271	320	80	E		418	180	80	W		
124	267	60	N		272	320	80	E		419	180	78	W		

125	262	65	N	273	320	80	E	420	30	60	E
126	265	70	N	274	320	80	E	421	32	65	E
127	275	75	N	275	230	80	N	422	33	58	E
128	135	48	S	276	230	80	N	423	215	70	W
129	135	48	S	277	230	80	N	424	210	68	W
130	210	33	W	278	230	80	N	425	215	58	W
131	201	33	W	279	230	80	N	426	213	72	W
132	220	80	W	280	265	65	N	427	90	45	S
133	22	80	E	281	265	65	N	428	90	40	S
134	50	90	S	282	185	55	W	429	60	60	S
135	40	30	E	283	200	85	W	430	65	63	S
136	265	72	N	284	300	75	N	431	58	59	S
137	315	75	N	285	280	50	N	432	61	60	S
138	265	72	N	286	195	85	W	433	63	58	S
139	240	70	N	287	195	85	W	434	65	64	S
140	175	65	W	288	190	85	W	435	30	50	E
141	15	70	E	289	195	80	W	436	40	70	E
142	85	42	S	290	200	70	W	437	45	68	E
143	75	70	S	291	240	65	N	438	43	72	E
144	250	85	N	292	245	60	N	439	41	69	E
145	251	86	N	293	250	70	N	440	150	35	W
146	250	80	N	294	240	70	N	441	153	40	W
147	250	79	N					442	146	38	W

Epithermal Veins (Field Measurements)											
No.	Strike	Dip	Dip Quad	No.	Strike	Dip	Dip Quad	No.	Strike	Dip	Dip Quad
0	342	73	E	53	52	80	S	105	300	75	N
1	340	70	E	54	250	56	N	106	280	50	N
2	341	76	E	55	251	70	N	107	195	85	W
3	338	68	E	56	255	42	N	108	197	88	W
4	340	70	E	57	255	65	N	109	190	85	W
5	67	50	S	58	251	56	N	110	195	80	W
6	65	60	S	59	253	60	N	111	200	70	W
7	350	70	E	60	55	79	S	112	240	65	N
8	179	80	W	61	255	80	N	113	245	60	N
9	173	78	W	62	251	78	N	114	250	70	N
10	175	65	W	63	73	80	S	115	240	70	N
11	179	72	W	64	65	68	S	116	40	72	E
12	340	65	E	65	66	72	S	117	40	71	E
13	188	73	W	66	67	66	S	118	55	78	S
14	55	54	S	67	61	65	S	119	0	55	E
15	51	76	S	68	67	59	S	120	10	60	E
16	235	80	N	69	67	65	S	121	356	67	E
17	233	83	N	70	67	70	S	122	305	50	N

18	231	78	N	71	75	65	S	123	300	50	N
19	58	67	S	72	55	80	S	124	298	54	N
20	181	70	W	73	235	70	N	125	300	60	N
21	183	73	W	74	245	80	N	126	15	65	E
22	332	70	E	75	245	78	N	127	15	65	E
23	68	80	S	76	243	75	N	128	315	55	N
24	125	65	S	77	65	80	S	129	310	60	N
25	124	70	S	78	68	81	S	130	315	70	N
26	311	65	N	79	62	78	S	131	304	70	N
27	315	70	N	80	241	72	N	132	315	50	N
28	312	80	N	81	243	70	N	133	315	60	N
29	313	69	N	82	181	80	W	134	200	53	W
30	317	86	E	83	8	81	E	135	205	50	W
31	319	67	E	84	200	78	W	136	200	54	W
32	314	78	N	85	201	81	W	137	210	50	W
33	315	75	N	86	20	68	E	138	200	50	W
34	321	65	E	87	28	80	E	139	199	45	W
35	141	70	W	88	25	80	E	140	200	55	W
36	142	78	W	89	175	68	W	141	240	75	N
37	144	67	W	90	170	70	W	142	240	80	N
38	340	80	E	91	175	67	W	143	235	70	N
39	342	89	E	92	178	87	W	144	315	35	N
40	225	56	W	93	175	78	W	145	315	40	N
41	221	78	W	94	55	65	S	146	313	39	N
42	227	76	N	95	54	70	S	147	200	85	W
43	228	68	N	96	50	68	S	148	200	85	W
44	225	81	W	97	300	66	N	149	300	87	N
45	44	70	E	98	302	70	N	150	310	85	N
46	45	80	E	99	120	65	S	151	300	78	N
47	47	76	S	100	127	60	S	152	300	85	N
48	45	81	E	101	265	65	N	153	302	80	N
49	55	78	S	102	265	66	N	154	297	70	N
50	58	79	S	103	185	55	W	155	260	55	N
51	53	76	S	104	200	85	W	156	260	55	N
52	55	72	S								

CURRICULUM VITAE

	Name – Surname:	Mehmet ÇAM
	Nationality:	*******
	Birth Place & Date:	******** _ **/**/****
	Mobile:	*** *** ** **
	E-mail:	*******@**.***.**
Education	:	**1999-2003** Foreign Language High School (English) (Burhaniye-Balıkesir) **2004-2008** Dokuz Eylül University. Engineering Faculty, Department of Geological Engineering (B.Sc.). **2010-2014** Sivas Cumhuriyet University. Engineering Faculty, Department of Geological Engineering (M.Sc.). Supervisor: Assoc.Prof.Dr. Tefik Fikret SEZEN **2014-2017** Muğla Sıtkı Koçman University Engineering Faculty, Department of Geological Engineering (M.Sc.). Supervisor: Prof.Dr. İlkay KUŞCU **2017-2024** Muğla Sıtkı Koçman University Engineering Faculty, Department of Geological Engineering (Ph.D). Supervisor: Prof.Dr. İlkay KUŞCU
Basic and Work Oriented Softwares	:	MS OFFICE, Mapinfo, CorelDraw, Global Mapper WinTensor, Microsoft Office Applications, Computer Operating Certificate (Ministry of Education).
Military Service	:	**.**.**** - **.**.**** Turkish Armed Forces - General Command of Gendarmerie

Experiences

July 2012 - March 2014 Research Assistant, Sivas Cumhuriyet University

March 2014 - Research Assistant, Muğla Sıtkı Koçman University

Educational Practices

-2007 Summer Practice

Jeoteknik Mühendislik, *****-*****

(Tel No: **** *******)

-2008 Summer Practice

Uysal Kırmataş Tesisleri, *******-*********

(Tel No: **** *******)

-Field Geological Mapping Camp

Supervisor: Prof. Dr. T**** G*****

-B.Sc. Thesis

İzmir Fayının Doğu Segmentinin Jeolojisi ve Depremselliği

Supervisor: Prof. Dr. U*** İ***

Attended Meetings

-ATAG (Active Tectonic Working Group of Turkey)

Muğla – 2014 (Member of Organization Committee)

-ISEMG (International Sympozium on Eastern Mediterrenean Geology)

Muğla - 2014 (Member of Organization Committee)

-71st Geological Congress of Turkey

Ankara – 2018 (Oral Presentation)

-EGU2018 European Geosciences Union – General Assembly

2018 – Vienna (Poster Presentation)

-EGU2023 European Geosciences Union – General Assembly

2013 – Vienna (Poster Presentation)